A new hybrid Additive Manufacturing process combining Selective Laser Melting and Laser Shock Peening

THÈSE N^O 9088 (2018)

ÉCOLE POLYTECHNIQUE FÉDÉRALE DE LAUSANNE

POUR L'OBTENTION DU GRADE DE DOCTEUR ÈS SCIENCES

PAR

Nikola KALENTICS

acceptée sur proposition du jury:

Prof. Y. Bellouard, président du jury
Prof. R. Logé, Dr E. Boillat, directeurs de thèse
Prof. A. Clare, rapporteur
Dr D. Rostohar, rapporteuse
Dr M. Strobl, rapporteur

ÉCOLE POLYTECHNIQUE
FÉDÉRALE DE LAUSANNE

Suisse
2018

Acknowledgments

This thesis marks a final step of a four-year long journey on which I was privileged to be accompanied and supported by a number of extraordinary people. Today, I would like to express my immense gratitude to them.

First and foremost, to my thesis advisor Roland Logé, for giving me the opportunity and then the freedom and support to explore different directions during the development of this project. His belief in these ideas, expert guidance, vision and mentorship have made all this possible.

To my thesis co - advisor, Eric Boillat, from whom I have learned the first things about SLM and for his help in many technical and machine related issues over the years.

To the thesis committee, composed of Prof. Yves Bellouard, Dr. Danijela Rostohar, Prof. Adam Clare and Prof. Markus Strobl, for their valuable time and effort to review this manuscript and provide a much appreciated feedback.

To my dear colleagues from the LMTM lab, with whom I have shared unforgettable moments and who have all, in one way or another, contributed to this thesis. Special thanks to Mathijs for all his help with the day to day activities, and Cyril for his help with the SEM. Special thanks goes to Jamasp, Andreas, Kei, Manuel, Navid and Hossein who have directly contributed to the content of this thesis. Thanks to everyone who participated to the spectacular table tennis matches during the breaks, especially Kei, Manuel, Navid, Hossein, Gaojun and Oscar. These moments will be treasured. Thanks to Joëlle for taking care of all administrative tasks. And Annick, Priscille, Margaux, Céline and Rita for your kindness and for making LMTM team great as it is.

Special thanks to everyone who made it all the way to Novi Sad for the wedding and shared those memorable moments with Aleksandra and me. To my friends all over the world, for all their time and patience and sometimes for simply being there.

Finally, a warmest thank you goes to my parents Katica and Vojislav, sisters Zaga and Marija, brother Marko, and my wife Aleksandra for having nothing but unlimited support, encouragement and sincere love.

Lausanne, 21.09.2018.   *Nikola Kalentics*

Abstract

Additive Manufacturing (AM) in whole and especially Selective Laser Melting (SLM) are already making a revolution in the way parts are designed and manufactured with the ability to produce lightweight parts with unprecedented complex geometries which are otherwise impossible to manufacture. These advantages are becoming more apparent and acknowledged in the manufacturing world and are reflected in a constant and rapid yearly growth (e.g. an 80% increase in the number of sold metal AM machines in 2017 compared to the year before).

This thesis represents an experimental study focused on two major limitations of the SLM process: i) accumulation of tensile residual stresses (TRS) and ii) non optimal microstructures in SLM parts. In order to address these limitations, a novel hybrid additive manufacturing process entitled 3D Laser Shock Peening (3D LSP) was developed and patented. 3D LSP repetitively introduces Laser Shock Peening (LSP), a well-known surface post treatment, during the building phase of SLM in order to introduce beneficial compressive residual stresses (CRS) and subsequently decrease part distortion, improve microstructure, increase fatigue life and reduce crack density.

The thesis is composed of 10 chapters. The first three chapters give an introduction to SLM and LSP, the problem statement, and a thorough analysis of the state of the art. Results obtained during this PhD are described in six chapters associated to six papers. Among the 6 papers, four have been published and two are planned to be submitted for publication in international peer-reviewed journals.

In the fourth chapter (first paper), LSP treatments were applied on SLM samples made out of two different steel grades in their rough as – built (AB) surface state and led to a clear conversion of detrimental TRS into more beneficial CRS. In the next chapter (paper), the accumulation of CRS due to the repetitive nature of the 3D LSP process is quantified. The LSP effects on the microstructure and the ability to improve recrystallization kinetics of the treated material is then shown in Chapter 6. In Chapter 7, the 3D LSP method is applied on a titanium alloy (Ti6Al4V) with a demonstrated 75% reduction in geometrical distortion compared to the SLM AB part. The next (8th) chapter demonstrates that 3D LSP can produce 316L steel parts with unrivaled fatigue life, i.e. a 15 times increase compared to the SLM AB state (non-machined surface), and more than 57 times increase compared to conventionally made parts (machined surface). The 9th chapter addresses the ability to reduce crack density in SLM parts made of a nickel based super alloy (CM247LC). 3D LSP showed a reduction of up to 95% compared to the SLM AB state. The final chapter summarizes all investigated effects of 3D LSP and gives a vision on potential future research.

The thesis stands as a series of initial, feasibility studies showing the potential of a novel hybrid additive manufacturing process. They represent stepping stones towards more detailed and focused future research in each of the investigated fields.

Résumé

La fabrication additive dans son ensemble et en particulier la fusion sélective par laser **(Selective Laser Melting - SLM)** constituent dès à présent une révolution puisqu'elles permettent de concevoir et de fabriquer des pièces légères avec des géométries complexes impossibles à obtenir jusqu'ici. Ces avantages sont de plus en plus significatifs et reconnus dans le monde industriel et se reflètent par une croissance constante et rapide (avec une augmentation de 80% du nombre de machines vendues en 2017 par rapport à l'année précédente).

Cette thèse présente une étude expérimentale centrée sur deux des principales limitations du procédé **SLM** : i) l'accumulation de contraintes résiduelles en traction **(Tensile Residual Stresses TRS)** et ii) l'obtention de microstructures non optimales dans les pièces obtenues. Afin de faire face à ces limitations, une nouvelle technique de fabrication additive hybride nommée « 3D Laser Shock Peeing » **(3D LSP)** ou Grenaillage Laser 3D, a été développée et brevetée. Le procédé **3D LSP** introduit la technique du Grenaillage Laser, déjà très utilisée en post traitement de surface, pendant la phase de fabrication, afin d'induire des contraintes résiduelles compressives **(CRS)** bénéfiques dans la pièce. Cela permet par conséquent de réduire les distorsions, d'améliorer la microstructure, de **réduire la densité de fissures et enfin d'augmenter la tenue en fatigue**.

Cette thèse est composée de 10 chapitres. Les trois premiers chapitres proposent une introduction aux techniques **SLM** et LSP, la présentation de la problématique ainsi qu'une analyse complète de l'état de l'art. Les résultats obtenus durant ce travail de thèse sont décomposés en six chapitres correspondants à six publications. Parmi ces six articles, quatre ont déjà été publiés et deux sont sur le point d'être soumis à publication dans des journaux internationaux avec comité de lecture.

Dans le chapitre quatre (première publication), des traitements par LSP sont appliqués à la surface d'échantillons fabriqués par SLM. Dans des échantillons de deux nuances d'acier différentes à l'état brut de fabrication **(As-Built - AB),** les traitements ont entraîné une nette transformation des contraintes de traction préjudiciables, en contraintes de compression bénéfiques. Dans le chapitre (article) suivant, l'accumulation des contraintes compressives dues à la nature répétitive du procédé 3D LSP est quantifiée. L'impact du LSP sur la microstructure et sur la capacité à améliorer la cinétique de recristallisation dans le matériau traité est montré dans le chapitre six. Dans le chapitre sept, la méthode 3D LSP est appliquée à un alliage de titane (Ti6Al4V). Une réduction des distorsions géométriques de 75% par rapport à une pièce brute de fabrication est démontrée. Le chapitre suivant (8ème) montre que le procédé 3D LSP permet de fabriquer des pièces en acier 316L avec une durée de vie en fatigue jamais atteinte auparavant, 15 fois plus longue que des pièces brutes de fabrication additive (surface non traitée) et plus de

57 fois plus longue que des pièces obtenues par fabrication conventionnelles (surface traitée). Le 9ème chapitre traite de la possibilité de réduire la densité de fissures dans des pièces en superalliage à base nickel (CM247LC) obtenues par SLM. Le procédé 3D LSP apporte une réduction de fissuration de 95% par rapport à l'état brut de fabrication additive. Le dernier chapitre résume tous les effets étudiés du 3D LSP et ouvre des perspectives de recherches futures.

Ce travail de thèse couvre une série d'études de faisabilité et montre le potentiel d'une nouvelle méthode de fabrication additive hybride. Celles-ci représentent des étapes indispensables avant de passer à des études plus détaillées et précises dans chacun des domaines étudiés.

Mots Clés: Fusion Sélective par Laser, Grenaillage Laser, 3D LSP, contraintes résiduelles, microstructure, recristallisation, microdureté, distorsion, tenue en fatigue, densité de fissures

Contents

Chapter 1 Introduction

1.1 Additive Manufacturing

Additive Manufacturing (AM) is defined by ISO/ASTM 52900 terminology standard as "a process of joining materials to make objects from 3D model data, usually layer upon layer, as opposed to subtractive and formative manufacturing methodologies" [1]. AM (widely known as 3D printing) emerged in the 1980s with the development of stereolithography [2] and was used primarily for prototyping. Nowadays, AM is changing the production as we know it. Some consider that it will have bigger influence on the production than any other process in recent history and even go to the extent of calling it an industrial revolution [3].

Conventional manufacturing processes are usually based on removal of material from a larger block using various technologies such as machining or forging until the desired shape is reached. They require expensive cutting tools that need to be used in multiple operations or corresponding molds that have to be built each time a new shape or size of a product is wanted, which is in both cases time-consuming and costly. AM process functions on a completely opposite principle - instead of subtracting, material is added in a layerwise method, as a single layer of material is built upon a previous one. Such process gives the possibility to create almost any shape including intricate internal channels, lattice and other complex structures, that were impossible to produce before. In addition to the geometrical freedom that it brings, AM also minimizes time to the market, enhances quality, lowers costs and opens the ability to produce multi-material parts [3]–[5].

There are more than 30 different AM processes that can be classified by various criteria, one of them is the classification into: powder bed, direct material deposition and liquid bed processes, as shown in Figure 1.
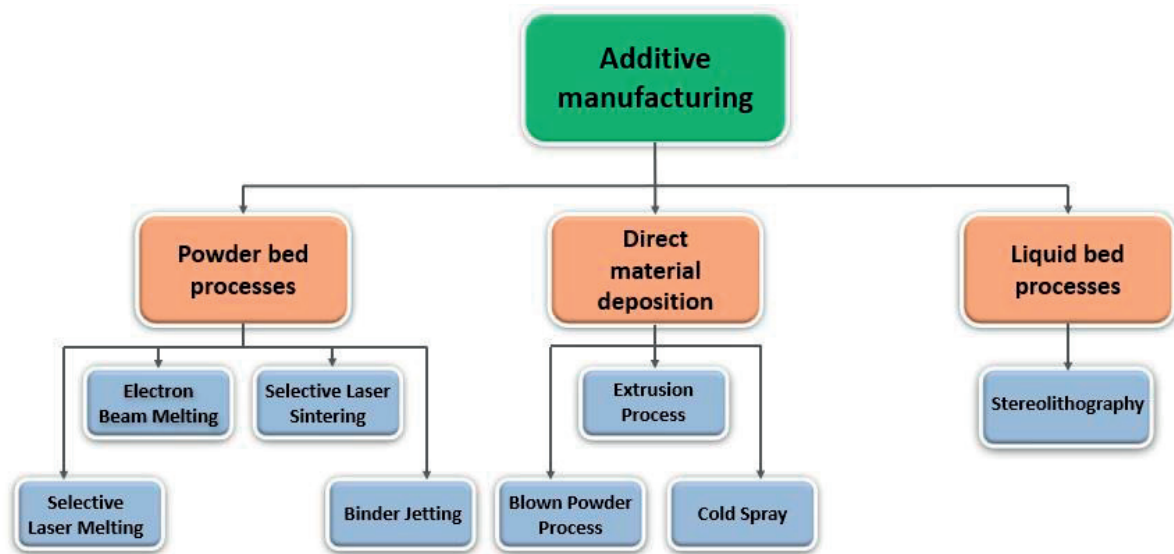
Fig. 1 AM processes division into powder bed, direct material deposition and liquid bed processes.

AM technologies have the ability to use different types of materials including plastics, ceramics, metals and composite materials. This thesis will only focus on the metal AM. Parts made with metal AM can offer similar or better material properties than parts made with traditional processes while reducing the amount of used material, waste and weight of the product, development time or even the production costs [3], [6], [7]. This, combined with the ability to produce parts with unique features and innovative design, makes AM-produced parts ideally suited for high-value, low-volume production of complex parts in sectors such as the aerospace, medical/dental, tooling and motorsports industries. Metal AM is one of the sectors with immense growth rise and its expanding research and development departments are constantly offering new discoveries. Metal AM shows extraordinary results, as the market value has risen an incredible 5.5 times in the past eight years as shown in Figure 2 [8].
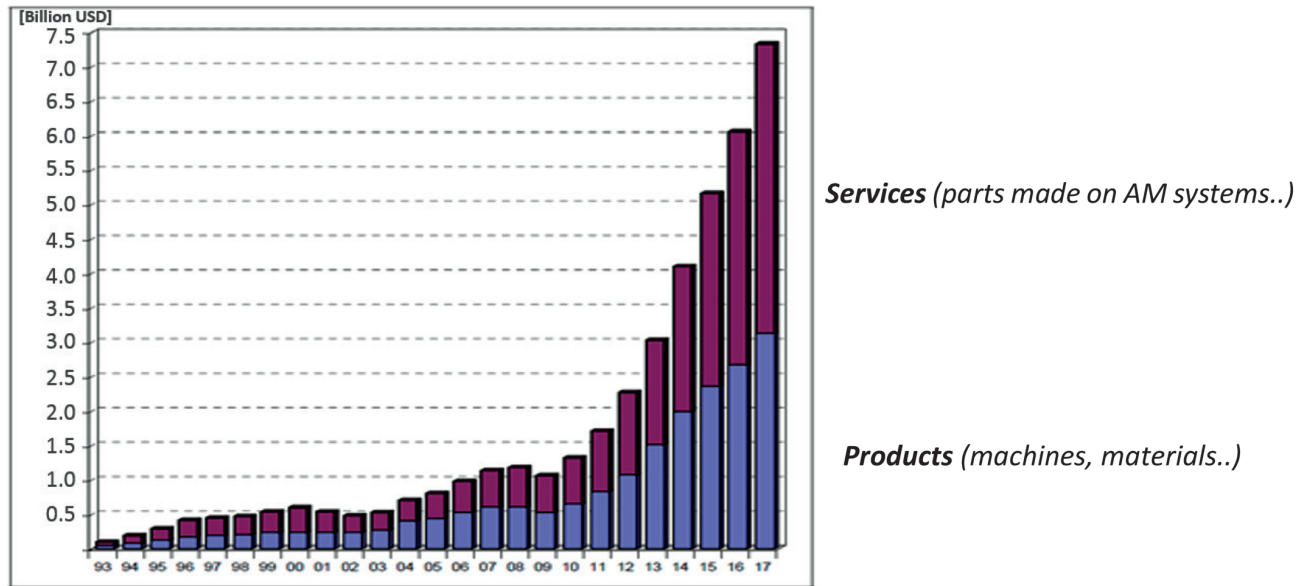
Fig. 2 Market share of AM [8].

In 2017, a surge in the number of sold metal AM machines has been observed. A total of 1,778 machines has been sold, which represents an 80% increase compared to the previous year [8]. This is an increase of 2.2 times over the last 2 years and 8.75 times over the last 5 years which is shown in Figure 3. Such extraordinary rise in the number of sold machines and the expiration of some patents in the AM field resulted in the increase in the number of companies which are producing industrial AM machines (from 97 in 2016 to 135 in 2017 [8]).

This remarkable and almost exponential growth which can be observed in Figures 2 and 3 is quite unique when compared to other industrial fields and can be attributed to the maturing of the AM technology and a clear shift from the prototyping applications to the production phase.
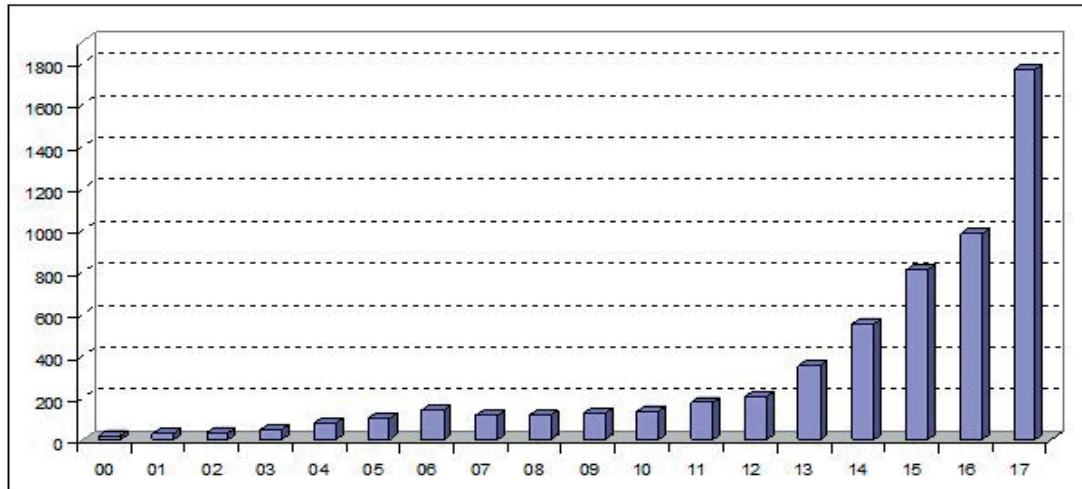
Fig. 3 Number of metal AM machines produced yearly [8].

Ascribed to its advantages, AM has a possibility of being widely applied in numerous sectors. It was observed a while ago how natural materials such as wood or bone are noticeably lightweight due to their porous cellular structure, yet they remain extraordinarily strong and able to absorb impact. Nevertheless, it was simply not feasible to imitate these natural structures using traditional subtracting manufacturing technologies. AM makes manufacturing of such lightweight parts possible, which is of great potential for aerospace and automotive industries that strive to make lightest possible aircrafts and vehicles while preserving safety in order to achieve savings in fuel consumption. With AM, manufacture of complex cross-sectional areas like the honeycomb cell [9] and lattice structures with cavities and cut-outs is enabled. This has sparked great interest among the biggest companies. Airbus revealed a cabin bracket optimized for weight saving that has no impact on functionality and stated that they intend to produce aircraft parts that weigh 30%–55% less and reduce used raw material by 90% [10]. General Electric Company (GE) has recently acquired Concept Laser and Arcam, two leading AM machine producers [11], [12]. Now part of the GE Additive, they have managed to drastically improve their production by AM (such as building a helicopter engine consisting of only 16 instead of 900 separate components, that were also 40% lighter and 60% cheaper [13]). Another important application is the production of fuel nozzles for their LEAP engines. In this case, the AM fuel nozzles are 5 times more durable, and made as a single part instead of being assembled from 20 parts when made conventionally (Figure 4). They are also 25% lighter and 30% cheaper to produce by means of AM [13]. GE Additive researches application of AM in various fields with various partners. Together with the Czech government, they agreed to build a new factory for the development and production of the world's first turboprop engine with 3D printed

4

components. On account of AM, engineers were able to consolidate 845 parts into just 11 components which will help speed up production, reduce fuel burn by up to 20%, achieve 10% more power and lower the engine's weight [14].

Fig. 4 GE fuel nozzle for the LEAP engine [15].

1.2 Selective Laser Melting

In this thesis we will explore Selective Laser Melting (SLM), which is a laser based powder bed metal AM process. It was developed by Dr. Fockele and Dr. Schwarze and the first patent was filed to the German patent office in 1996 [16]. In this process, a powder layer is deposited on a substrate with a roller or a rake and selectively melted by a laser beam piloted by the CAM system. Using a system of mirror scanners, every layer is selectively scanned and melted according to its respective cross section which is derived from the CAD model of the part (Figure 5). A new layer of powder is then placed on the work area and the process is repeated until the solid three-dimensional part in the desired shape is created. At the end the remaining loose powder is removed from the building chamber and can be reused in another building process.
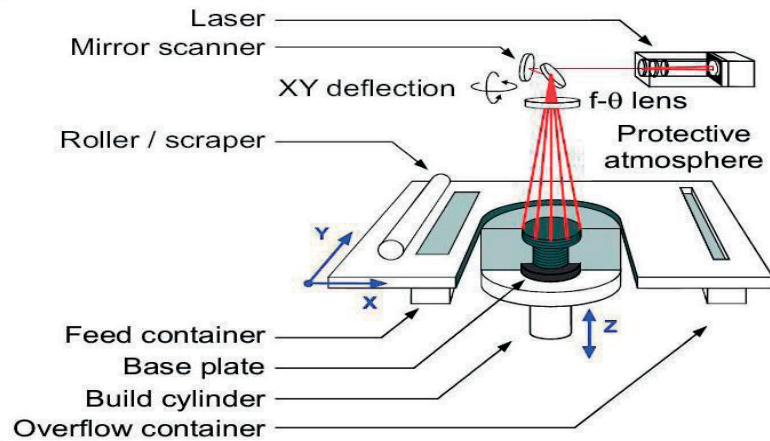
Fig. 5 The SLM process scheme [17].

SLM is an innovative technology that enables production of highly complex geometries and unique inner structures that are otherwise very challenging or impossible to manufacture. Originally used only for making prototypes or tooling parts, SLM now has a broad application in aeronautical, aerospace and medical industry as can be seen in Figure 6. Large manufacturers such as Boeing, Airbus and General Electric stated that they have opted to AM and SLM due to cost and time reductions as well as reduction in the number of required parts [18], [19] which is decreasing the need for time-consuming and complex assembly steps. Traditional manufacturing commonly uses components with simple geometries in order to facilitate production, however, such designs are often not optimized for the function of these parts. SLM allows geometrical freedom in creating complex lattice structures or bionic designs for weight reduction, and offers design of components with same functional specifications by using less materials. SLM has been tested on various materials, but research focus is based mainly on steel, titanium and nickel based alloys because of their widespread applications [20]. Representative alloys of each group (stainless steels 316L, PH1; titanium Ti6Al4V and a nickel based CM247LC) have been selected in this thesis due to their widespread applications, and used for illustrating the thesis scope.

However, the SLM production is still considerably more expensive in comparison to the conventional production methods due to the high machine costs, slow production speed and high material cost (powder production remains expensive for the moment), and this is the reason why parts made by SLM need to bring certain "added value" to be economically feasible. With the constant increase in the number of produced SLM machines, an increase in their productivity and volume of consumed materials, and because the respective patents are expiring, we are observing a fall in machine and powder prices.

6
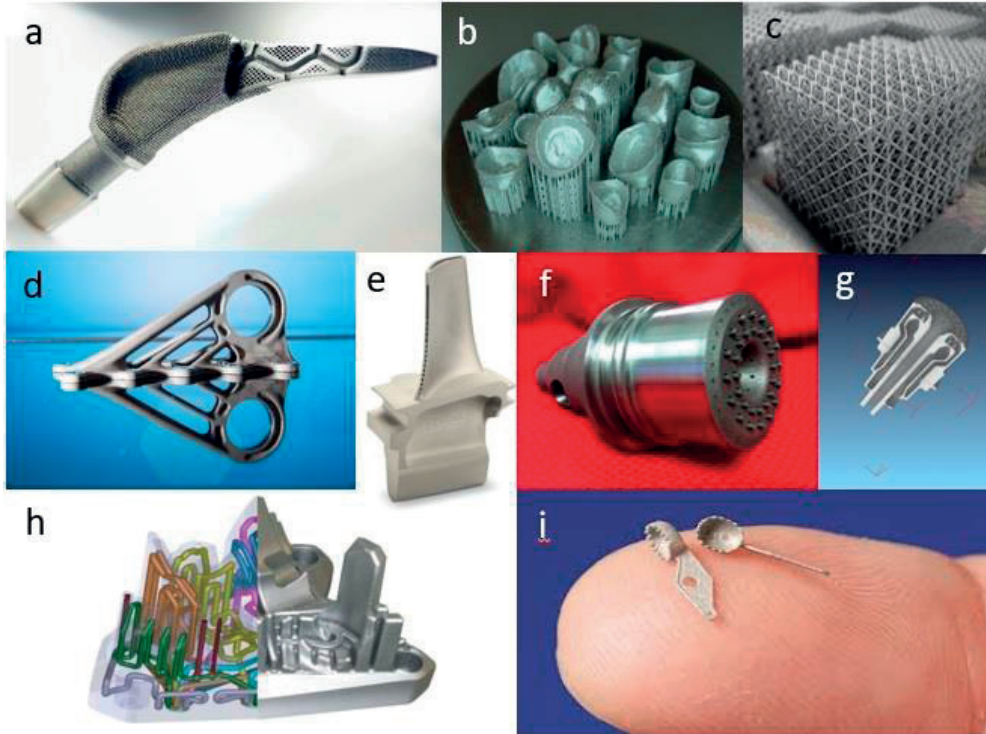
Fig. 6 SLM selected applications: a) hip implant [21]; b) dental implants [22]; c) lattice structure [23]; d) Airbus bracket [10]; e) gas turbine blade [6]; f) and g) NASA rocket engine injector and its cross-section [7]; h) conformal cooling channels [24]; i) small features [25].

1.2.1 Limitations of Selective Laser Melting

Although the parts built by SLM have mechanical properties comparable to those built by traditional processes [17], [26]–[34], some of the most significant drawbacks of SLM remain the build-up of detrimental tensile residual stresses (TRS) during the building process and the undesirable columnar microstructure. While the highly textured microstructure leads to non-optimal anisotropic mechanical properties [30], [35]–[41], TRS can have a detrimental effect on fatigue life [42], distortion of the final part [29], [37], [43]–[45], and delamination [46], [47] or cracking during the building phase [48], [49].

The quality of SLM produced parts is highly dependent on the applied processing parameters. The main parameters (Figure 7) are the laser power P (W), scanning speed V (mm/s), hatch

distance h (mm) i.e. distance between two scanning lines of the laser, and the layer thickness t (mm). Their ratio defines the applied volumetric energy density E_v [50]–[52]:

$$E_v = \frac{P}{V*h*t} \quad \left[{^J}/{_{mm^3}} \right]$$

These parameters are material dependent and non-optimal values are the prime cause of many SLM related defects. Insufficient volumetric energy density, usually a combination of a high scanning speed, low laser power and an increased layer thickness, can lead to an unstable and discontinuous melt pool and will have an effect on the density of the produced part. Typically such processing conditions will create porosities due to the lack of fusion between the melt pool and the solidified layer underneath, i.e. will create lack of fusion type porosities [53]. On the other hand, high volumetric energies due to a low scanning speed or high power, usually cause extensive material evaporation and the so called keyhole porosities [54]. Although SLM defects will not be in the focus of this thesis, this discussion illustrates that only an optimal combination of laser power, scanning speed, hatch distance and layer thickness can provide high density parts. The processing window being often quite narrow, there is a strong motivation for finding new degrees of freedom to better control other features such as the part microstructure and state of residual stresses.
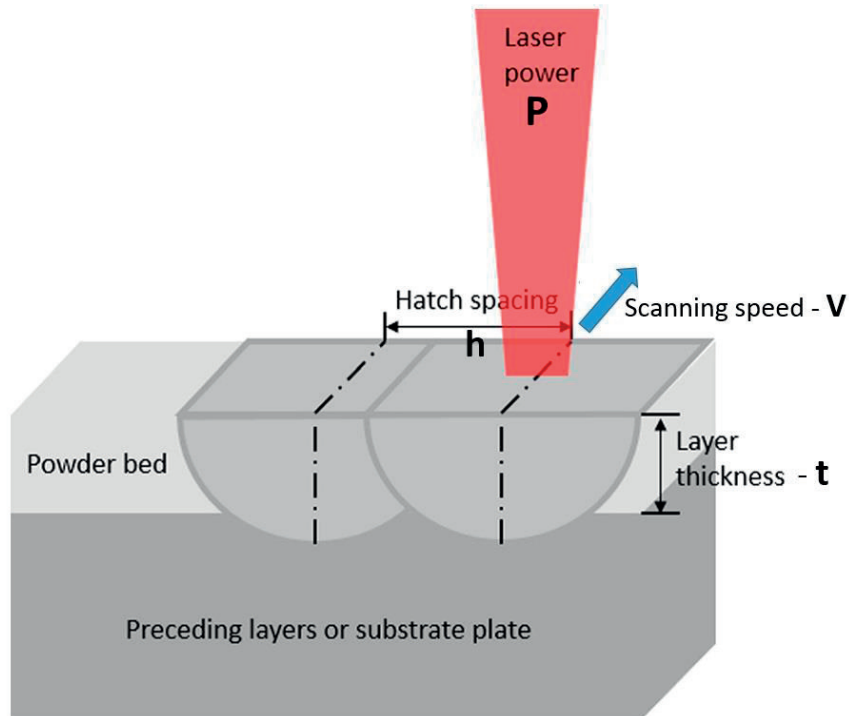
Fig. 7 Schematic of the SLM processing parameters: Laser power, scanning speed, layer thickness, hatch spacing, modified from [20].

SLM microstructure

During the SLM process, due to the low density of the powder bed (around 50%) and thus a low thermal conductivity of the surrounding powder, the heat deposited by the laser beam is mostly extracted through the substrate and the previously solidified layers of the part being built. This leads to a large thermal gradient G (K/m) and directional solidification along the vertical build direction. If the ratio between the thermal gradient G and the velocity of the solidification growth V (m/s) is high enough, an epitaxial grain growth from the substrate will occur resulting in a columnar microstructure (Figure 8) [55]. Epitaxy is a term used for the heterogeneous nucleation process in which grain nucleation takes place on the material liquid/solid boundary: in the SLM case, it is on the substrate for the initial layers [35]. Opposed to this process is the homogeneous nucleation which occurs directly in the liquid phase of the material and results in equiaxed grains with similar dimension in all three axes.

During SLM, the melt pool includes the molten powder but also a part of the previously solidified layer underneath (Figure 7). This enables good bonding between layers but also leads to the extension of grains across several layers. Consequentially, the SLM microstructure is most of the time columnar and the grain size can extend considerably through multiple layers as a result of an epitaxial growth along the build direction, as illustrated in Figure 8. The combination of a coarse elongated grain structure with a strong crystallographic texture (<100> direction parallel to the build direction, in cubic structures) leads to non-optimal anisotropic mechanical properties of the parts made by SLM, which represents one of the major limitations of the process [30], [36], [56]–[60].
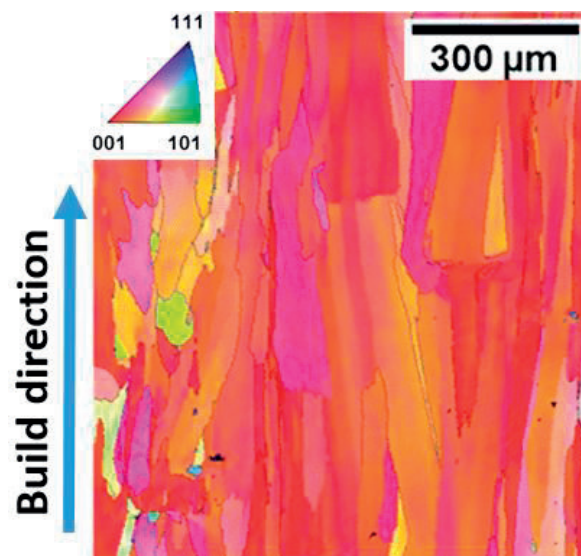
Fig. 8 Columnar grains in 316L stainless steel processed by SLM [55].

Different approaches have been used to try to control the microstructure of SLM samples. Since grain orientation and grain size are directly influenced by the heat conduction and cooling rates during the solidification phase of the building process, attempts were made to control the thermal gradients and produce more beneficial equiaxed and finer-grained microstructure. Although fine tuning SLM process parameters such as the hatching distance, scanning speed or laser power can vary the cooling rate to a certain degree, the acceptable process windows are usually quite narrow [50], [61]–[64]. For example by increasing the scanning speed we create an unstable discontinuous melt pool which leads to lack of fusion type of pores, while a decreased scanning speed and increased energy density lead to large keyhole type porosities. This results in adverse part density which strongly affects the mechanical properties of the part. Low part density used to be a long lasting major limitation of SLM and its predecessor Selective Laser Sintering which limited their use to mostly prototyping applications. The ability to achieve part densities above 99% is what enabled SLM to be used in industrial applications, and such densities are only achievable in rather narrow processing windows [50], [64], [65]. This virtually eliminates the possibility of fine tuning the part microstructure by varying important process parameters such as scanning speed, hatching distance or laser power.

Residual stresses in SLM parts

The accumulation of large TRS during the building phase of SLM is the main cause of many inherent drawbacks of the SLM process such as significant geometrical distortion of the produced part, reduction in fatigue life, cracking or even delamination during the building phase of the process (Figure 9).
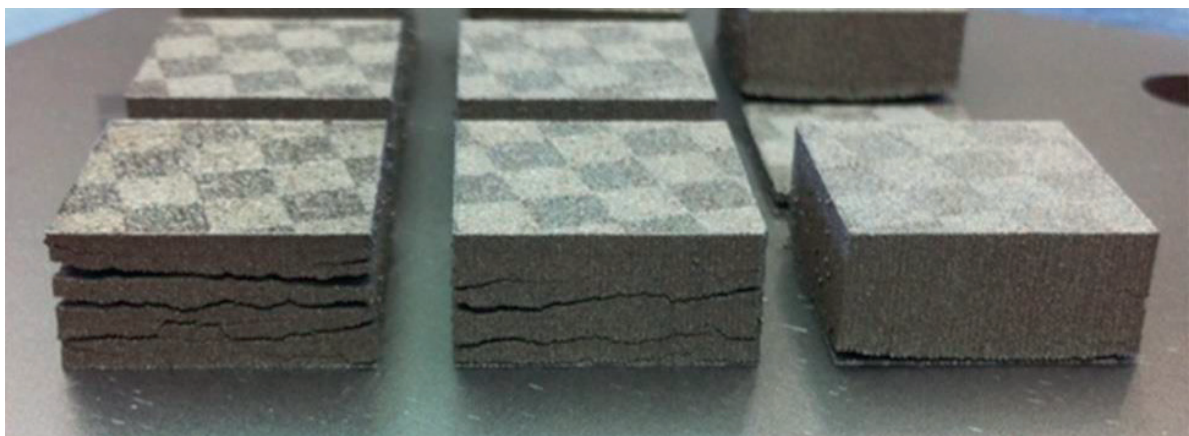
Fig. 9 Severe delamination of SLM parts [46].

In the SLM process there are two mechanisms responsible for the creation of residual stresses [46], [66]. The first one is the temperature gradient mechanism (TGM). Due to the introduced heat from the laser, previously solidified layers underneath the laser spot are rapidly heated and due to a relatively slow heat conduction by the underlying layers, as already mentioned, large thermal gradients occur. As the heated upper layers of the solid substrate expand, the underlying solidified layers that have cooled down will however prevent this expansion, which, in the end, results in the introduction of compressive residual stresses (CRS) in the upper layers (Figure 10a). As these top layers cool down they start to shrink, but since their deformation is inhibited by the underlining layers, TRS are formed in the top layers and CRS in the underlying layers (Figure 10b).
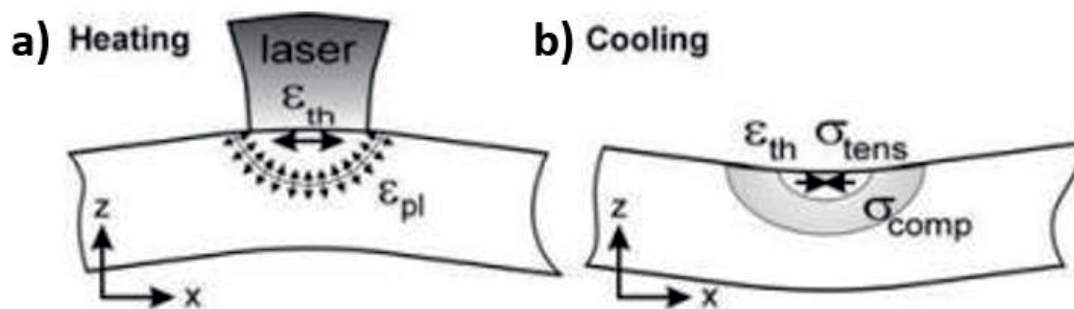
Fig. 10 Temperature gradient mechanism, a) heating phase, b) cooling phase [66].

The second and the more pronounced mechanism introducing residual stresses in SLM parts is induced by the cooling phase of the melt pool on the layer [46], [66]. As the melt pool cools down and solidifies, it shrinks due to thermal contraction. Since this motion is again constrained by the underlying solid structures, TRS are introduced in the top layers and CRS in the layers below, thus reaching a state of equilibrium (Figure 11).
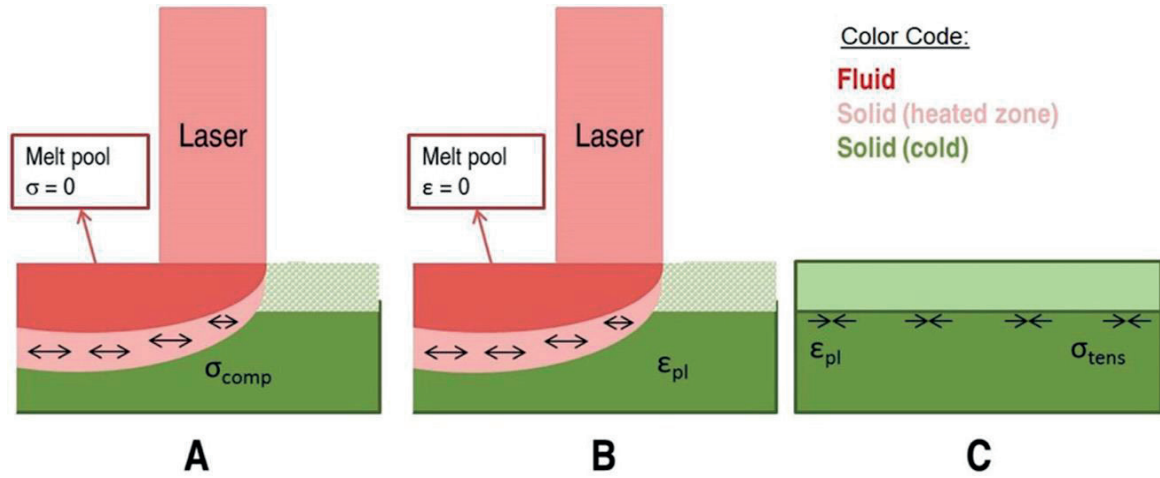
Fig. 11 Formation of tensile residual stresses due to thermal contraction of the solidifying layer [46].

The accumulated residual stresses can induce strong macroscopic deformation of the SLM part, and be so severe that they can even cause plastic deformation of the baseplate on which the part is manufactured. This is one of the reasons for which much effort has been placed into finding ways and methods that would minimize residual stresses. Different methods have been developed to control and reduce residual stresses in SLM parts. These methods include in situ preheating [44], [67]–[69], adapting scanning strategies [44], [45], or using different post treatments such as annealing. In some instances, annealing demonstrates up to 70% reduction of residual stresses [66], [69]. All these processes have shown improvement in reducing the TRS, however, they remain incapable to completely remove them, or to introduce beneficial CRS that would enhance fatigue life. In addition, post-process heat treatment cannot prevent failure occurring during the building phase of SLM (see Figure 9).

Accumulation of TRS in large SLM-produced parts causes significant geometrical distortion issues which can lead to important challenges, e.g. for overhangs (Figure 12) and thin wall structures, frequently produced by SLM.
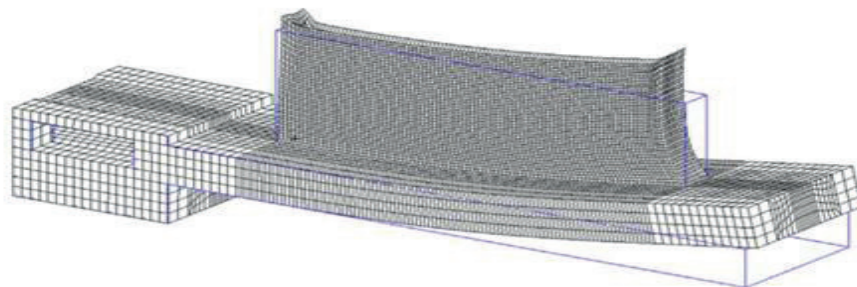
Fig. 12 Distortion of an overhang in an SLM produced part [70].

Tensile residual stresses can also be a major cause of cracking in materials such as Ni - based super alloys [38], [48], [49] (Figure 13). Several cracking mechanism have been reported in literature [71]–[74], most notably Solidification Cracking and Liquation Cracking. Solidification Cracking occurs in zones where the material is in a partially solid state (solidifying melt pool) as a result of entrapment of remaining liquid in the interdendritic regions [72]. Due to the existence of TRS introduced by the solidification of the material, the entrapped liquid zones can act as crack initiation sites. Liquation Cracking was noticed in the Heat Affected Zone (HAZ) during welding [73]. In the HAZ, phases with lower melting point are partially remelted and form a liquid film along the grain boundaries. Since the liquid film cannot withstand the TRS induced by the solidification shrinkage, cracks are formed in these regions. Although cracking mechanisms in various Ni - based superalloys is still a matter of debate, all of them require TRS state which act as a driving force for crack initiation.

Ni - based superalloys have a major importance in high temperature applications [75], [76], such as in gas and turbine jet engines, because of their excellent creep and corrosion resistance at elevated temperatures [77]. From an industrial perspective, however, any part containing excessive cracks should be rejected. Thus, controlling the TRS and removing cracks is of a high importance for promoting SLM into these fields of application.
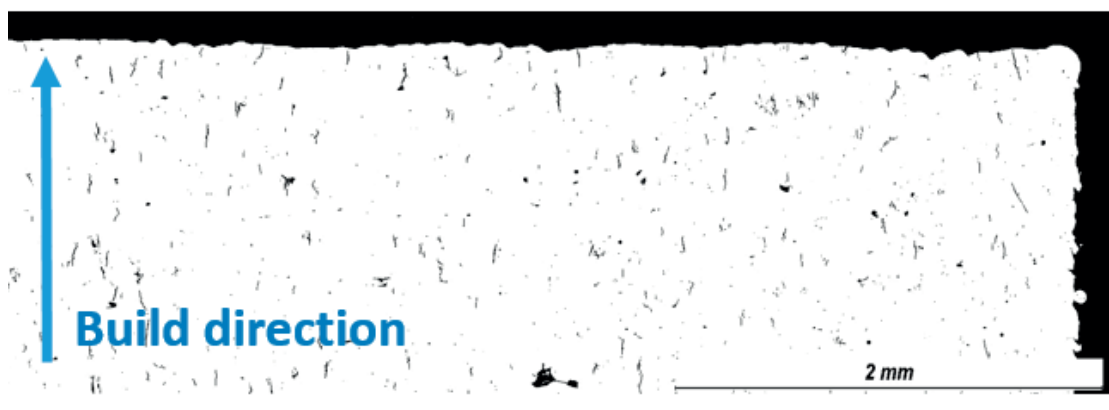
Fig. 13 Cracks in the Ni – based superalloy (CM247LC) made by SLM in the scope of this work.

Finally, TRS can have a negative effect on fatigue life of SLM parts [28]. When an external tensile load is placed on the part, TRS in the near surface will have a cumulative effect and enhance crack nucleation and propagation rates, resulting in a decrease of lifetime. Compressive stresses, on the other hand, and as shown in Figure 14, tend to prevent crack initiation, or to close them down, with a resulting beneficial effect on fatigue life. This is the main reason why having an

ability to tailor residual stresses in SLM parts, and replace TRS by compressive RS in the near surface region, is of paramount importance for promoting SLM to wider industrial applications.

1.3 Laser Shock Peening

Laser Shock Peening (LSP) is a well-known surface treatment. It is used for the purpose of introducing plastic deformation and CRS into the subsurface region of the treated material. These CRS introduced by LSP can extend several millimeters into the material and are able to counteract the external tensile stresses applied on the part and decrease the crack propagation rate, thus enhancing fatigue life (Figure 14) [78]–[80]. The beneficial influence of LSP was shown on a wide range of materials such as stainless steel [80], aluminum alloys [81]–[84], titanium alloys [79], [85], [86], nickel based alloys [87]–[89] etc.
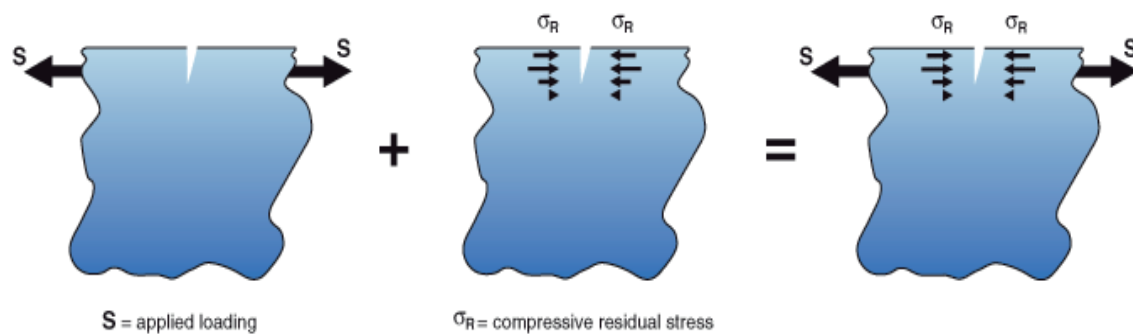
Fig. 14 Illustration of the effect of TRS and CRS on crack growth [90].

The schematic of the LSP process is shown in Figure 15. The surface is first covered with an opaque absorbent coating that is laser ablated while forming plasma on the surface. The purpose of the opaque layer is to prevent melting and ablation of the part surface [78] while still preserving a high surface quality. A transparent confining overlay (usually water or glass) is placed on top of the ablative layer. A pulsed laser with a pulse duration in the nanosecond range [78], [91] is used to vaporize the ablative layer and create a plasma which continues to absorb the laser energy for the whole duration of the laser pulse. The hydrodynamic expansion of the heated plasma in the confined region between the material surface and the confining overlay creates a high – amplitude, short duration shock wave [92]–[95]. The shock wave pressure is on the order of GPa [78], [91], [96], which can therefore be much larger than the dynamic yield strength of the material. Once the peak pressure exceeds this threshold [97]–[99], the shock wave induces plastic deformation and compressive residual stresses, thereby modifying near-surface

microstructure and mechanical properties [78]. Due to the high strain rates (typically around $10^6 s^{-1}$) [100], the LSP process can have an effect on grain size and is linked to enhanced material properties and increased hardness at the surface and in the subsurface. LSP induced residual stresses can reach a depth of several millimeters and influence fatigue life, wear and corrosion resistance.

The ablative layer prevents melting and ablation of the surface, thus making LSP a purely mechanical and cold-working process. Different materials can be used for this layer: aluminum [93], [101]–[103], copper [104], lead [105], vinyl tape [106]–[108], zinc [103] or black paint [94], [109], [110]. It has been shown that black paint has the best absorption ability to standard LSP lasers (532nm and 1064nm wavelength) [106]. If the ablative layer is not used, the laser pulse will ablate and remelt a shallow layer of the material surface and this configuration is known as Laser Shock Peening without Coating (LSPwC) [111]–[113]. A transparent overlay (confining medium) is used to prevent the plasma from expanding away from the surface and to increase the peak pressure by up to two orders of magnitude [28,29]. There are a few different media used as a transparent layer, such as glass [106], [116], [117] or quartz [105], [106], [118], [119], but the most widely used medium is water [93], [94], [107], [110], [120], as it is cheap and easy to implement.
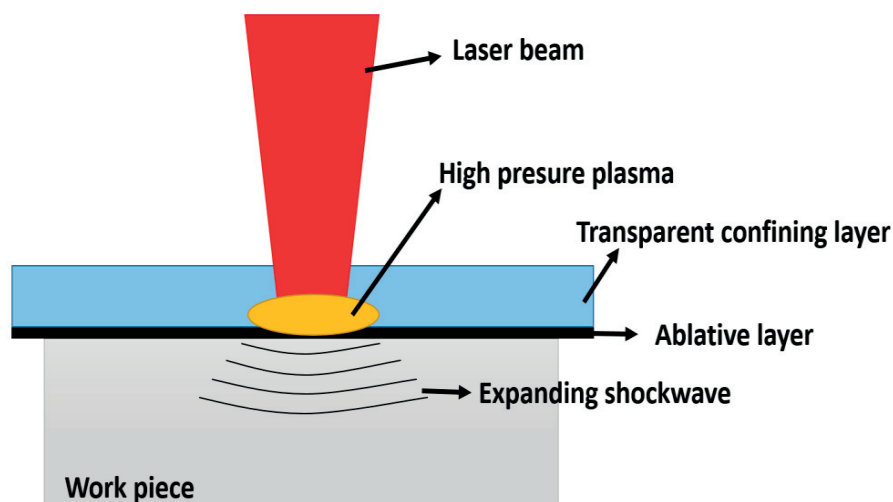
Fig. 15 Schematic of the LSP process, modified from [91].

In practical applications, LSP has been able to demonstrate superior results and therefore to replace the conventional Shot Peening (SP) process. LSP achieves about 4-5 times deeper CRS

than SP [110], [121]–[124] and consequently leads to higher fatigue strength [125]–[127], which is the main beneficial effect of LSP. In addition, the LSP process leads to increased wear resistance [128], and better surface finish compared to SP [91], [129]. Due to the induced CRS, LSP can also be used to mitigate stress corrosion cracking [111], [130], [131] which represents a growth of a surface crack resulting from aggressive environment and TRS. Both LSP and SP increase the surface roughness [91], [97], [100], but contrary to SP, the surface can be polished after LSP without significantly removing the beneficial CRS [91], which in the end leads to a lower surface roughness [109], [110], [132]. LSP can also produce an increase in metal surface hardness of the treated area [113], [133], [134], the magnitude of which depends on LSP conditions such as power density [135], [136], number of impacts per unit area [93], [137], peak pressure [112], [138], as well as the alloy type and microstructure.

LSP is a complex process with a variety of parameters such as laser energy, laser pulse duration and frequency, number of overlapping shot repetitions, beam shape and size, material of the ablative and confining medium, etc. All these have an impact on the process results. By enhancing material performance, LSP enables more efficient component designs which, similarly to SLM, can promote the decrease of the part weight, extend its lifetime and improve its performance.

LSP application

LSP was developed in the 1970s at the Battelle Columbus Laboratories in the USA [139]–[141] while many of the theoretical foundations of the process have been placed in France [92], [114], [142]. Over time LSP was further developed for commercial applications [143]. This is also demonstrated by the quantity of patents, as the first two major patents were issued in 1974 [144] and 1983 [145] respectively, and only in a five-year period (1996-2001) General Electric Company alone has received twenty-three US patents based on LSP [109]. LSP is in fact applied in many areas similar to those of SLM. LSP is especially used for many products in the aerospace industry, both commercial and military. These parts include turbine blades and rotor components (Figure 16a) [146], [147], gear shafts [148], landing components (Figure 16b) [149], and bearing components [150]. For example, General Electric Aircraft Engines applied LSP on the leading edges of turbine fan blades which resulted in improving the durability of the fan blades as well as the resistance to foreign object damage [147]. LSP is now being commonly used also for treatment of gas and steam turbine blades [151]. Toshiba has been using a low energy - high overlap rate underwater LSPwC approach for the treatment of nuclear reactors (Figure 16e) [152]. LSP also enables service providers such as Metal Improvement Company to treat components both off- and on-site (Figure 16c) [152], and components can be successfully laser

16

peened regardless of their size. In addition, LSP is now also being applied in the biomedical field to help controlling corrosion rate of medical implants (Figure 16d) [153], [154].
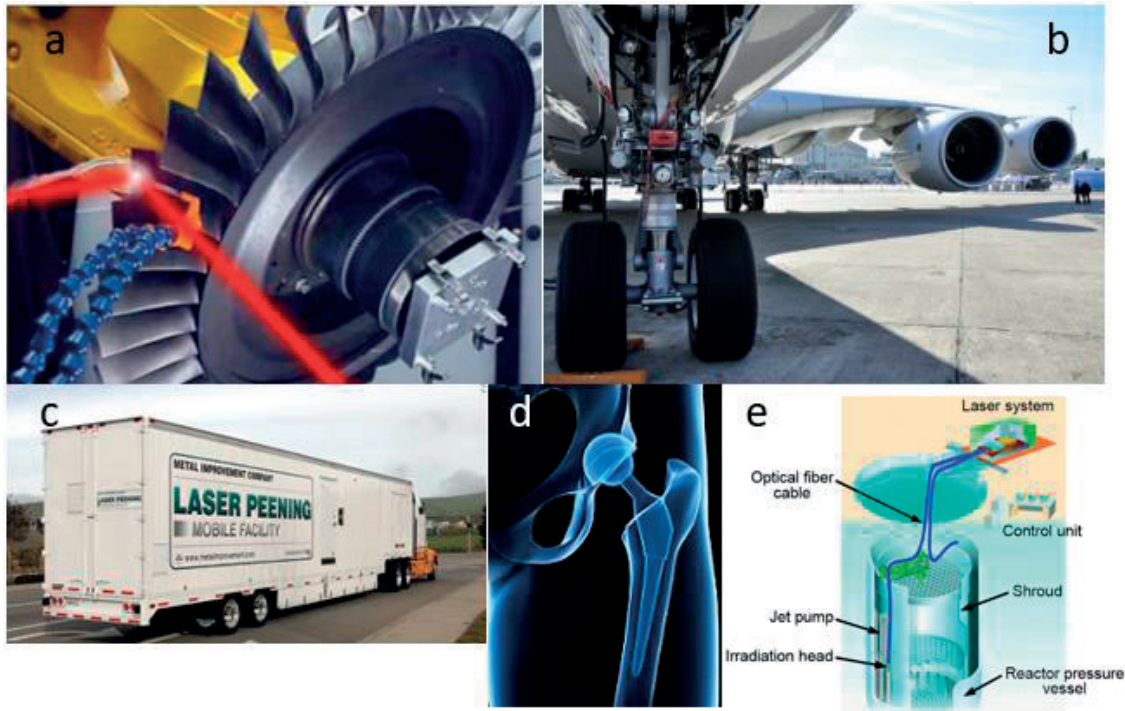
Fig. 16 LSP applications: a) turbine blade [155]; b) landing gear [149]; c) on-site LSP [156]; d) hip implant [157]; e) nuclear reactor [152].

Chapter 2 State of the art

In this chapter we will be looking at different approaches that are being investigated and sometimes applied to address some of the inherent drawbacks of the SLM process such as the beforehand mentioned inadequate microstructure, accumulation of TRS and its effect on geometrical distortions, cracking and decreased fatigue life. We will show a brief overview of these approaches and try to state the improvements that they bring, but will also explain the limitations of each of them in order to gain an overview of the current trends in addressing these SLM drawbacks. We will also try to compare them to the goals that have been set in this thesis.

2.1 Laser remelting

This process uses a laser to remelt previously fused material upon every built layer, or after several layers have been produced. The power density of the laser is usually low either by decreasing the laser power or increasing the spot size and scanning speed, such that the laser will only remelt the previously deposited layer and not vaporize the material. Remelting effects will vary in respect to the material itself, as well as to other parameters such as the laser power, scanning speed and strategy. Laser remelting of SLM parts has been investigated and it has demonstrated a decrease in part porosity, improved surface roughness of the top layer (Figure 17), finer microstructure, and increased microhardness [158]–[160], but it was able to achieve only a partial TRS relaxation in the top layer (e.g. about 55% in [69]).
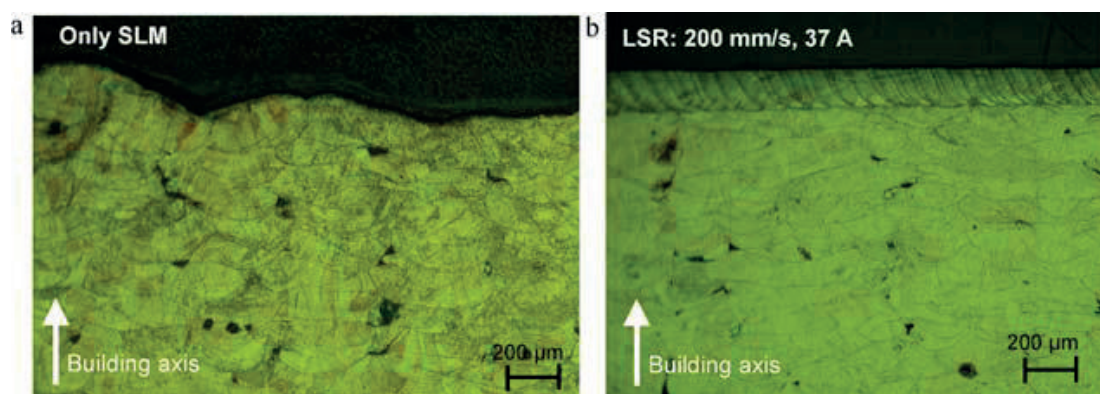
Fig. 17 Decrease in surface roughness of 316L stainless steel: a) as-built SLM condition; b) sample with remelting of the top layer [160].

Drawbacks of the process mainly refer (i) to the longer manufacturing time since the laser beam should make an increased number of scans, and (ii) to the inability to fully reduce the TRS. The process is also unable to introduce beneficial CRS in the part.

2.2 Preheating

Preheating is an in situ method that is often applied to reduce the accumulation of residual stresses during the building process. It is thought that high cooling rates lead to high TRS [69], and that reducing thermal gradients reduces cooling rates and helps mitigating the stresses. In order to do so, material preheating is applied which increases the powder bed temperature. The standard process that is widely available on most of the commercially available or lab machines is the baseplate preheating shown in Figure 18. It uses a heat source placed underneath the baseplate to heat up the baseplate and keep it at a predefined constant temperature. However, as the part becomes larger as it is being produced, the baseplate heating is less and less effective in maintaining a constant temperature of the top layer of the part.
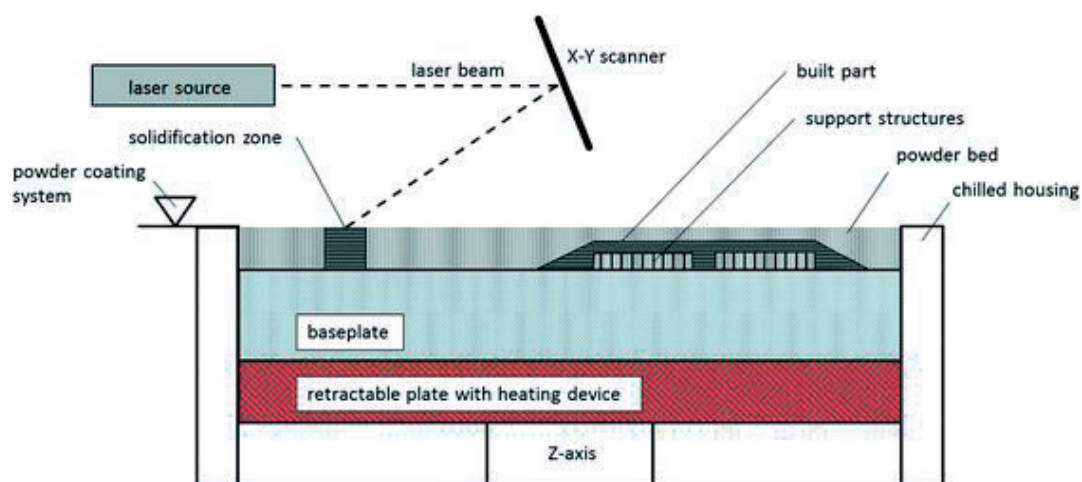
Fig. 18 Baseplate preheating in an SLM process [161].

Another preheating method consists in using another high power laser and focusing it on the part top surface (Figure 19). Such an approach can achieve significantly higher temperatures, e.g. up to 2500°C with ceramics [162], or 1200°C with alloys prone to cracking such as Ni-based superalloys [163], [164].
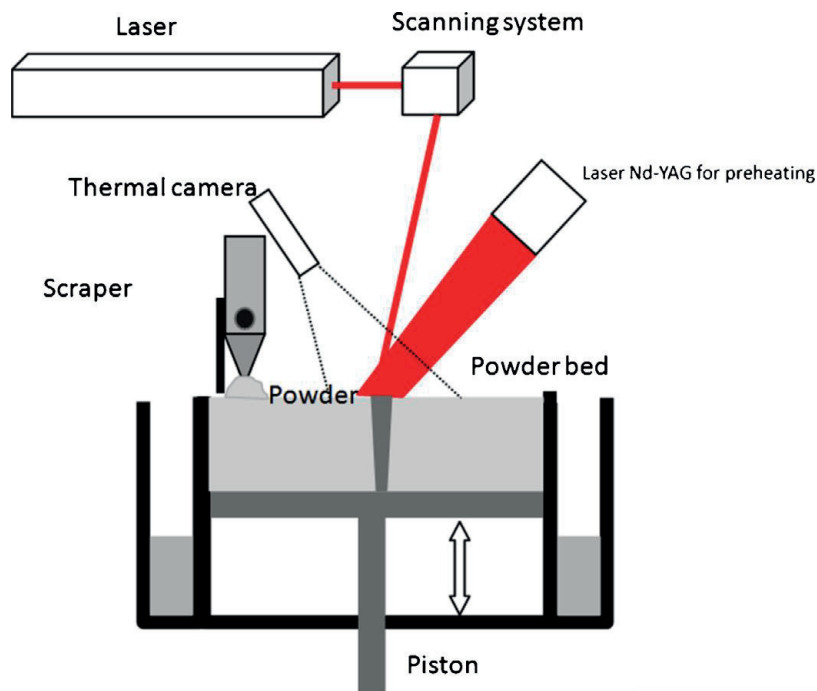
Fig. 19 High temperature preheating of the top surface with an additional laser [162].

Experiments on a chrome molybdenum steel (JIS SCM440) showed a clear inverse relationship between bed temperature and TRS [69]. For example, preheating the baseplate to 160°C resulted in a decrease of the TRS in the top layer by 40% [69]. Although baseplate preheating has shown success in reducing TRS at higher temperatures, the temperature is usually applied up to 200°C. Indeed, higher chamber temperatures have a beneficial effect on the TRS but have a negative impact on mechanical properties such as yield strength and fatigue limit [165], [166].

2.3 Heat treatment

A stress-relieving heat treatment is a post treatment which involves heating the SLM part in a furnace, and keeping it at the desired temperature for a certain period of time (Figure 20). As an example, TRS can be reduced up to 70% in steel heated at 600°C for one hour [69]. The main drawback of the stress relieving heat treatment is that besides adding one more step in the processing sequence, it can only be performed after the part has been manufactured. Therefore,

it cannot help reducing TRS during the SLM building phase, while these can sometimes cause part delamination/cracking and process failure.
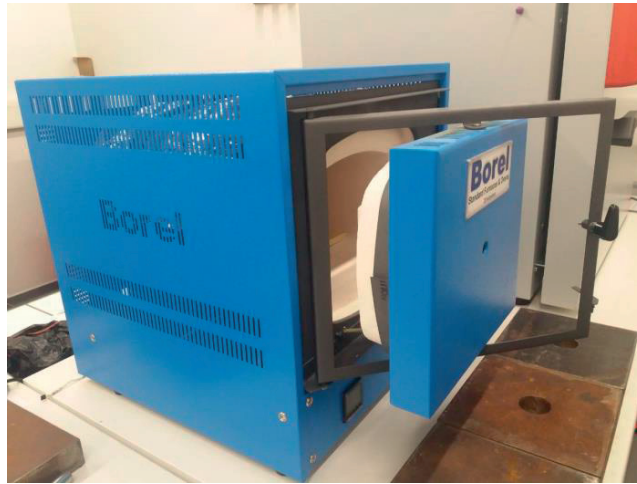
Fig. 20 Heat treatment furnace from Borel SA at LMTM, EPFL.

2.4 Hot Isostatic Pressing (HIP)

Hot Isostatic Pressing (HIP) is a well-known thermomechanical post treatment that applies a high pressure inert gas at elevated temperatures on a part with the primary goal of closing down internal porosities in the bulk, and thus increasing the part density (Figure 21). Usually the applied pressure does not exceed 200 MPa, while the temperature can reach up to 2000°C [167], [168]. It has been widely used for cast parts in applications where the density is of crucial importance, e.g. in aerospace and medical fields [167], [168]. It is also widely applied on SLM parts with the goal of increasing the density [169], [170]. Based on the HIP parameters such as the defined temperature, pressure, duration of the process and similarly to the effects of the heat treatment post process, some of the residual stresses can be relieved.
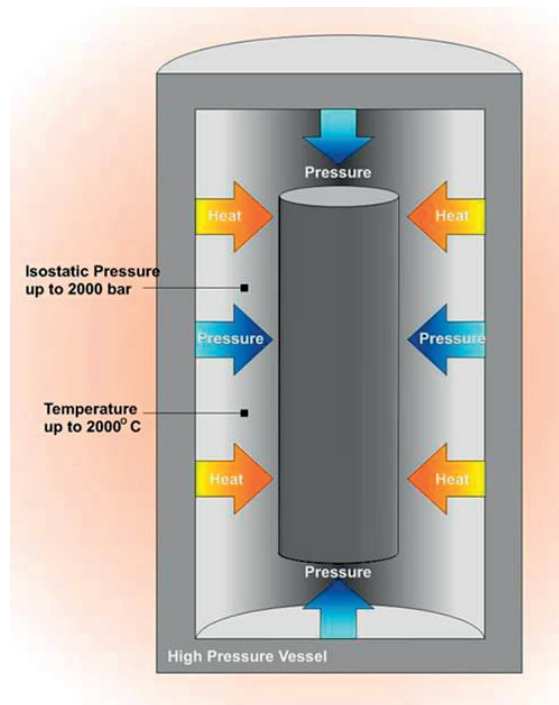
Fig. 21 Schematic of the HIP process [171].

As with the heat treatment, HIP is a post process and thus cannot address problems that occur during the building phase of SLM, such as cracking and delamination. Another disadvantage relates to the temperature level and holding time needed for the porosity closure which promotes substantial grain growth in most metallic alloys, with detrimental effects on properties such as the yield strength [170], [172], [173]. This undesired microstructure evolution may remove some or all of the beneficial effects of the increased density. It should be mentioned that with the constant development of the SLM process and the accompanying increase in the obtained densities, there is less and less a strict requirement for HIP treatments intended to close down porosities.

Furthermore, the equipment needed to achieve and sustain high pressures at elevated temperatures is complex and expensive. There is therefore a strong motivation to find cheaper and less time consuming methods to address the drawbacks of the SLM process.

2.5 Hybrid Selective Laser Melting processes

The concept of hybrid SLM process consists of an in situ application of a conventional manufacturing process such as milling [174], or a surface post treatment such as sliding Severe Plastic Deformation (SPD) [175], Shot Peening [175], or Laser Shock Peening [176] *during* the building phase of Selective Laser Melting, with the goal of improving some of the properties of the produced part.

2.5.1 Selective Laser Melting and machining

Hybrid Selective Laser Melting processes coupled with in situ machining are additive – subtractive processes in which after a certain number of SLM layers, a machining (milling) step is applied (Figure 22). Hybrid SLM and machining is most widely explored hybrid SLM process and such machines produced by the Japanese company Matsuura are already available [174].
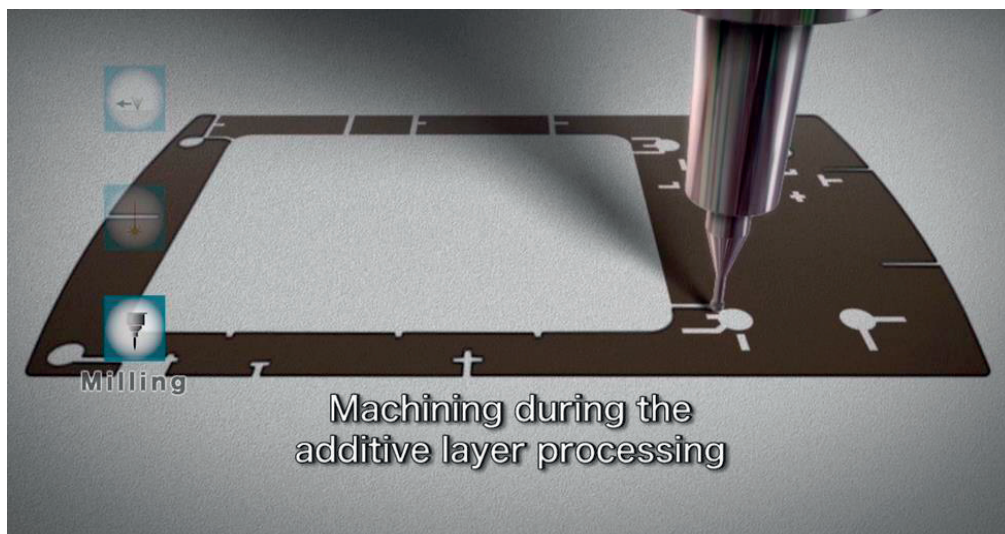
Fig. 22 Machining step during Selective Laser Melting [174].

By sequentially applying a milling step during SLM, parts with improved surface finish and geometrical accuracy can be produced. This is especially important for parts with complex geometries such as conformal cooling channels, since they are usually difficult to polish in a post processing step. Although this approach can improve the geometrical accuracy of the produced

part, it is not able to address other drawbacks such as delamination and cracking, or decreased fatigue life due to TRS or inappropriate microstructure.

2.5.2 Selective Laser Melting and Sliding Severe Plastic Deformation

Severe Plastic Deformation (SPD) surface post treatments are used to increase the strength of metals by grain refinement due to very large plastic deformation [175], [177], [178]. Sliding SPD is one such treatment that was investigated as a potentially suitable candidate for developing an in situ hybrid SLM process [175]. Similarly to conventional milling, sliding SPD uses a tool and a multi axis motion to treat the surface of the part. Unlike milling, the lead angle of the tool is negative and hence it does not cut the material, but instead causes surface deformation, as shown in Figure 23. As the tool moves through the surface of the part, a prow is created in front of the tool and the material is plastically deformed, thereby introducing CRS in the near surface region.
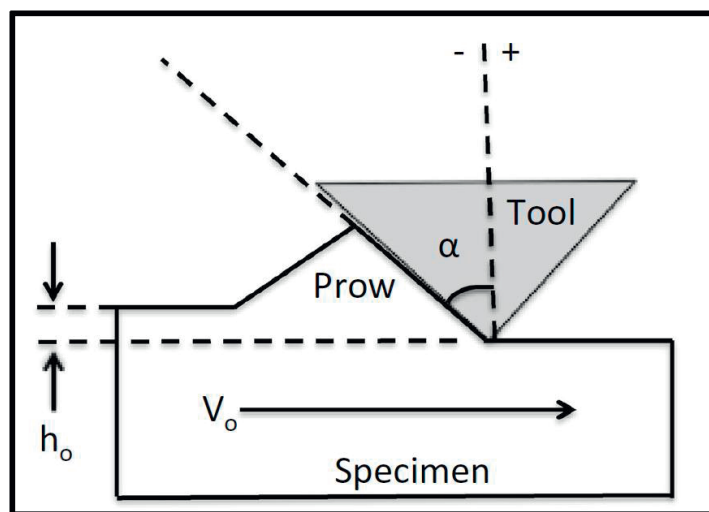
Fig. 23 Schematic of the sliding SPD process [175].

Book and Sangid have performed Sliding SPD on AlSi10Mg [175] and have shown beneficial effects when the process is repeatedly applied during the building stage of SLM. An increase in microhardness of 20-25%, up to 300 microns from the surface, which gradually decreases back to the baseline values around the depth of 1mm, accompanied with grain refinement, were reported.

One of the disadvantages of the process is related to the high roughness of the as-built condition: surface peaks fold into adjacent valleys, which leads to the initiation of cracks. The authors suggest however that such surface cracks might be re-solidified and closed during subsequent remelting. Another disadvantage of the process is the low productivity, since the applied tool velocity is reported only around $5\frac{mm}{s}$. Studies were done on AlSi10Mg, and the higher hardness of steel, titanium or nickel based alloys, widely processed by SLM, might cause wear problems for the tool. An additional drawback of this process is the difficulty to apply it selectively over a portion of an SLM layer, since around the treated zone a prow would be created which might collide with the powder coater and pose a problem during subsequent layer deposition. Another concern is that due to the horizontal (lateral) component of the applied force on the surface of the part, the process might deform thin walls of an SLM cross section, thus making it unsuitable for fine features and complex SLM geometries.

2.5.3 Selective Laser Melting and Shot Peening

Shot Peening (SP) is a cold work surface treatment process, in which a stream of high velocity beads is directed on a surface of a part (Figure 24). Upon contact, the kinetic energy of the shot particle is transferred to the surface of the part creating plastic deformation in the near-surface zone, thereby inducing compressive residual stresses and thus improving the fatigue life of the part [179].

Fig. 24 Shot Peening of turbine blades with high velocity beads [180].

Although SP is widely used as a post treatment of SLM parts [181]–[183] to improve surface roughness and increase fatigue life, there are technical limitations for its application within an in situ process. The most obvious one is the contamination of the powder bed by the shot peening media, usually 0.6 to 1mm in diameter [175], [184], exceeding by far the size of SLM powder particles, or the SLM layer thickness. Book and Sangid have, in their study on AlSi10Mg [175], proposed the use of Fine Particle Shot Peening (FPSP) in which the shot particles would be the SLM powder itself. But due to the smaller size of the shot peening medium and thus a significantly decreased kinetic energy, the corresponding effects on microhardness and microstructure were negligible. As suggested by the authors, a potential solution would consist in increasing peening time. One can actually doubt that improved processing parameters would lead to a sufficiently deep affected zone such that the introduced beneficial changes are not thermally cancelled out by the subsequent SLM rebuilding steps.

2.5.4 3D LSP – SLM and Laser Shock Peening

3D Laser Shock Peening (3D LSP) is a novel hybrid approach in Additive Manufacturing (AM) patented [185] during the course of this PhD work by the Laboratory of Thermomechanical Metallurgy (LMTM) at the Ecole Polytechnique Fédérale de Lausanne (EPFL). The novelty of this approach is the introduction of Laser Shock Peening (LSP) during the building phase of Selective Laser Melting (SLM), in order to better control the microstructure, selectively increase hardness, tailor residual stresses and consequently reduce distortions, decrease crack density and increase fatigue life of SLM parts (Figure 25). The approach may reduce and potentially eliminate the need for post processing, while improving mechanical properties of the finished part anywhere in the bulk of the material. 3D LSP is able to convert the near-surface detrimental TRS inherent to the SLM process into more beneficial CRS [186], over a larger depth [176] compared to conventional 2D (surface) LSP. The improvement comes from the periodic use of LSP throughout the volume of the part, while it is being built by SLM, instead of just as a surface treatment of a finished part. Performing LSP treatment periodically does provide an accumulated beneficial effect [176]. This means that all well-known improvements of the conventional LSP process are no longer limited just to a shallow depth below the surface layer: with 3D LSP, the treatment can be introduced selectively throughout the bulk of the material. Mechanical properties of the produced part are also tailored and selectively improved, with the possibility of addressing the critical sections that are otherwise difficult to reach with conventional methods (internal voids, lattice structures, etc.).
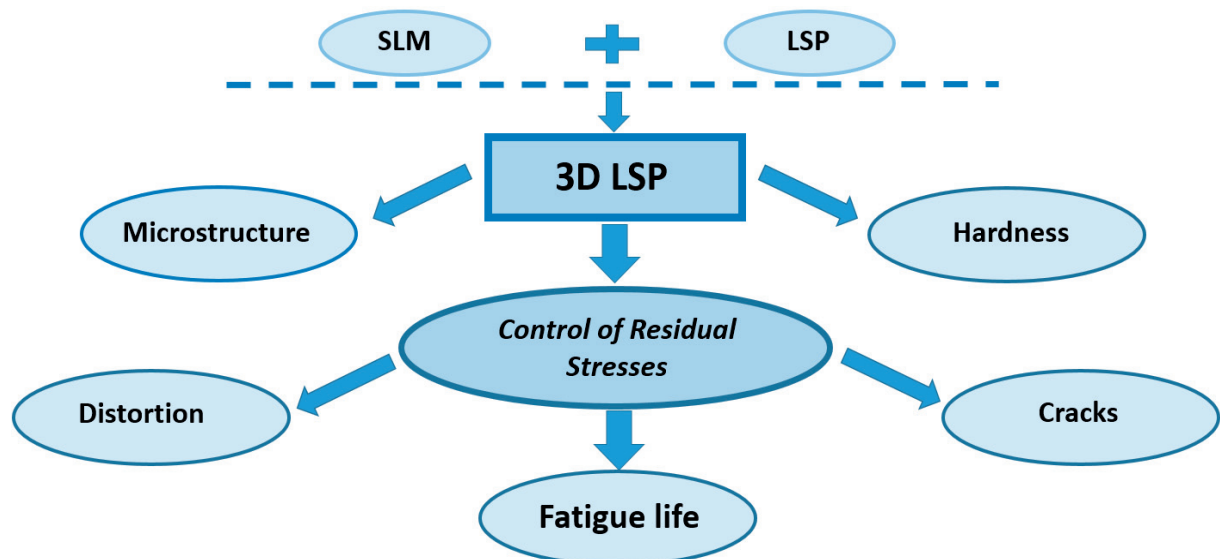
Fig. 25 Schematic of the 3D LSP process and the scope of its beneficial effects.

In order to successfully apply LSP during the SLM building step, water as a confining medium has to be avoided due to the powder bed used in the SLM process. As a substitute, an automated device with a solid state confinement shown in Figure 26 has been devised. The automated device can, depending on the application, be comprised out of a multilayered system that includes both a confining and an ablative layer.

Fig. 26 Illustration of the 3D LSP system.

A schematic of the main components of the 3D LSP process is shown in Figure 27 [185]. The SLM process is done in a repetitive manner, with an SLM laser in a continuous mode (1), directed with a scanning head (2) onto a surface of freshly deposited powder. After a layer is selectively scanned, the building platform (3) is lowered by the thickness of the SLM layer and the hopper (4) deposits fresh powder (5). After a certain number of SLM layers, the mentioned multilayered device comprised out of a confining layer (8) and an ablative layer (9) is activated and covers the surface of the previously built SLM layer. Then, as in conventional LSP, a nanosecond laser in a pulsed mode (10) is applied, creating a high pressure shock wave at the surface of a previously solidified SLM layer and introducing plastic deformation and compressive residual stresses in the part. The number of SLM layers after which the LSP is applied is dependent on the material and on the desired volume and depth of CRS meant to be introduced to the material. After the LSP

treatment, the device is moved and the SLM building process is continued. During this period, a new ablative layer (12) is introduced to the bottom side of the confining layer (8) so that it is ready for its next application. The old ablative layer is removed (as a consumable) and winded on an exchangeable reel system (11). The operation sequence is repeated until completion of the part (6), after which the unused powder (7) is removed and recycled. As in a conventional SLM process, optional preheating can be applied (15, 16).
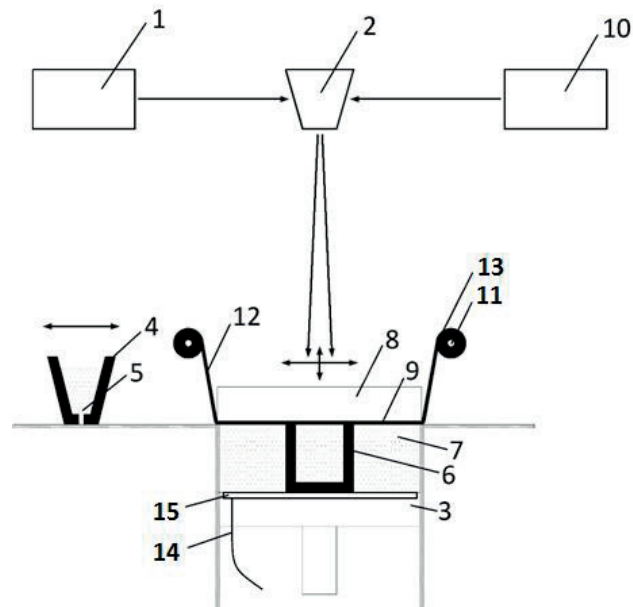
Fig. 27 Schematic illustration of the LSP process: 1. SLM laser, 2. Scanning head, 3. Building platform, 4. Hopper, 5. Fresh powder, 6. Part during the building phase, 7. Unused powder, 8. Confining layer, 9. Ablative layer, 10. Pulsed laser, 11. Exchangeable reel system 12. Reel with the unused ablative layer, 13.Excess ablative layer on a reel, 14. Preheating cord, 15. Preheating plate [185].

2.6 Comparison between different approaches

The disadvantages of the SLM process have been identified a long time ago, and numerous techniques and mechanisms have been developed or combined in an attempt to reduce or even completely remove them. In this chapter we have tried to briefly introduce some of the proposed literature solutions, analyzing some of their most evident advantages and disadvantages. A comparative summary is given in Table 1.

It can be observed that, while majority of these approaches have managed to reduce TRS to a certain extent, with associated improvements in geometrical accuracy, some of them have however created unwanted counter-effects such as increased grain size and undesired microstructure. More importantly, most of these methods are incapable of selectively introducing a beneficial (compressive) stress state, which limits any improvement in fatigue life or tendency for delamination or cracking during the SLM building phase.

Method/ Improvements	In situ		Post treatment		Hybrid SLM			
	Preheating	Laser remelting	Heat treatment	HIP	SLM + Machining	SLM + Sliding SPD	SLM + Shot Peening	3D LSP SLM + LSP
Reduction of TRS	+	+	+	+	\	++	+	++
Introduction of CRS	\	\	\	\	\	++	\	++
Geometrical accuracy	+	+	+	+	++	++	+	++
Fatigue life	\	\	\	−/++	\	+	\	++
Crack density/ delamination during SLM	+	\	\	\	\	+	\	++
Microhardness	\	+	+	+	\	++	\	+
Microstructural Improvement	\	+	\	−	\	++	\	+
Compatibility for in situ application	++	++	--	--	++	−	+	++

++ Very good
+ Good
\ No effect
− Bad
-- Very bad

Table 1 Comparison between different approaches designed for improving the quality of SLM parts.

Chapter 3 Scope of the Thesis

The purpose of this chapter is to define the thesis statement and the main objectives that were addressed. In addition, we will give an outline of the thesis and explain its structure.

In the first two chapters we have given an insight in the field of Additive Manufacturing and more precisely Selective Laser Melting. We have addressed the major advantages they are bringing to the manufacturing community in the light of their rapid market share growth, but have also described the inherent drawbacks which are currently limiting their widespread applications. We have shown different literature approaches addressing these drawbacks, and analyzed the main advantages and disadvantages of each process. We have further described 3D Laser Shock Peening (3D LSP) as the process on which this thesis will concentrate. The announced potential advantages of 3D LSP, summarized in Table 1 and compared to the other literature methods, will be substantiated in the coming chapters. The main topics addressed in this thesis can be summarized as:

3D Laser Shock Peening leads to:

- **Selective conversion of detrimental (tensile) to beneficial (compressive) residual stresses in the bulk of an SLM part**
- **A selective increase in stored energy allowing for 3D microstructure design by playing on the local hardness and possible recrystallization by post heat treatment**
- **An increase in geometrical accuracy of SLM parts**
- **A substantial increase in SLM parts fatigue life**
- **A significant reduction in crack density in alloys prone to SLM cracking (e.g. Ni – based superalloys)**

Thesis outline and objectives

The objective of this thesis is to experimentally show and quantify improvements of the SLM process by the 3D LSP approach in five different areas which are described in the above thesis

statement. The results reported in this work are meant to attract further interest both from academia and industry such as to intensify activities in this field.

The thesis is constructed in a cumulative manner and its core is comprised out of a collection of six distinct paper manuscripts which have been published, submitted, or are about to be submitted to international peer-reviewed journals. All 6 papers focus on different aspects of the 3D LSP process which have never been investigated so far, and are tracing paths in different fields described in the thesis statement. They all connect to experimental results accumulated during the course of the four years of this PhD work.

The manuscript is divided in 10 chapters, laid down as follows:

Chapter 1 – Introduction. This chapter gives a brief introduction to the Additive Manufacturing field, and more precisely Selective Laser Melting with its main applications, advantages and inherent disadvantages. Finally the basics of the of conventional surface Laser Shock Peening treatment are provided.

Chapter 2 – State of the art. Major drawbacks of the SLM process and the state of the art in different approaches to improve them are explained. Advantages and disadvantages of each method are detailed, and a comparisons to the 3D LSP process are given.

Chapter 3 – Scope of the thesis with the thesis statement, objectives and structure outline.

Chapter 4 – Tailoring residual stress profile of Selective Laser Melted parts by Laser Shock Peening. In this chapter we have addressed the ability of conventional LSP treatments to convert tensile residual stresses into more beneficial compressive residual stresses, in parts made by SLM. This represents an initial feasibility study for which the results were not easily anticipated due to the total absence of literature in that area, and the rough surface state of SLM parts in the as-built surface condition which was expected to cause trouble.

Chapter 5 – 3D Laser Shock Peening – a new method for the 3D control of residual stresses in Selective Laser Melting. This chapter has addressed the way the 3D LSP process develops a residual stress field. The main issue was to evaluate whether the introduced CRS would be thermally relaxed by the subsequent rebuilding steps of the SLM process, or instead if they would accumulate and improve (in magnitude / penetration depth) compared to those encountered in conventional surface LSP post treatments.

Chapter 6 – Laser shock peening: a promising tool for tailoring metallic microstructures in selective laser melting. Here we address the ability of LSP to selectively increase the stored energy in an SLM part. The effect is demonstrated from the resulting changes in recrystallization kinetics during a post heat treatment. The paper therefore demonstrates the possibility to tailor

the microstructure in 3D, alternating between recrystallized equiaxed grains in areas of interest (LSP treated), and the as–built columnar microstructure (non treated zones).

Chapter 7 – 3D Laser Shock Peening as a way to improve geometrical accuracy in Selective Laser Melting. In this manuscript we describe the ability of 3D LSP to decrease geometrical distortions in parts caused by SLM induced TRS. The 3D LSP process is shown to be able to compensate for the tensile stresses by selectively introducing counteracting CRS.

Chapter 8 – Hybrid Additive Manufacturing of ultra-durable metal parts. Chapter 8 represents one of the most important outputs of the whole 3D LSP process. In this chapter we have shown that by accumulating CRS in the subsurface region of an SLM part, we are able to increase fatigue life in bending by more than 57 times compared to conventionally made material, and by more than 15 times compared to SLM samples in the rough as – built surface state.

Chapter 9 – Reducing crack density in Selective Laser Melting by 3D Laser Shock Peening. This chapter describes the ability of the 3D LSP process to decrease the crack density in a Ni – based superalloy by a staggering 95%. With further optimization of 3D LSP parameters the ability to process crack free parts out of such alloys seems to be at a grasp. Currently such alloys are not sold on the market due to the excessive amount of (crack) defects.

Chapter 10 – Conclusions and future perspectives. We summarize the various benefits of the 3D LSP process which were investigated during the thesis. We also describe potential paths for further research in this field.

Chapter 4

Tailoring residual stress profile of Selective Laser Melted parts by Laser Shock Peening

Nikola Kalentics[1,*], Eric Boillat[1], Patrice Peyre[2], Snežana Ćirić-Kostić[3], Nebojša Bogojević[3], Roland E. Logé[1]

1. Thermomechanical Metallurgy Laboratory – PX Group Chair, Ecole Polytechnique Fédérale de Lausanne (EPFL), CH-2002 Neuchâtel, Switzerland

2. Processes and Engineering in Mechanics and Materials Laboratory (PIMM), CNRS-ENSAM Paristech,151 Bd de l'Hôpital, 75013 Paris, France

3. Faculty of Mechanical and Civil Engineering in Kraljevo, University of Kragujevac, Serbia

Contribution:

Nikola Kalentics designed the experiment, assisted in the Laser Shock Peening treatments, did the residual stress measurements, interpretation of results and wrote the manuscript.

Abstract

The paper describes a new approach in controlling and tailoring residual stress profile of parts made by Selective Laser Melting (SLM). SLM parts are well known for the high tensile stresses in the as – built state in the surface or subsurface region. These stresses have a detrimental effect on the mechanical properties and especially on the fatigue life. Laser Shock Peening (LSP) as a surface treatment method was applied on SLM parts and residual stress measurements with the hole - drilling method were performed. Two different grades of stainless steel were used: a martensitic 15-5 precipitation hardenable PH1 and an austenitic 316L. Different LSP parameters were used, varying laser energy, shot overlap, laser spot size and treatments with and without an ablative medium. For both materials the as-built (AB) residual stress state was changed to a more beneficial compressive state. The value and the depth of the compressive stress was analyzed and showed a clear dependence on the LSP processing parameters. Application of LSP on SLM parts showed promising results, and a novel method that would combine these two processes is proposed. The use of LSP during the building phase of SLM as a "3D LSP" method would possibly give the advantage of further increasing the depth and volume of compressive residual stresses, and selectively treating key areas of the part, thereby further increasing fatigue life.

1. Introduction

Selective laser melting (SLM) is a part of a large family of Additive Manufacturing (AM) processes. Over the last decades more than thirty different types of Additive Manufacturing processes have been developed [1], [2], with SLM being one of the most researched over the past years.

However, although the mechanical properties have become close to those of bulk materials [3]–[14], SLM has some inherent drawbacks such as warping, cracking and detrimental tensile residual stresses (TRS). A large degree of shrinkage occurs during liquid - solid transformation, thus accumulating considerable tensile residual stresses on the surface of the SLM produced components. The complex residual stresses (RS) that arise during cooling are regarded as key factors responsible for the distortion and even delamination of the final parts [9], [10], [15]–[17]. These residual stresses may even cause process failure during the building phase [18].

The last melted layer shrinks during cooling while the layer underneath, already solidified constrains it and prevents further shrinking [15], [16]. Since this mechanism occurs for each layer at each step of the SLM process, large tensile residual stresses accumulate inside the

38

manufactured component which cause significant and detrimental anisotropy of the mechanical properties of produced parts [5], [17], [19]–[21], thus limiting their application.

Different methods have arisen to reduce residual stresses. In situ heating (e.g. build plate heating; reheating of the melt pool) is commonly used [15], [22]. Adapting scanning strategies can also have a strong impact on residual stresses [15], [23]. As a post treatment, annealing is widely used and has demonstrated in some cases a 70 percent reduction of residual stresses [24]. Although these methods have demonstrated certain improvements of the final residual stress state, they have shown to be unable to completely remove tensile residual stresses. In the case of annealing, as a post treatment it is limited to addressing this issue only after the building process is done, and as such it cannot address the issue of stress accumulation that can cause process failure.

In the present paper, a novel strategy is proposed for tailoring residual stresses in parts manufactured by SLM by using another laser treatment – Laser Shock Peening. The goal of this approach is to fully transform the residual stress state from a detrimental tensile to a beneficial compressive residual stress (CRS) in the near surface region. Additional benefit of the proposed approach is that it might be introduced as an in situ treatment during the SLM process.

Laser Shock Peening (LSP) is a high strain rate (on the order of $10^6 s^{-1}$) [25], surface treatment process, that is similarly to Shot Peening (SP) and Ultrasonic Shot Peening (USP) used to introduce compressive residual stresses and plastic deformation into the surface of the material. The compressive stress can reach a depth of several millimeters and may counteract some or all of the tensile stress, decrease the crack propagation rate, effectively reduce the stress intensity factors, enhance the fatigue crack closure effect and increase the critical stress of crack propagation, thus improving the fatigue performance of metal materials (Figure 1) [26]–[29]. This positive effect of LSP was shown on many different materials such as aluminum alloys [25], [26], [30], [31], titanium alloys [28], [32], [33], nickel based alloys [34]–[36], stainless steel [29] etc.
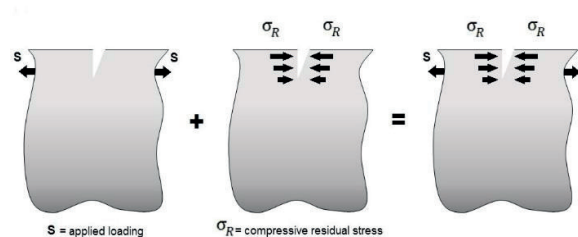
Fig. 1 Effect of tensile and compressive stresses on the crack growth propagation.

It has been shown that the residual stresses can be directly related to the fatigue life of samples [25], [27]–[29], [31]–[33], [37], [38] with a clear beneficial effect of compressive stresses in the near surface region. It was also observed that the depth of the compressive residual stresses has

a direct influence on the fatigue life. The larger the depth, the longer CRS will interact with the surface crack, resulting in a slower crack propagation and a longer fatigue life. Compared to other similar processes such as Shot Peening (SP) or Ultrasonic Shot Peening (USP), LSP treatment introduces CRS to a larger depth, thus leading to an increase in fatigue life of LSP samples compared to SP and USP samples [27], [32], [39], [30], [40]–[42]. The proposed strategy of combining SLM with LSP has a goal of further increasing the depth and amount of CRS in the near surface region.

2. Experimental setup

2.1 Material

Materials used in this paper are two grades of stainless steel, PH1 and 316L. PH1 with a standard denomination 15-5 PH, is a martensitic precipitation hardenable stainless steel made by the SLM machine producer EOS (EOS GmbH, Germany). PH1 has an ultimate tensile strength (UTS) of 1150 MPa [43] and provides excellent mechanical properties, especially in the precipitation hardened state. It is widely used in medical, aerospace and other engineering applications requiring high hardness and strength. PH1 samples were produced on an EOSINT M280 additive manufacturing machine, with a closed set of parameters and a fixed scanning strategy provided by the machine producer for this powder.

316L is a widely used austenitic stainless steel and has an UTS of 760 MPa [44]. The powder that was used was DIAMALLOY 1003 obtained from Sulzer Metco, Switzerland. These samples were produced on a Concept laser M2 (Concept Laser GmbH, Germany) machine equipped with a fiber laser operated in continuous mode at a wavelength of 1070 nm and a spot size of 90 microns. The parameters laser power, scanning speed, hatch distance and powder layer thickness were 125 W, 600 mm/s, 0.105 mm and 0.03 mm, respectively. A bi-directional scanning strategy that was parallel to the part edges was used in every layer without a change in scanning direction between layers. This was done to deliberately create large tensile residual stresses and to show the ability of the LSP process to address even such stresses and to convert them to CRS.

The chemical composition of both PH1 and 316L stainless steel is shown in Table 1.

	Cr	Ni	Cu	Mn	Si	Mo	Nb	C	Fe
PH1	14 – 15.5	3.5- 5.5	2.5 -4.5	max 1	max 1	max 0.5	0.15 - 0.45	max. 0.07	Balance
316L	17	12	/	/	2.3	2.5	/	0.03	Balance

Table 1 Chemical composition of PH1 and 316L stainless steel, wt.% [43].

2.2 Laser Shock Peening

Laser shock peening (LSP) experiments were made at the PIMM laboratory at CNRS-ENSAM Paristech [45]. The laser source used is a 7.1 ns at 532 nm Nd:YAG GAIA - class laser from Thales Laser company. The beam spatial energy distribution is "top-hat" and the pulse shape is near - Gaussian. LSP processing parameters are shown in Table 2. Round laser spots of 1, 2 and 5 mm diameter were used with the laser energy of 0.4, 1.6 and 10J respectively. This ratio of the spot size and the energy kept the power density constant at 7.2 GW/cm^2. The pressure at the surface of the treated part was estimated at 4.7GPa using an empirical equation $P\,(GPa) = 1.75\,\sqrt{I_0}(\frac{GW}{cm^2})$ [46]. Pulse frequency was 1Hz, and the overlap of 40% was used for all spot sizes with and without a protective ablative coating. Also one sample with an overlap of 80% was treated with a 1mm spot size without an ablative coating. In order to avoid ablation of the surface of the samples, in some cases an ablative layer was used. For this purpose a sacrificial aluminum tape of 70μm thickness from 3M™ was placed on top of the sample. In other cases, the ablative layer was not applied, and the results in these two conditions were compared.

Spot size (mm)	E (J)	I_0 (GW/cm²)	P (GPa)	Frequency (Hz)
1	0.4	7.2	4.7	1
2	1.6	7.2	4.7	1
5	10	7.2	4.7	1

Table 2 LSP processing parameters: spot size; E - laser energy; I_0- power density; P - estimated pressure at the surface; frequency.

2.3 Residual stress determination using the hole drilling method

Residual stresses have been measured with the hole drilling method (HDM) according to the ASTM standard E837 [16], [47]. It is a widely used technique for the determination of in depth residual stress profiles in parts especially after surface treatments such as LSP, USP, SP [47]–[52]. The measuring device is the RESTAN-MTS 3000 from SINT Technology (Figure 2a). A 1,8mm diameter hole is drilled into the piece to be analyzed. Residual stresses relax at the hole location causing strains also to change. A strain gauge rosette with three grids measures these strains (Figure 2b). Residual stresses are given by the theory of Kirsch [53], adjusted with experimental coefficients for blind hole analysis. Residual stresses were measured at a total of 36 points from the surface up to 1mm in depth. Since the goal was to achieve more precise results of residual stresses in the near surface region, a variable depth increment was applied. In the region from the surface up to the depth of 100µm, measurements were made every 10µm. From 0.1mm up to 0.5mm in depth, measurements were made every 25µm, and from 0.5mm up to 1mm every 50µm.

Fig. 2 a) Hole drilling device RESTAN-MTS 3000 from SINT Technology; b) sample with attached strain gauge rosette for HDM.

3. Results and discussion

3.1 PH1 stainless steel

Figure 3 shows some of the most important parameters of a residual stress curve. These are the maximum amount of CRS - *Max CRS*, depth at which maximum CRS are observed – *Depth of max CRS*, depth at which change from CRS to TRS – *Depth of CRS*, and the value of CRS in the near surface region, at the depth of 20µm – *Surface RS*.
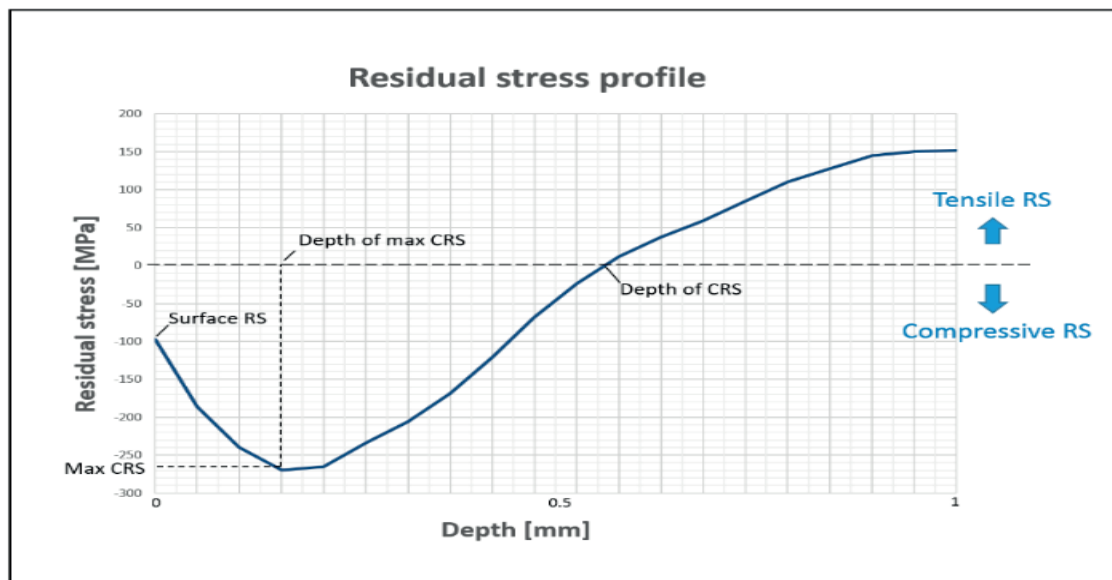
Fig. 3 Residual stress curve with the most important parameters indicated: *Max CRS* – maximum amount of CRS; *Depth of max CRS* - depth at which maximum CRS are observed; *Depth of CRS* - depth at which residual stresses change from CRS to TRS; *Surface RS* - value of CRS in the near surface region, at the depth of 20µm.

Residual stress measurements of the PH1 samples made by SLM in the as – built (AB) state show a low amount of compressive residual stresses (CRS) in the near surface region up to the depth of 183µm (Figure 4). Compressive residual stress in this near surface region of SLM samples is a rare observation. However, it was also observed that welded joints of martensitic stainless steels have such compressive residual stress state in the near surface zone [54]–[56]. The reason for their occurrence is that martensitic stainless steels experience a phase transformation during the

cooling period. During this phase change, the crystal lattice expands and the accumulated stresses due to the shrinkage are relaxed and inversed to a small negative value (i.e. to a compressive residual stress value) [44].

The maximum amount of the observed CRS is -230 MPa at the depth of 94µm which represents a 20% of its UTS of the material which is 1150 MPa. The value of the surface RS is -41 MPa (4% of the UTS). Beyond 183µm, the residual stress state changes towards tensile state. Above the depth of 183µm where the stresses are neutral, we can observe a sudden increase in TRS up to the depth of around 340µm where the TRS have a value of 435 MPa (38% of the UTS). Beyond this point we can see a slower increase in the amount of tensile stresses throughout the whole depth of the measurement.

Other samples made by SLM were treated with Laser shock peening. Table 3 gives an overview of results of residual stress measurements done on samples in the as-built and LSP treated state and a graphical representation is given in Figure 4.

LSP treatment	Max CRS [MPa] / percentage of the UTS [%]	Depth of max CRS [µm]	Depth of CRS [µm]	Surface RS [MPa] / percentage of the UTS [%]
1mm 40% NC	-421 / 37	142	406	-117 / 10
1mm 40% C	-530 / 46	115	403	-187 / 16
2mm 40% NC	-401 / 35	136	495	-103 / 9
2mm 40% C	-494 / 43	120	647	-165 / 14
5mm 40% NC	-325 / 28	139	620	-69 / 6
5mm 40% C	-412 / 36	113	788	-163 / 14
1mm 80% NC	-798 / 69	247	> 1mm (-266 MPa at 1mm)	-169 / 15
AB state	-230 / 20	94	184	-42 / 4

Table 3 Results of RS measurements: Max CRS / normalized by UTS; depth of max CRS; depth of CRS; Surface RS / normalized by UTS. Measurements are made in the as- built state (AB), or with LSP treatments of 1, 2 and 5mm, 40 and 80% overlap, and with and without an ablative coating (C / NC).
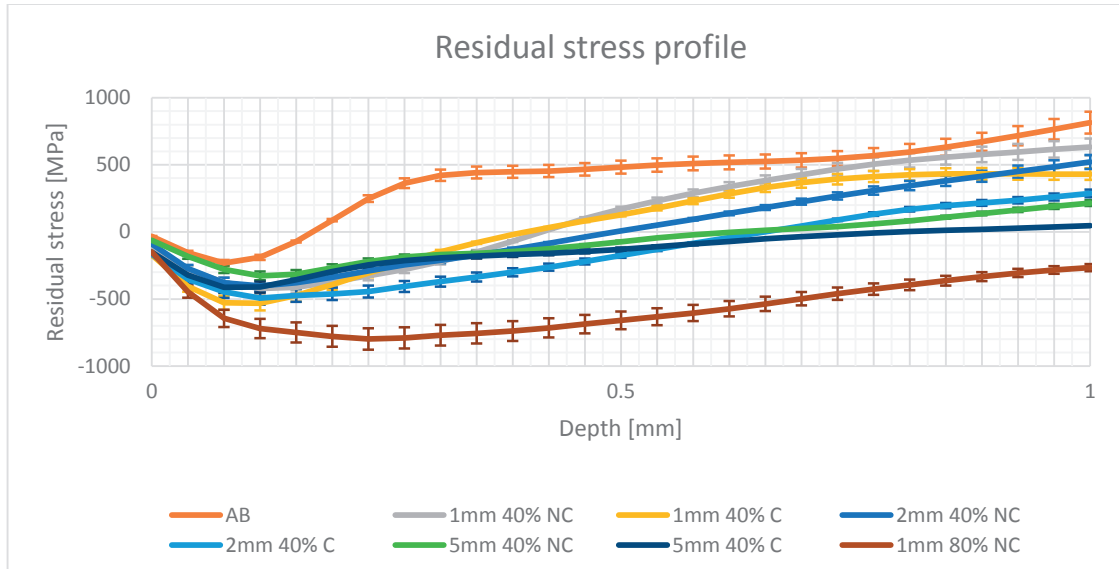
Fig. 4 Residual stress curves measured for samples in the as–built and different LSP treated states.

3.1.1 Maximum value of CRS

3.1.1.1 LSP treatment without an ablative coating

For an LSP treatment without an ablative coating (Figure 5), maximum CRS are -421 MPa for 1mm spot size (37% of the UTS), -401 MPa (35%) for 2mm and -325 MPa (28%) for 5mm, and they are observed at similar depths (136-142µm). These values make a significant improvement of 17%, 15% and 8% of the UTS respectively, compared to the as – built state which has CRS of -230 MPa (20%) at a depth of 94µm. It can be observed that smaller spot size leads to larger maximum values of residual stresses. This effect was observed in literature [57] and it is presumed that since LSP with smaller spots is more often applied for a same surface area compared to LSP with larger spots, the effect is more pronounced. It is somehow equivalent to a higher number of shots, which is discussed in section 3.1.4.
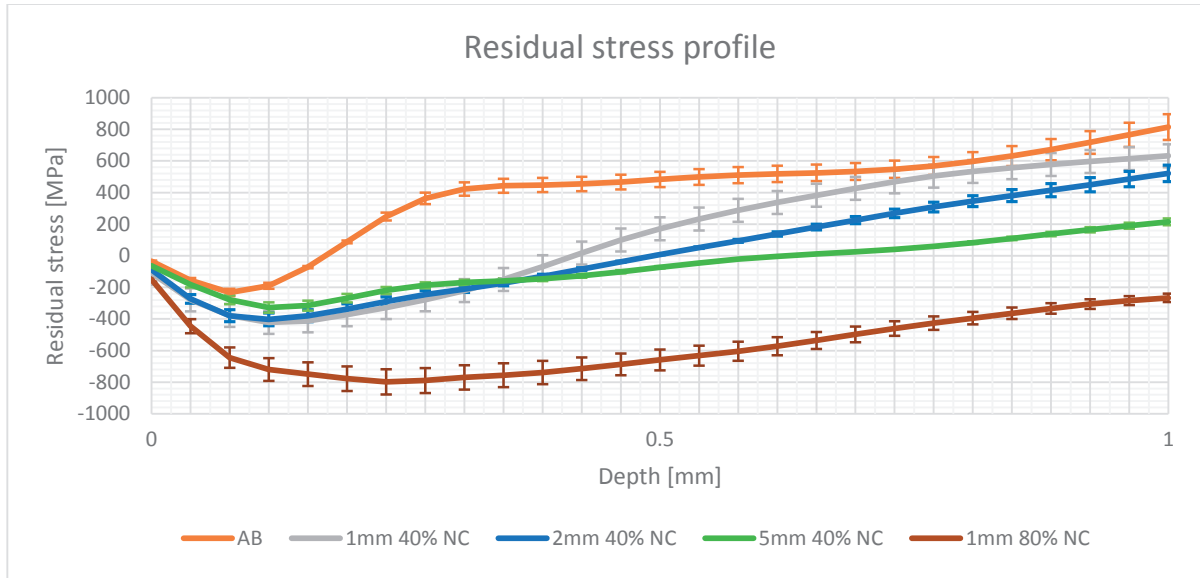
Fig. 5 Residual stress curves measured for samples in the AB and LSP treated states without an ablative coating.

3.1.1.2 LSP treatment with an ablative coating

Similar trends are observed in treatments with an ablative coating: -530 MPa for 1mm (46% of the UTS), -494 MPa (43 %) for 2mm and -412 MPa (36%) for 5mm. In this case, this maximum values are higher compared to the treatment without the ablative coating and they are observed closer to the surface (113-120µm). These values represent an even larger improvement compared to the as – built state of 26%, 23% and 16% of the UTS respectively which is shown in Table 4. Also an increase in CRS for LSP treatments with an ablative coating compared to those without an ablative coating can be observed. This is explained by the protective role of the ablative coating, since the plasma is created on its surface and not on the surface of the SLM sample. This prevents ablation and local melting of the sample surface and creation of TRS due to this melting. When the ablative coating is not applied, these TRS are decreasing the overall effect of the LSP process in both the max value of CRS and their depth.

46

LSP treatment	Max CRS compared to the AB state, and normalized by UTS; [%] of UTS	Surface RS compared to the AB state, and normalized by UTS; [%] of UTS
1mm 40% NC	17	6
1mm 40% C	26	12
2mm 40% NC	15	5
2mm 40% C	23	11
5mm 40% NC	8	2
5mm 40% C	16	10
1mm 80% NC	49	11

Table 4 Percentage of increase of maximum and surface CRS compared to the as built state and normalized by UTS.

3.1.2 Depth of CRS

3.1.2.1 LSP treatment without an ablative coating

If we look at the values of the depth of CRS, it can be observed that larger spot sizes lead to larger depths of CRS. For an LSP treatment without an ablative coating (Figure 5), compressive residual stresses are observed up to depths of 406μm, 495μm and 620μm for laser spots of 1mm, 2mm and 5mm respectively. This represents an increase compared to the as – built state of 121%, 169% and 278%. It can be observed that a smaller spot size leads to a smaller affected depth. This is due to the 2D attenuation of shock waves which occurs for smaller spot sizes, and that leads to decreased affected depth of the LSP treatment [27], [42], [58].

3.1.2.2 LSP treatment with an ablative coating

For samples treated with LSP treatment with an ablative coating (Figure 6), compressive residual stresses are observed up to the depth of 403μm, 647μm and 788μm for laser spots of 1mm, 2mm and 5mm respectively. This represents an increase compared to the as – built state of 119%, 252% and 329%. Similarly to the LSP treatment without an ablative coating, smaller spot size leads to smaller affected depths due to the 2D attenuation of shock waves [27], [42], [58]. Here, it can also be observed that the ablative coating due to its protective role, prevents local melting

on the sample surface and thus enhances the overall effect of the LSP process. This has also an effect of further increasing the depth of compressive stresses. In the case of a 2mm spot size an increase from 495µm to 647µm was observed and for the 5mm spot size an increase from 620µm up to 788µm. Compared to the AB state, this is an improvement from 169% to 252% for 2mm, and 278% to 329% for a 5mm spot size.
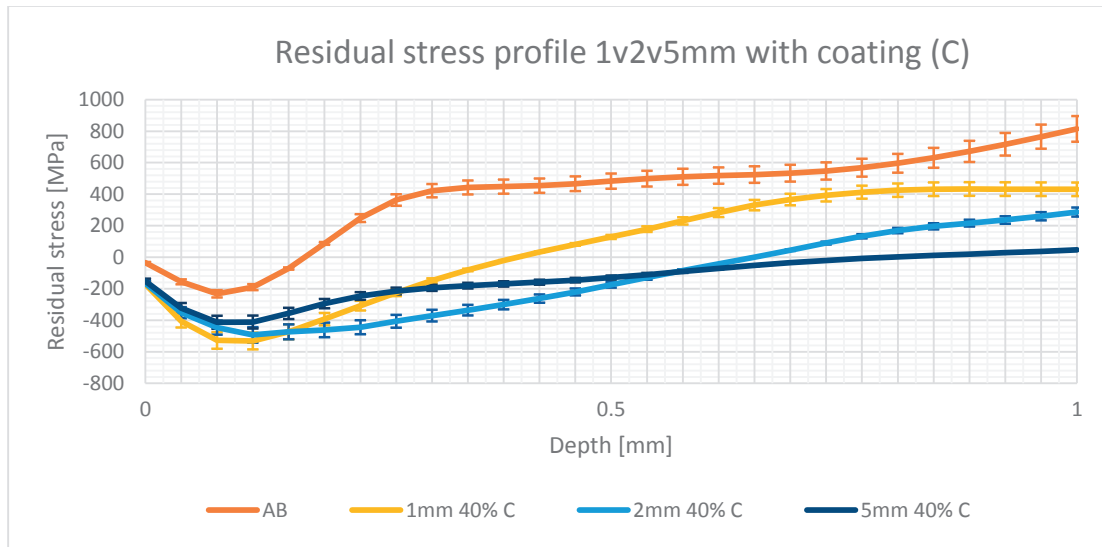
Fig. 6 Residual stress curves measured for samples in the AB and LSP treated states with protective coating.

3.1.3 Surface residual stresses

If we look at the values of the surface RS, it can be observed that the smaller spot sizes lead to larger CRS. The same tendency was observed in sections 3.1.1 and 3.1.2 in the case of the maximum amount and the depth of CRS. For samples treated without an ablative coating residual stresses are -117 MPa (10%) for 1mm spot size, -103 MPa (9%) for 2mm and -69 MPa (6%) for 5mm. This makes an increase of 6%, 5% and 2% of the UTS respectively, compared to the as – built state which has CRS of -42 MPa (4%).

For samples treated with an ablative coating, measured surface RS are -187 (16%), -165 (14%) and -163 MPa (14%) for 1, 2 and 5mm spot size respectively. This represents an increase compared to the AB state of 12%, 11% and 10% of the UTS. In the case of all 3 spot sizes, we can again see a significant influence of the ablative coating on the amount of CRS in the near surface region. For a 1mm spot size we can observe an increase from -117 MPa (10%) to -187 MPa (16%),

for 2mm from -103 MPa (9%) up to -165 MPa (14%) and for the 5mm from -69 MPa (6%) up to -163 MPa (14%) in the uncoated/coated state respectively.

3.1.4 Overlap rate

One sample was treated with a higher overlap rate of 80% and without an ablative coating. For this sample the smallest spot size of 1mm was used, as this value might be preferential for the LSP treatment of small and complicated parts made by SLM. These measurements showed a high increase in all the important features of the residual stress profile. Maximum residual stresses were -798 MPa (69%), observed at a depth of 247µm, compared to -421 MPa (37%) at 142µm for 1mm 40% overlap LSP treatment done also without a coating. These values represented the largest increase compared to the AB state with 49% increase of the UTS in the amount of CRS and a 163% increase in depth of the maximum CRS. Surface RS were -169 MPa (15%), which was an increase of 11% of the UTS compared to the AB state. Depth of the CRS, was above 1mm which was the range of the measurement. At the depth of 1mm they were still compressive with a value of -266 MPa (23%). With an increase by a factor of 2 in the overlap rate from 40% to 80%, we have an increase by a factor of 9 of the total number of shots on the treated surface. This large increase in the total number of shots leads to a significant increase in all measured RS parameters, i.e. maximum CRS, depth of max CRS, depth of CRS and surface RS, shown in Figure 5.

3.2 316L stainless steel

Since the PH1 SLM samples in the as built state showed unusual CRS in the near surface region, 316L SLM samples were used to show the potential of the LSP treatment on other materials and the ability to fully transform TRS to CRS. 316L was chosen because of its wide spread application, but also because it is an austenitic stainless steel that has a TRS state in the near surface region that is more common for SLM parts. The characteristic values in the AB and LSP treated states are shown in Table 5 and the curves of both samples made of 316L and PH1 with same treatments in Figure 7.

In the AB state, we observed TRS in the whole range from the surface up to the 1mm depth. The maximum value in the near surface region was 342 MPa at about 131µm which represents 45% of the UTS of the material (760 MPa).

LSP treatment with a 1mm spot size, no coating and 40% and 80% overlap was done. For the sample treated with a 40% overlap, CRS were observed up to the depth of 416μm. The maximum value of CRS was 266 MPa (35%) at 128μm, and surface RS were -103 MPa (14%). For the sample treated with an 80% overlap, CRS were observed up to the depth of 804μm. The maximum value of CRS was -729 MPa (96%) at 94μm and in the surface region -418 MPa (55%) at a 20μm depth. The maximum value of CRS represents 96% of the UTS of the material which indicates material strain hardening due to the high number of LSP shots on the surface in the 80% overlap LSP condition.

Tensile residual stresses are very efficiently converted to compressive residual stresses for 316L samples, and the asymptotic profile is qualitatively similar to that of the PH1 samples.

LSP treatment	Max RS[MPa]/ percentage of the UTS [%]	depth of max RS [μm]	depth of CRS [μm]	Surface RS [MPa]/ percentage of the UTS [%]
316L - AB	342 / 45	131	/	105 / 14
316L - 1mm 40% NC	-266 / 35	128	416	-103 / 14
316L - 1mm 80% NC	-730 / 96	94	804	-418 / 55

Table 5 Results of RS measurements: maximum RS / normalized by UTS; depth of maximum RS are observed; depth of CRS; surface RS /normalized by UTS. Measurements are made in the as- built state (AB), or with LSP treatments of 1mm, 40 and 80% overlap, without an ablative coating (NC).
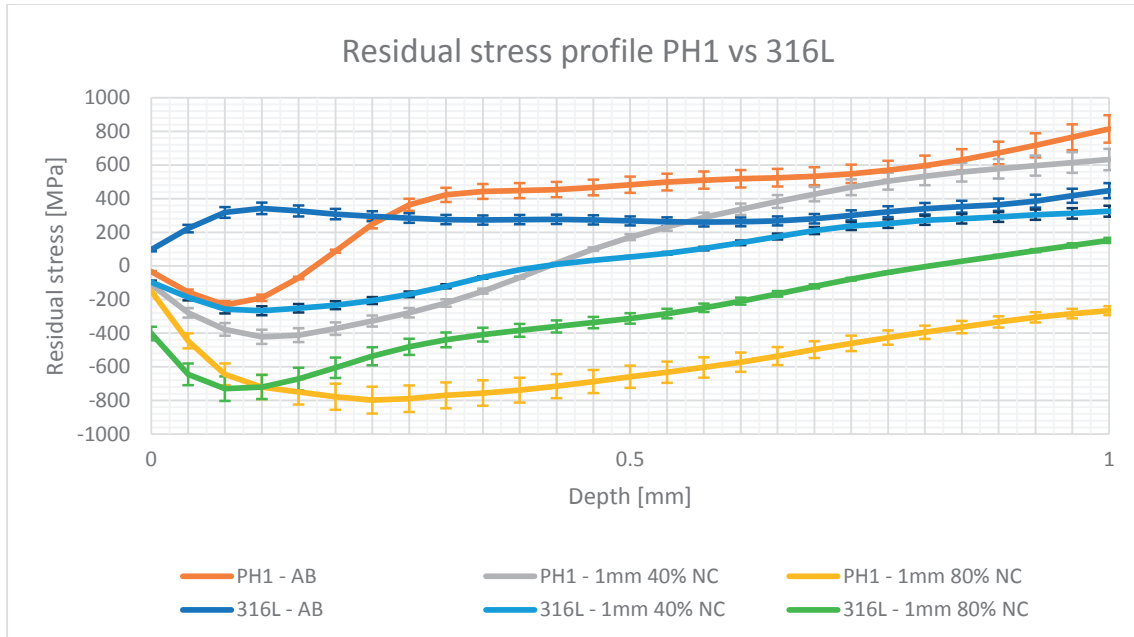
Fig. 7 Residual stress curves measured for both PH1 and 316L samples in the AB and LSP treated states without an ablative coating. Spot size was 1mm and overlaps 40% and 80%.

4. Conclusions

In this paper, the capability of the LSP treatment to alter the residual stresses of SLM parts was demonstrated. It was shown that in the case of the martensitic PH1 stainless steel, the maximum amount, depth of the profile and amount in the near surface region of the beneficial CRS can be drastically increased. Also, for the austenitic 316L stainless steel, the highly tensile state of the AB sample was changed to a beneficial CRS state. Various LSP processing parameters were used, with and without an ablative coating. It can be concluded that:

- Laser shock peening can be used to effectively and easily change the residual stress profile. Even with a single pass, the RS changes from tensile to compressive in the case of 316L, or in the case of PH1, the values of CRS are drastically increased and observed to larger depths.
- Smaller spot size leads to larger amount of residual stresses both in the near surface region and in the depth. These trends were observed both with and without an ablative coating.
- Larger spot sizes lead to increased depths of CRS.
- Ablative coating leads to larger and deeper CRS. This is true for the entire profile, in particular in the near surface region (at 20μm) and at the maximum value of CRS.

- When using an ablative coating the CRS increase is more pronounced for spot sizes of 2 and 5mm.
- Higher overlap rates (80%) lead to higher CRS and a deeper CRS profile. Although these LSP parameters give significantly better results, the associated higher number of impacts leads to longer processing time.

Further investigations will be done on the effect of the LSP treatment on the microstructure and the fatigue life of SLM parts. Also, the possibility of combining LSP treatment with SLM into a single machine will be addressed. The goal of using LSP during the building phase of SLM as a "3D LSP" method would be to tailor residual stresses throughout the part, especially focusing on critical points and in the near surface zone. This would possibly lead to increased depth and volume of CRS in the near surface region, which is known to have beneficial effects on fatigue life. Another goal would be to reduce the accumulation of TRS during the building phase, to avoid process failure for certain materials which are hard or even impossible to process by SLM (e.g. Ni-based superalloys).

References

[1] R. S. Gideon N. Levy, "Rapid manufacturing and rapid tooling with layer manufacturing (LM) technologies, state of the art and future perspectives. CIRP Ann—Manuf Technol 52 2:589-609," *CIRP Ann. - Manuf. Technol.*, vol. 52, no. 2, pp. 589–609, 2003.

[2] "Wohlers Report 2012." [Online]. Available: http://www.wohlersassociates.com/2012report.htm. [Accessed: 11-Sep-2015].

[3] E. Yasa, K. Kempen, J.-P. Kruth, L. Thijs, and J. Van Humbeeck, "Microstructure and mechanical properties of maraging steel 300 after Selective Laser Melting," presented at the Solid Freeform Fabrication Symposium Proceedings, 2010.

[4] L Thijs, J Van Humbeeck, K Kempen, E Yasa, JP Kruth, and M Rombouts, "Investigation on the inclusions in maraging steel produced by Selective Laser Melting," in *Innovative Developments in Virtual and Physical Prototyping*, 0 vols., CRC Press, 2011, pp. 297–304.

[5] T. Niendorf, S. Leuders, A. Riemer, H. A. Richard, T. Tröster, and D. Schwarze, "Highly Anisotropic Steel Processed by Selective Laser Melting," *Metall. Mater. Trans. B*, vol. 44, no. 4, pp. 794–796, May 2013.

[6] K. Kempen, L. Thijs, J. Van Humbeeck, and J.-P. Kruth, "Mechanical Properties of AlSi10Mg Produced by Selective Laser Melting," *Phys. Procedia*, vol. 39, pp. 439–446, 2012.

[7] H. Stoffregen, K. Butterweck, and E. Abele, "Fatigue Analysis in Selective Laser Melting: Review and Investigation of Thin-walled Actuator Housings," presented at the 25th Solid Freeform Fabrication Symposium 2014, Austin, Texas, 2014, pp. 635–650.

[8] D. Gu *et al.*, "Densification behavior, microstructure evolution, and wear performance of selective laser melting processed commercially pure titanium," *Acta Mater.*, vol. 60, no. 9, pp. 3849–3860, May 2012.

[9] X. Tan *et al.*, "Graded microstructure and mechanical properties of additive manufactured Ti–6Al–4V via electron beam melting," *Acta Mater.*, vol. 97, pp. 1–16, Sep. 2015.

[10] T. H. Becker, M. Beck, and C. Scheffer, "MICROSTRUCTURE AND MECHANICAL PROPERTIES OF DIRECT METAL LASER SINTERED TI-6AL-4V," *South Afr. J. Ind. Eng.*, vol. 26, no. 1, pp. 1–10, Mar. 2015.

[11] L. T. B. Vrancken, "Microstructure and mechanical properties of a novel β titanium metallic composite by selective laser melting," *Acta Mater.*, vol. 68, no. 15, pp. 150–158, 2014.

[12] E. Sallica-Leva, A. L. Jardini, and J. B. Fogagnolo, "Microstructure and mechanical behavior of porous Ti–6Al–4V parts obtained by selective laser melting," *J. Mech. Behav. Biomed. Mater.*, vol. 26, pp. 98–108, Oct. 2013.

[13] H. K. Rafi, D. Pal, N. Patil, T. L. Starr, and B. E. Stucker, "Microstructure and Mechanical Behavior of 17-4 Precipitation Hardenable Steel Processed by Selective Laser Melting," *J. Mater. Eng. Perform.*, vol. 23, no. 12, pp. 4421–4428, Sep. 2014.

[14] J.-P. Kruth, M. Badrossamay, E. Yasa, J. Deckers, L. Thijs, and J. Van Humbeeck, "Part and material properties in selective laser melting of metals," presented at the Proceedings of the 16th International Symposium on Electromachining, 2010.

[15] J.-P. Kruth, J. Deckers, E. Yasa, and R. Wauthle, "Assessing and comparing influencing factors of residual stresses in selective laser melting using a novel analysis method," *Proc. Inst. Mech. Eng. Part B J. Eng. Manuf.*, vol. 226, no. 6, pp. 980–991, Jun. 2012.

[16] C. Casavola, S. L. Campanelli, and C. Pappalettere, "Experimental analysis of residual stresses in the selective laser melting process," in *Proccedings of the XIth International Congress and Exposition, Orlando, Florida, USA*, 2008.

[17] K. Kunze, T. Etter, J. Grässlin, and V. Shklover, "Texture, anisotropy in microstructure and mechanical properties of IN738LC alloy processed by selective laser melting (SLM)," *Mater. Sci. Eng. A*, vol. 620, pp. 213–222, Jan. 2015.

[18] K. Kempen, B. Vrancken, S. Buls, L. Thijs, J. Van Humbeeck, and J.-P. Kruth, "Selective Laser Melting of Crack-Free High Density M2 High Speed Steel Parts by Baseplate Preheating," *J. Manuf. Sci. Eng.*, vol. 136, no. 6, p. 061026, Oct. 2014.

[19] L. Thijs *et al.*, "Strong morphological and crystallographic texture and resulting yield strength anisotropy in Selective Laser Melted tantalum," *Acta Mater.*, vol. 61, no. 12, pp. 4657–4668, Jul. 2013.

[20] T. E. L. Rickenbacher, "High temperature material properties of IN738LC processed by selective laser melting (SLM) technology," *Rapid Prototyp. J.*, vol. 19, no. 4, 2013.

[21] M. Simonelli, Y. Y. Tse, and C. Tuck, "Further Understanding of Ti6Al4V Selective Laser Melting Using Texture Analysis," *Proc. 23rd Annu. Int. Solid Free. Fabr. Symp. Austin TX*, 2012.

[22] D. Buchbinder, W. Meiners, N. Pirch, K. Wissenbach, and J. Schrage, "Investigation on reducing distortion by preheating during manufacture of aluminum components using selective laser melting," *J. Laser Appl.*, vol. 26, no. 1, p. 012004, 2014.

[23] A. S. Wu, D. W. Brown, M. Kumar, G. F. Gallegos, and W. E. King, "An Experimental Investigation into Additive Manufacturing-Induced Residual Stresses in 316L Stainless Steel," *Metall. Mater. Trans. A*, vol. 45, no. 13, pp. 6260–6270, Dec. 2014.

[24] M. Shiomi, K. Osakada, K. Nakamura, T. Yamashita, and F. Abe, "Residual Stress within Metallic Model Made by Selective Laser Melting Process," *CIRP Ann. - Manuf. Technol.*, vol. 53, no. 1, pp. 195–198, 2004.

[25] P. Peyre, R. Fabbro, P. Merrien, and H. P. Lieurade, "Laser shock processing of aluminium alloys. Application to high cycle fatigue behaviour," *Mater. Sci. Eng. A*, vol. 210, no. 1–2, pp. 102–113, Jun. 1996.

[26] U. Trdan, M. Skarba, and J. Grum, "Laser shock peening effect on the dislocation transitions and grain refinement of Al–Mg–Si alloy," *Mater. Charact.*, vol. 97, pp. 57–68, Nov. 2014.

[27] T. W. Charles S. Montross, "Laser Shock Processing and its Effects on Microstructure and Properties of Metal Alloys: A Review," *Int. J. Fatigue*, vol. 24, no. 10, pp. 1021–1036, 2002.

[28] R. K. Nalla, I. Altenberger, U. Noster, G. Y. Liu, B. Scholtes, and R. O. Ritchie, "On the influence of mechanical surface treatments—deep rolling and laser shock peening—on the fatigue behavior of Ti–6Al–4V at ambient and elevated temperatures," *Mater. Sci. Eng. A*, vol. 355, no. 1–2, pp. 216–230, Aug. 2003.

[29] I. Nikitin, B. Scholtes, H. J. Maier, and I. Altenberger, "High temperature fatigue behavior and residual stress stability of laser-shock peened and deep rolled austenitic steel AISI 304," *Scr. Mater.*, vol. 50, no. 10, pp. 1345–1350, May 2004.

[30] Y. K. Gao, "Improvement of fatigue property in 7050–T7451 aluminum alloy by laser peening and shot peening," *Mater. Sci. Eng. A*, vol. 528, no. 10–11, pp. 3823–3828, Apr. 2011.

[31] M. Dorman, M. B. Toparli, N. Smyth, A. Cini, M. E. Fitzpatrick, and P. E. Irving, "Effect of laser shock peening on residual stress and fatigue life of clad 2024 aluminium sheet containing scribe defects," *Mater. Sci. Eng. A*, vol. 548, pp. 142–151, Jun. 2012.

[32] J. J. Ruschau, R. John, S. R. Thompson, and T. Nicholas, "Fatigue crack nucleation and growth rate behavior of laser shock peened titanium," *Int. J. Fatigue*, vol. 21, Supplement 1, pp. S199–S209, Sep. 1999.

[33] E. Maawad, H.-G. Brokmeier, L. Wagner, Y. Sano, and C. Genzel, "Investigation on the surface and near-surface characteristics of Ti–2.5Cu after various mechanical surface treatments," *Surf. Coat. Technol.*, vol. 12, no. 205, pp. 3644–3650, 2011.

[34] A. S. Gill, A. Telang, and V. K. Vasudevan, "Characteristics of surface layers formed on inconel 718 by laser shock peening with and without a protective coating," *J. Mater. Process. Technol.*, vol. 225, pp. 463–472, Nov. 2015.

[35] D. Karthik and S. Swaroop, "Laser shock peening enhanced corrosion properties in a nickel based Inconel 600 superalloy," *J. Alloys Compd.*, vol. 694, pp. 1309–1319, Feb. 2017.

[36] Y. Li *et al.*, "The strengthening mechanism of a nickel-based alloy after laser shock processing at high temperatures," *Sci. Technol. Adv. Mater.*, vol. 14, no. 5, p. 055010, Oct. 2013.

[37] M. A. S. Torres and H. J. C. Voorwald, "An evaluation of shot peening, residual stress and stress relaxation on the fatigue life of AISI 4340 steel," *Int. J. Fatigue*, vol. 24, no. 8, pp. 877–886, Aug. 2002.

[38] A. H. Clauer, J. H. Holbrook, and B. P. Fairand, "Effects of Laser Induced Shock Waves on Metals," in *Shock Waves and High-Strain-Rate Phenomena in Metals*, M. A. Meyers and L. E. Murr, Eds. Springer US, 1981, pp. 675–702.

[39] A. King, A. Steuwer, C. Woodward, and P. J. Withers, "Effects of fatigue and fretting on residual stresses introduced by laser shock peening," *Mater. Sci. Eng. A*, vol. 435–436, pp. 12–18, Nov. 2006.

[40] O. Hatamleh, "A comprehensive investigation on the effects of laser and shot peening on fatigue crack growth in friction stir welded AA 2195 joints," *Int. J. Fatigue*, vol. 31, no. 5, pp. 974–988, May 2009.

[41] C. A. Rodopoulos, J. S. Romero, S. A. Curtis, E. R. de los Rios, and P. Peyre, "Effect of controlled shot peening and laser shock peening on the fatigue performance of 2024-T351 aluminum alloy," *J. Mater. Eng. Perform.*, vol. 12, no. 4, pp. 414–419.

[42] A. K. Gujba and M. Medraj, "Laser Peening Process and Its Impact on Materials Properties in Comparison with Shot Peening and Ultrasonic Impact Peening," *Materials*, vol. 7, no. 12, pp. 7925–7974, 2014.

[43] "EOS Metal Materials for Additive Manufacturing." [Online]. Available: http://www.eos.info/material-m. [Accessed: 12-Oct-2016].

[44] A.B. Spierings, T.L. Starr, and K. Wegener, "Fatigue performance of additive manufactured metallic partsnull," *Rapid Prototyp. J.*, vol. 19, no. 2, pp. 88–94, Mar. 2013.

[45] D. Courapied *et al.*, "Laser adhesion test for thermal sprayed coatings on textured surface by laser," *J. Laser Appl.*, vol. 28, no. 2, p. 022509, May 2016.

[46] D. Courapied, L. Berthe, P. Peyre, F. Coste, J.-P. Zou, and A.-M. Sautivet, "Laser-delayed double shock-wave generation in water-confinement regime," *J. Laser Appl.*, vol. 27, no. S2, p. S29101, Feb. 2015.

[47] C. Correa *et al.*, "Random-type scanning patterns in laser shock peening without absorbing coating in 2024-T351 Al alloy: A solution to reduce residual stress anisotropy," *Opt. Laser Technol.*, vol. 73, pp. 179–187, Oct. 2015.

[48] J. P. Nobre, M. Kornmeier, A. M. Dias, and B. Scholtes, "Use of the hole-drilling method for measuring residual stresses in highly stressed shot-peened surfaces," *Exp. Mech.*, vol. 40, no. 3, pp. 289–297, Sep. 2000.

[49] C. Rubio-González *et al.*, "Effect of laser shock processing on fatigue crack growth and fracture toughness of 6061-T6 aluminum alloy," *Mater. Sci. Eng. A*, vol. 386, no. 1–2, pp. 291–295, Nov. 2004.

[50] U. Trdan, J. A. Porro, J. L. Ocaña, and J. Grum, "Laser shock peening without absorbent coating (LSPwC) effect on 3D surface topography and mechanical properties of 6082-T651 Al alloy," *Surf. Coat. Technol.*, vol. 208, pp. 109–116, Sep. 2012.

[51] N. S. Rossini, M. Dassisti, K. Y. Benyounis, and A. G. Olabi, "Methods of measuring residual stresses in components," *Mater. Des.*, vol. 35, pp. 572–588, Mar. 2012.

[52] G. S. Schajer, "Relaxation Methods for Measuring Residual Stresses: Techniques and Opportunities," *Exp. Mech.*, vol. 50, no. 8, pp. 1117–1127, Jul. 2010.

[53] V. M. Measurements, "Measurement of residual stresses by the hole drilling strain gage method," Tech Note TN-503-6, 2007.

[54] R. H. Leggatt, "Residual stresses in welded structures," *Int. J. Press. Vessels Pip.*, vol. 85, no. 3, pp. 144–151, Mar. 2008.

[55] D. Thibault, P. Bocher, and M. Thomas, "Residual stress and microstructure in welds of 13%Cr–4%Ni martensitic stainless steel," *J. Mater. Process. Technol.*, vol. 209, no. 4, pp. 2195–2202, Feb. 2009.

[56] A. Griffiths, W. Nimmo, B. Roebuck, G. Hinds, and A. Turnbull, "A novel approach to characterising the mechanical properties of supermartensitic 13 Cr stainless steel welds," *Mater. Sci. Eng. A*, vol. 384, no. 1–2, pp. 83–91, Oct. 2004.

[57] P. Peyre, R. Fabbro, L. Berthe, X. Scherpereel, and A. Le Cornec, "Laser shock processing with small impacts," 1996, vol. 2789, pp. 125–132.

[58] P. Peyre, L. Berthe, X. Scherpereel, and R. Fabbro, "Laser-shock processing of aluminium-coated 55C1 steel in water-confinement regime, characterization and application to high-cycle fatigue behaviour," *J. Mater. Sci.*, vol. 33, no. 6, pp. 1421–1429, Mar. 1998.

Chapter 5

3D Laser Shock Peening – a new method for the 3D control of residual stresses in Selective Laser Melting

Nikola Kalentics[1,*], Eric Boillat[1], Patrice Peyre[2], Cyril Gorny[2], Christoph Kenel[3], Christian Leinenbach[3], Jamasp Jhabvala[1], Roland E. Logé[1]

1. Thermomechanical Metallurgy Laboratory – PX Group Chair, Ecole Polytechnique Fédérale de Lausanne (EPFL), CH-2002 Neuchâtel, Switzerland

2. Processes and Engineering in Mechanics and Materials Laboratory (PIMM), CNRS-ENSAM Paristech,151 Bd de l'Hôpital, 75013 Paris, France

3. Empa-Swiss Federal Laboratories for Materials Science and Technology, Dübendorf, Switzerland

Contribution:

Nikola Kalentics designed the experiment, assisted in the Laser Shock Peening treatments, did the residual stress measurements, interpretation of results and wrote the manuscript.

Abstract

This paper describes a hybrid additive manufacturing process – 3D Laser Shock Peening (3D LSP), based on the integration of Laser Shock Peening (LSP) with Selective Laser Melting (SLM). The well-known tensile residual stresses (TRS) in the as – built (AB) state of SLM parts in the subsurface region have a detrimental effect on their fatigue life. LSP is a relatively expensive surface post treatment method, known to generate deep CRS into the subsurface of the part, and used for high end applications (e.g. aerospace, nuclear) where fatigue life is crucial. The novel proposed 3D LSP process takes advantage of the possibility to repeatedly interrupt the part manufacturing, with cycles of a few SLM layers. This approach leads to higher and deeper CRS in the subsurface of the produced part, with expected improved fatigue properties. In this paper, 316L stainless steel samples were 3D LSP processed using a decoupled approach, i.e. by moving back and forth the baseplate from an SLM machine to an LSP station. A clear and significant increase in the magnitude and depth of CRS was observed, for all investigated process parameters, when compared to the AB SLM parts, or those traditionally LSP (surface) treated.

1. Introduction

Selective Laser Melting (SLM) is a part of a large family of Additive Manufacturing (also known as 3D printing) processes [1]–[3], and also the most studied over the past years. In the SLM process the part is built layer by layer out of a metallic, ceramic, polymer or composite powder. At each step, a powder bed is deposited on a substrate and selectively melted by a laser beam. Using a laser beam deflection system, each layer is scanned according to the corresponding part cross section, as calculated from the CAD (computer-aided design) model. After selective consolidation, a new powder layer is deposited, and the operation sequence is repeated until completion of the part. At the end, the unused powder is removed and can be reused in another building process. This manufacturing method leads to the ability to produce parts with high added value and very complex geometries, which would otherwise be difficult or impossible to produce. Typical examples concern lattice structures used for aerospace and medical applications, bionic design for weight reduction, conformal cooling channels in molds, etc.

Although the mechanical properties of parts made by SLM have become close to those produced by conventional processes [3]–[13], SLM still has several inherent limitations, one of them being the accumulation of detrimental tensile residual stresses (TRS), illustrated in Figure 1. During the SLM process, the top layer which was melted last has shrunk upon cooling, with however a magnitude which is limited by the continuity with the underlying (already solidified) material [14],

58

[15]. From one layer to another, large TRS accumulate inside the manufactured component, resulting either in reduced fatigue life or in distortion of the final part [6], [14], [15], [19], [20]. High stresses can even lead to process failure (cracking) *during* the building phase [21].

Different methods have been used to control and reduce residual stresses. In situ heating (e.g. by substrate preheating or laser remelting) is commonly used [15], [22]–[24]. Adapting scanning strategies has also been shown to strongly impact residual stresses [15], [19]. As a post treatment, annealing is widely used and has demonstrated in some cases a 70 percent reduction of residual stresses [24], [25]. Although these methods do bring improvements in the final residual stress state, they have shown to be unable to completely remove TRS, and are unable to introduce compressive residual stresses (CRS) which improve fatigue life. Furthermore, process failure cannot be avoided with post-processing treatments, which means that materials for which in situ heating or optimized scanning strategies are not successful simply cannot be processed by SLM.

Laser Shock Peening (LSP) is a high strain rate ($\sim 10^6 s^{-1}$) [26] surface treatment method, similar to Shot Peening (SP) and Ultrasonic Shot Peening (USP), used to introduce CRS in the near surface region of the material. LSP is well-known to result in an increased fatigue life, resistance to stress corrosion cracking, and fretting fatigue, for a variety of metallic materials [27]–[29]. Introduced CRS can reach a depth of up to one millimeter (depending on the treated material), counteract some or all of the tensile stress in the near surface region, decrease the crack propagation rate, effectively reduce the stress intensity factors, enhance fatigue crack closure effects and increase the critical stress for crack propagation, therefore improving the fatigue performance of metallic materials (Figure 2) [27]–[30].

Initial investigation on the application of LSP as a conventional surface treatment method on parts made by SLM has shown that LSP is able to convert the TRS into more beneficial CRS in the subsurface region [31]. The residual stresses were successfully transformed for all considered LSP parameters. However, conventional LSP remains a surface post treatment, and cannot address the bulk accumulation of high TRS *during* the SLM building phase.

In the present paper, a novel hybrid additive manufacturing process – 3D Laser Shock Peening (3D LSP) is described. 3D LSP is a process patented [32] by the Laboratory of Thermomechanical Metallurgy (LMTM) at the Ecole Polytechnique Fédérale de Lausanne (EPFL). It is shown to successfully allow the 3D control of residual stresses in SLM parts. In particular, the detrimental TRS state inherited from SLM is converted into beneficial CRS in the surface region, over a depth larger than that obtained with conventional surface LSP (Figure 1). The 3D LSP process is actually able to accumulate CRS in any critical zone in the bulk of the part. The idea consists in combining SLM and LSP processes, by applying the LSP treatment every few SLM layers. For such an

approach to be fully functional and able to produce large parts, the LSP laser with a corresponding scanning head must be integrated into the SLM machine.
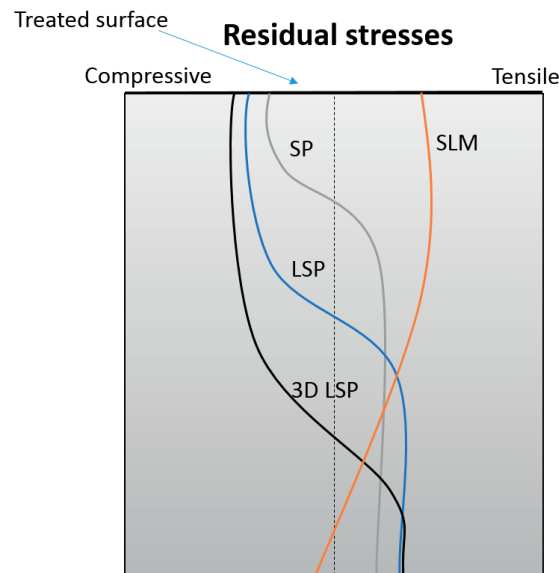
Fig. 1 Schematic representation of residual stresses in SLM parts, showing the influence of Shot Peening (SP), Laser Shock Peening (LSP), and 3D LSP.

The effects of residual stresses on the fatigue life have been extensively investigated [27]–[29], [33] and the beneficial role of compressive stresses in the near surface region has been demonstrated without any ambiguity. It was also observed that the depth of CRS plays a significant influence on fatigue life. The larger the depth (for a given magnitude), the more near surface cracks will be mitigated, and the longer the fatigue life. Although the LSP setting is more complex than the more conventional SP (or even Ultrasonic SP), it is still irreplaceable as a surface treatment of parts with tight specifications such as those encountered for nuclear or aerospace applications, due to the larger CRS depth (Figure 1) [27], [34]–[39]. By repeating the LSP treatment on a number of SLM layers in the subsurface region, 3D LSP aims at increasing both the CRS magnitude and depth compared to a conventional surface LSP process, with therefore an expected further improvement in fatigue life.
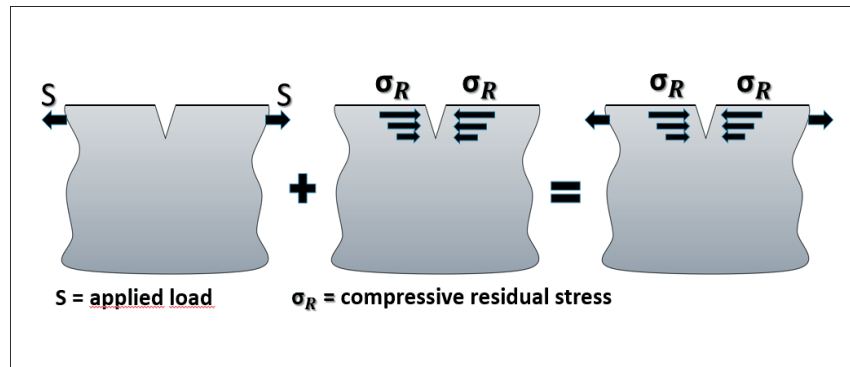
Fig. 2 Effect of tensile and compressive stresses on the crack growth propagation and fatigue life.

2. Experimental setup

2.1 Material and SLM parameters

The reference material used here is the widely used 316L austenitic stainless steel, with an ultimate tensile strength (UTS) of 760 MPa [17]. The powder was DIAMALLOY 1003, obtained from Sulzer Metco, Switzerland. The chemical composition is shown in Table 1. Selective Laser Melting was performed with a Concept M2 (Concept Laser GmbH, Germany) equipped with a fiber laser operated in continuous mode at a wavelength of 1070 nm and a spot size of 90 microns. The specimen geometry was a 20x20x7 mm^3 cuboid on a 3 mm thick support structure. The chosen SLM processing parameters were: laser power 125 W, scanning speed 600 mm/s, hatch distance 0.105 mm, and layer thickness 0.03 mm. A bi-directional scanning strategy parallel to the part edges was used without a change in scanning direction between layers to deliberately create large residual stresses. Processing was performed under N_2 atmosphere, and the O_2 content was controlled to be below 1 % throughout the process.

	Cr	Ni	Si	Mo	C	Fe
316L	17	12	2.3	2.5	0.03	Balance

Table 1 Chemical composition of 316L stainless steel, wt. %.

2.2 Laser Shock Peening

Laser Shock Peening (LSP) experiments were done using the facility described in [40]. The laser source was a Nd:YAG GAIA - class laser from Thales Laser company with a pulse duration of 7.1 ns, operating at 532 nm. The beam spatial energy distribution is "top-hat" and the pulse shape is near - Gaussian. Round laser spots of 1 and 5 mm diameter were used with a laser energy per pulse of either 0.4J or 10J. The ratio of spot size and energy per pulse was chosen such as to keep a constant power density of 7.2 GW/cm^2. The advantage in using lower energies per pulse (for a given power density) is to open the use of more readily accessible lasers, often functioning at higher repetition rates and therefore possibly increasing productivity. Furthermore, with the current state of the art, lower pulse energies could be delivered via a bundle of optical fibers [41], which is another advantage for the compactness of the machine.

The pressure created at the surface of the part was estimated to 4.7 GPa using the empirical equation $P\ (GPa) = 1.75\ \sqrt{I_0}(\frac{GW}{cm^2})$ [42]. Pulse frequency was 1Hz, and the overlap of 40% and 80% was used for both spot sizes without a protective ablative layer.

2.3 Residual stress determination using the hole drilling method

Residual stresses measurements were done with the hole drilling method (HDM). This technique is widely used for determination of in depth residual stress profiles, especially after surface treatments such as LSP, USP, or SP [43]–[48]. The measuring device was the RESTAN-MTS 3000 from SINT Technology (Figure 3a), and the measurements were done according to the ASTM standard E837 [14] [43]. The HDM measurement is done by positioning a strain gauge rosette (Figure 3b) on the measured surface, and drilling a 1,8mm diameter hole through it into the surface. As the hole is drilled, residual stresses relax at the hole location causing strains to change. Residual stresses are given by the theory of Kirsch [49]. A variable depth increment of the drill was applied. In the region from the surface up to 100µm depth, measurements were made every 10µm. From 0.1mm to 0.5mm, the step increased to 25µm, and from 0.5mm to 1mm, it increased further to 50µm. This procedure resulted in a total of 36 points measured over a total depth of 1 mm.

Fig. 3 a) Hole drilling device RESTAN-MTS 3000 (SINT Technology); b) sample with attached strain gauge rosette.

Figure 4 shows the most relevant parameters of a typical residual stress profile. These are (i) the maximum amount of CRS - *Max CRS*, (ii) the depth at which the maximum CRS is observed – *Depth of max CRS*, and (iii) the depth at which a transition from CRS to TRS occurs – *Depth of CRS.*
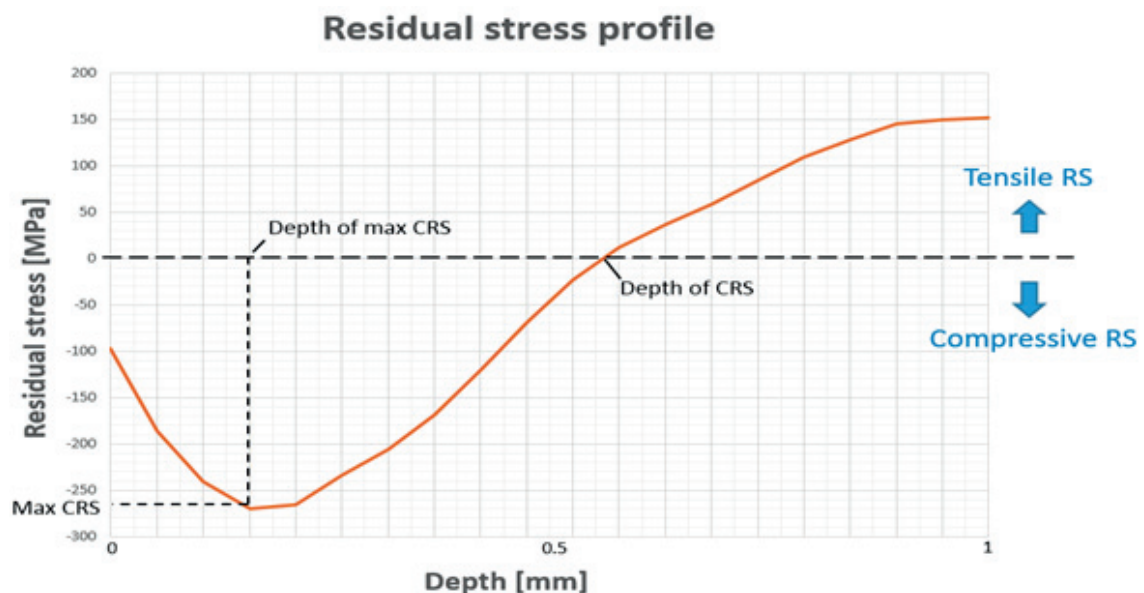

Fig. 4 Residual stress profile displaying the most relevant parameters: *Max CRS* – maximum amount of CRS; *Depth of max CRS* - depth at which the maximum CRS is observed; *Depth of CRS* - depth at which a transition from CRS to TRS occurs.

3. Results and discussion

3.1 As–built state

Residual stress measurement of the 316L SLM samples in the AB state are shown in Table 2. The high tensile value of 342 MPa at 131µm depth represents 45% of the material UTS (760 MPa). Stresses are tensile from the surface up to the depth of more than 1mm (Figure 5), which is typical for parts made by SLM.

3.2 LSP treated state

SLM samples attached to the baseplate were removed from the SLM machine and treated with LSP. LSP treatments operated with 1mm and 5mm spot size, and 40% or 80% overlap were done. A total of four samples were treated for each LSP processing condition. After LSP treatment, one of the four samples of each LSP processing condition was removed from the baseplate and analyzed, while the remaining three samples were sent back to the SLM machine for a rebuilding step of 1, 3 and 10 new layers. Results of residual stress measurements done on samples in the AB and LSP treated states are given in Table 2. The corresponding stress profiles are shown in Figure 5.

From Table 2 it can be observed that an increase in the overlap rate from 40% to 80% leads to an overall increase in CRS for both the 1mm and 5mm spot size. This is in agreement with the previous investigation done on PH1 stainless steel, where it was also observed that (i) a larger spot size leads to deeper CRS, and (ii) a smaller spot size leads to higher max RS [31]. As already discussed in [31], result (i) comes from a geometrical effect associated to the use of a too small spot size, which results in a strong 2D attenuation of shockwaves, and therefore to a decreased plastically affected depth of the LSP treatment [27], [35], [50]. Result (ii) is in agreement with [51], and this effect can be explained from the increased number of impacts by a smaller spot size on a given surface area.

The maximum value of CRS occurred when using a 1 mm spot size with 80 % overlap: the stress value represents 96% of the material UTS. This indicates cyclic hardening of the 316L due to the high number of LSP shots to which the surface is subjected in the 80% overlap LSP condition [52]. Regardless of the chosen LSP parameters, TRS of the AB state are systematically converted to CRS. Smaller spot sizes lead to larger maximum CRS which is in agreement with previous results

obtained on a different material [31]. This is especially evident for the 80% overlap case where reducing the spot size from 5 to 1 mm led to an increase of 45% of UTS. A larger spot size tends however to increase the LSP affected zone depth: an increase from 416 μm to 686 μm is observed, for the 40% overlap case. The effect is less pronounced for the 80% overlap case, but still present. The relationship between the spot size and the LSP affected zone depth is due to the 2D attenuation of shock waves [27], [31], [53]. Higher overlap expectedly led to both higher maximum CRS and deeper CRS, but at the cost of an increased LSP treatment time.

Since the LSP laser is meant to be integrated with an SLM machine, laser related questions such as repetition rate, laser size, laser beam delivery and guiding methods should be addressed. The effect of laser spot size requires attention, since laser features differ significantly for the proposed two sets of LSP processing parameters. To reach the desired power density, the energy per pulse jumps from 400mJ with a 1 mm spot, to 10 J with a 5mm spot. Since the reported results with the two spot sizes do not vary too much from each other, especially for the 80% overlap case, lower energy lasers (around 400mJ per pulse) are likely to be beneficial, due to their smaller size, reduced cost and higher repetition rate. Taking into consideration both spot size and available repetition rates, the LSP treatment time is potentially reduced by a factor 4 when using smaller spot sizes. Furthermore, lower energies in the ns range can be coupled into an optical fiber delivery system, and make use of a scanning head (similar to those used in SLM). These considerations explain why a spot size of 1mm was chosen for all further investigations related to 3D LSP.

LSP treatment	Max RS[MPa]/ percentage of the UTS [%]	depth of max RS [μm]	depth of CRS [μm]
AB	342 / 45	131	/
1mm 40%	-266 / 35	128	416
1mm 80%	-730 / 96	94	804
5mm 40%	-246 / 32	207	696
5mm 80%	-390 / 51	241	963

Table 2 Results of RS measurements: maximum RS / normalized by UTS; depth of maximum RS; depth of CRS. Measurements are made in the as-built state (AB), or with LSP treatments of 1mm and 5mm, 40 and 80% overlap, without an ablative coating.
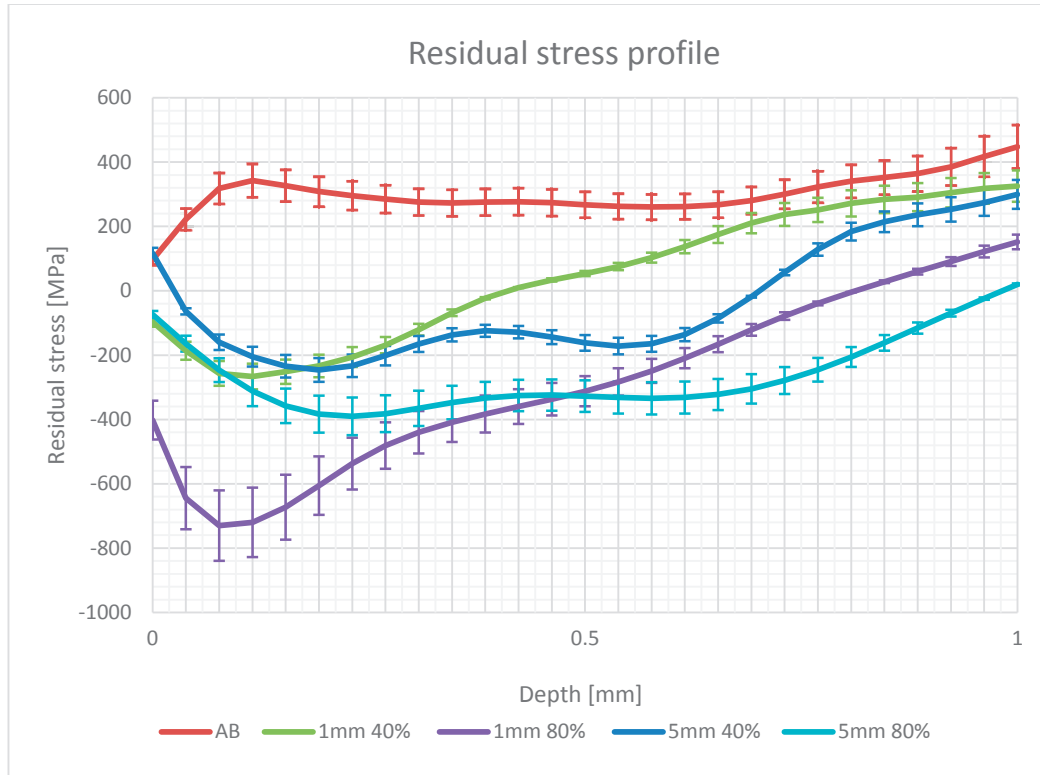
Fig. 5 Residual stress curves measured for samples in the AB and LSP treated states. Spot size was 1mm and 5mm with an overlap of 40% and 80%.

3.3 3D LSP

After the initial LSP treatment, for each group of LSP processing parameters, three treated samples were left attached to the baseplate. The baseplate with these samples was returned to the SLM machine for a rebuilding phase. After careful re-alignment, powder was refilled and *n* additional new layers were rebuilt (Figure 6). The number *n* of new layers was 1, 3 or 10. The SLM parameters and scanning strategy were kept the same, including the layer thickness of 30 μm. After the rebuilding phase, the samples were removed from the SLM machine, and the LSP treatment was repeated, using a 1 mm spot size and an overlap rates of 40% and 80%.
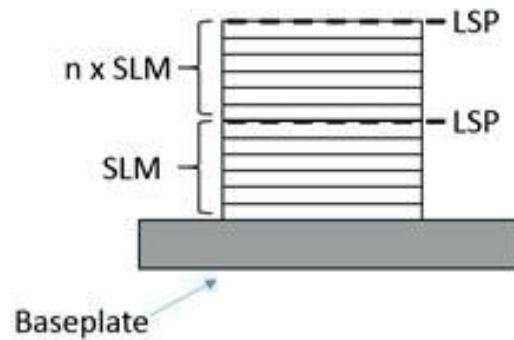
Fig. 6 Schematic description of the 3D LSP process.

3.3.1 3D LSP, 40% overlap

Residual stress measurements for the AB, LSP treated and 3D LSP treated samples are shown in Table 3, and a graphical representation of the stress profiles is given in Figure 7. 3D LSP samples have a very similar max RS of -345MPa (45% of UTS), -368 MPa (48%) and -358 MPa (47%) for *n* = 1, 3 and 10 SLM layers, respectively. This represents a significant increase of Max RS when compared to a conventional surface LSP treatment, leading to an improvement of 30%, 38% and 35%, respectively. This result was not obvious, due to the possible relaxation of stresses from thermal effects induced by the SLM rebuilding step, and the associated generation of tensile stresses. However, an accumulation of CRS was observed for all 3D LSP processing parameters (Figure 7 and 8). This indicates that the stress relaxation caused by the subsequent laser melting of even multiple *n* SLM layers during the rebuilding step is not the dominant effect, and that the 3D LSP does lead to a clear increase in magnitude and depth of CRS compared to a conventional LSP treatment.

The depth of CRS varied from 416 μm for the conventional LSP treatment, to 652 μm, 668 μm and 767 μm for the 3D LSP cases (*n* = 1, 3 and 10), showing an increase of 57%, 65% and 84%. The general trend which can be extracted from these results is that an increase in *n* leads to an increased depth of CRS. As mentioned above, this result was not straightforward. Since the melting and solidification of an SLM layer is very fast, it introduces a limited amount of heat and does not lead to full stress relaxation. CRS can therefore accumulate. The details of these mechanisms will however require further investigation. It is expected that there will be a critical value n_c beyond which the cumulative effects on the magnitude and depth of CRS will start decreasing. The value of n_c itself should be a function of SLM processing parameters and scanning strategy. In the present case, as mentioned in section 2.1, the least favorable SLM

67

parameters and scanning strategy were selected on purpose, to show the potential of the 3D LSP process, hence leaving space for further improvement.

LSP treatment, 40% overlap	Max RS[MPa]/ percentage of the UTS [%]	depth of max RS [μm]	depth of CRS [μm]
AB	342 / 45	131	/
LSP	-266 / 35	128	416
3D LSP $n = 1$	-345 / 45	170	652
3D LSP $n = 3$	-368 / 48	202	686
3D LSP $n = 10$	-358 / 47	131	767

Table 3 Results of RS measurements: maximum RS / normalized by UTS; depth of maximum RS; depth of CRS. Measurements are made in the as-built state (AB); LSP treatments of 1mm, 40% overlap; 3D LSP 1mm 40% with 1, 3 and 10 rebuilt layers.

Fig. 7 Residual stress curves measured for samples in the AB, LSP 1mm 40% and 3D LSP 1mm 40% with 1, 3 and 10 rebuilt layers.

3.3.2 3D LSP, 80% overlap

Residual stress measurements after treatments with 80% overlap are shown in Table 4 and Figure 8. 3D LSP samples had a max RS of -667 MPa (88% of UTS), -707 MPa (93%) and -756 MPa (99%) for n = 1, 3 and 10 SLM layers, respectively. These values are very similar to those produced by a conventional LSP treatment (-730 MPa or 94% of UTS), which already indicate a high strain hardening level due to a high density of shots when working with an 80% overlap.

The depth of CRS was increased from 804 µm for the conventional LSP treatment to over 1mm, beyond the maximum depth investigated with the current hole drilling experimental setup. At the 1mm depth, remaining compressive stresses were 38 MPa, 52 MPa and 254 MPa for n = 1, 3 and 10, respectively. This is not only a significant increase compared to the conventional LSP treatment, but also compared to the LSP treatment with 5mm spot size (see Table 2 and Figure 5). These results illustrate the relevance of choosing a small spot size in 3D LSP, as the LSP affected zone depth can be even higher than the one produced by larger spot sizes in conventional LSP treatments. Similarly to the 40% overlap case, an increase in n leads to a significant increase in depth of CRS.

LSP treatment, 80% overlap	Max RS[MPa]/ percentage of the UTS [%]	depth of max RS [µm]	depth of CRS [µm]
AB	342 / 45	131	/
LSP	-730 / 96	94	804
3D LSP n = 1	-667 / 88	165	> 1mm (-38 MPa at 1mm)
3D LSP n = 3	-707 / 93	126	> 1mm (-52 MPa at 1mm)
3D LSP n = 10	-756 / 99	243	> 1mm (-254 MPa at 1mm)

Table 4 Results of RS measurements: maximum RS / normalized by UTS; depth of maximum RS; depth of CRS. Measurements are made in the as-built state (AB); LSP treatments of 1mm, 80% overlap; 3D LSP 1mm 80% with 1, 3 and 10 rebuilt layers.
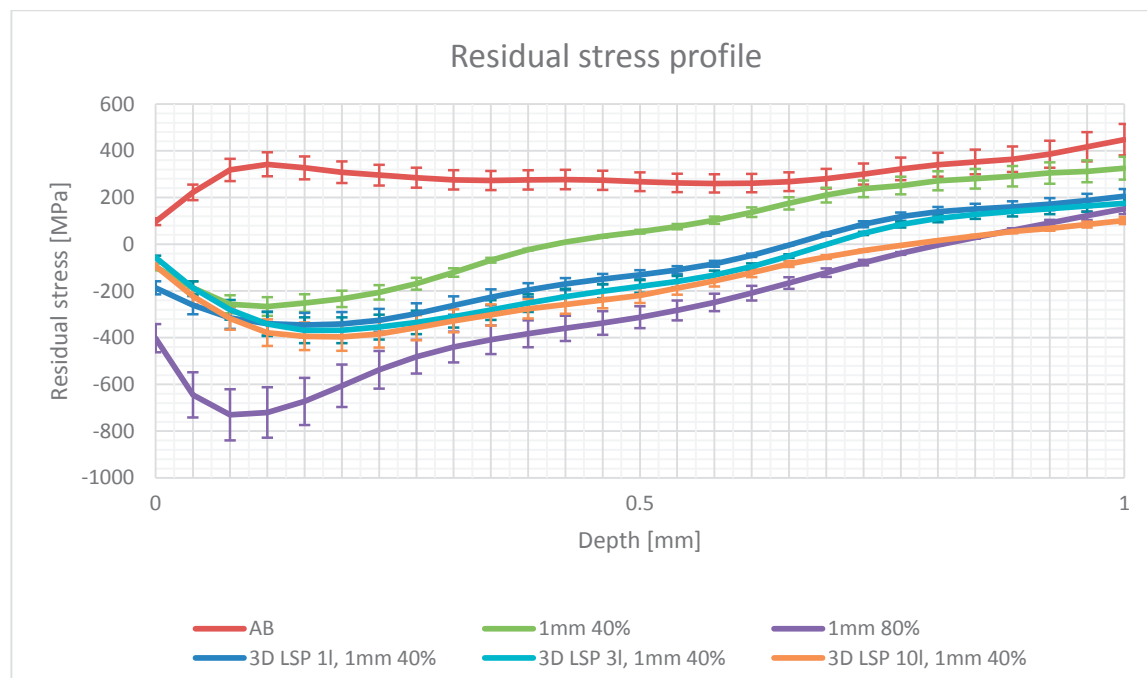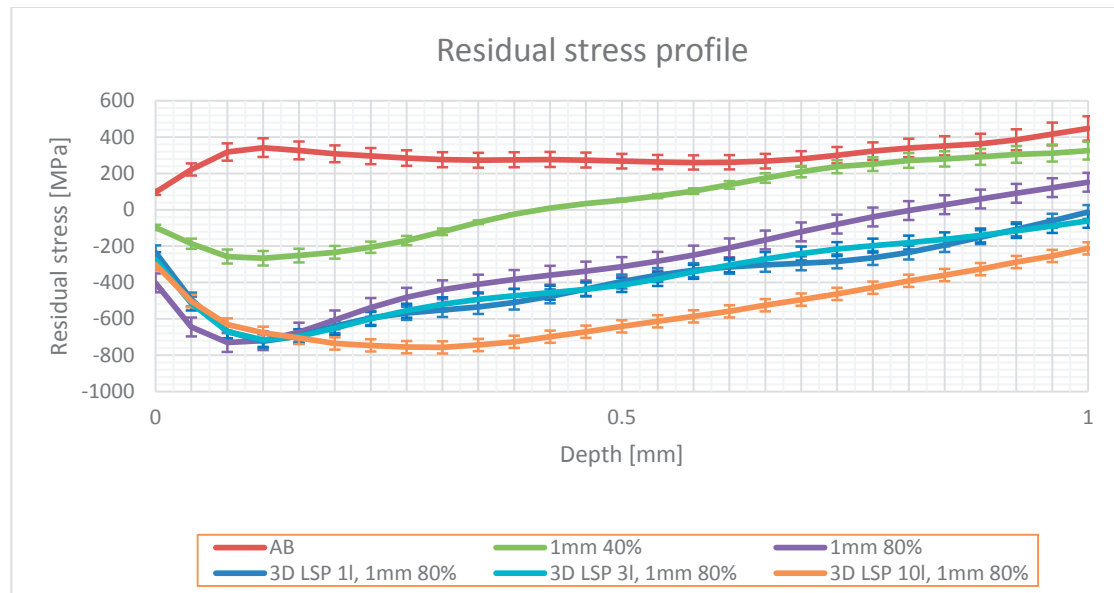
Fig. 8 Residual stress curves measured for samples in the AB, LSP 1mm 80% and 3D LSP 1mm 80% with 1, 3 and 10 rebuilt layers.

4. Conclusions and future work

In this paper, we have demonstrated the capability of an LSP treatment to change the residual stress state of SLM parts. Tests were performed on an austenitic 316L stainless steel, for which a highly tensile state of the AB sample was converted into a CRS state. It was also shown that if SLM building phase alternates with LSP treatments, both the magnitude and depth of maximum CRS can be significantly increased. Various LSP processing parameters were tested, and it can be concluded that:

- A conventional LSP treatment easily converts TRS into a CRS state.
- A smaller spot size leads to a larger maximum CRS.
- A larger spot size leads to increased depth of CRS.
- Higher overlap rates (80%) lead to higher CRS and deeper CRS profiles due to a larger density of impacts on the treated surface. Although this LSP processing condition leads to better results, it increases the LSP treatment time.
- 3D LSP increases both the magnitude and depth of CRS. This was observed for all processing conditions.
- 3D LSP with a reduced spot size and pulse energy can produce deeper CRS than those induced by a conventional LSP treatment with a larger spot size and pulse energy. This

70

was observed for both 40% and 80% overlap, and proves the interest of using lower energy pulsed lasers with higher repetition rates and reduced processing time. Such lasers are also better suited for implementation into a single SLM-LSP hybrid machine, being smaller in size, cheaper, and more easily adaptable in terms of beam delivery and positioning.

- Increasing the number of SLM layers between LSP treatments leads to an increase of CRS depth.

Further work will focus on (i) more accurate investigation of the effects of the number of SLM layers between two subsequent LSP treatments, (ii) the development of a prototype machine for building larger samples with optimized spatial distribution of tensile and compressive stresses, (iii) the assessment of fatigue life of 3D LSP treated samples, and the comparison with samples subjected to a conventional surface LSP treatment.

Another research direction will relate to the manufacturing of materials which are known to fail in SLM conditions due to the accumulation of high TRS, and for which the combination with 3D LSP is anticipated to be beneficial.

References

[1] "Wohlers Report 2012." [Online]. Available: http://www.wohlersassociates.com/2012report.htm. [Accessed: 11-Sep-2015].

[2] R. S. Gideon N. Levy, "Rapid manufacturing and rapid tooling with layer manufacturing (LM) technologies, state of the art and future perspectives. CIRP Ann—Manuf Technol 52 2:589-609," *CIRP Ann. - Manuf. Technol.*, vol. 52, no. 2, pp. 589–609, 2003.

[3] W. E. Frazier, "Metal Additive Manufacturing: A Review," *J. Mater. Eng. Perform.*, vol. 23, no. 6, pp. 1917–1928, Jun. 2014.

[4] L Thijs, J Van Humbeeck, K Kempen, E Yasa, JP Kruth, and M Rombouts, "Investigation on the inclusions in maraging steel produced by Selective Laser Melting," in *Innovative Developments in Virtual and Physical Prototyping*, 0 vols., CRC Press, 2011, pp. 297–304.

[5] H. Stoffregen, K. Butterweck, and E. Abele, "Fatigue Analysis in Selective Laser Melting: Review and Investigation of Thin-walled Actuator Housings," presented at the 25th Solid Freeform Fabrication Symposium 2014, Austin, Texas, 2014, pp. 635–650.

[6] T. H. Becker, M. Beck, and C. Scheffer, "MICROSTRUCTURE AND MECHANICAL PROPERTIES OF DIRECT METAL LASER SINTERED TI-6AL-4V," *South Afr. J. Ind. Eng.*, vol. 26, no. 1, pp. 1–10, Mar. 2015.

[7] X. Tan *et al.*, "Graded microstructure and mechanical properties of additive manufactured Ti–6Al–4V via electron beam melting," *Acta Mater.*, vol. 97, pp. 1–16, Sep. 2015.

[8]   L. T. B. Vrancken, "Microstructure and mechanical properties of a novel β titanium metallic composite by selective laser melting," *Acta Mater.*, vol. 68, no. 15, pp. 150–158, 2014.

[9]   E. Sallica-Leva, A. L. Jardini, and J. B. Fogagnolo, "Microstructure and mechanical behavior of porous Ti–6Al–4V parts obtained by selective laser melting," *J. Mech. Behav. Biomed. Mater.*, vol. 26, pp. 98–108, Oct. 2013.

[10] H. K. Rafi, D. Pal, N. Patil, T. L. Starr, and B. E. Stucker, "Microstructure and Mechanical Behavior of 17-4 Precipitation Hardenable Steel Processed by Selective Laser Melting," *J. Mater. Eng. Perform.*, vol. 23, no. 12, pp. 4421–4428, Sep. 2014.

[11] J.-P. Kruth, M. Badrossamay, E. Yasa, J. Deckers, L. Thijs, and J. Van Humbeeck, "Part and material properties in selective laser melting of metals," presented at the Proceedings of the 16th International Symposium on Electromachining, 2010.

[12] E. Yasa, K. Kempen, J.-P. Kruth, L. Thijs, and J. Van Humbeeck, "Microstructure and mechanical properties of maraging steel 300 after Selective Laser Melting," presented at the Solid Freeform Fabrication Symposium Proceedings, 2010.

[13] K. Kempen, L. Thijs, J. Van Humbeeck, and J.-P. Kruth, "Mechanical Properties of AlSi10Mg Produced by Selective Laser Melting," *Phys. Procedia*, vol. 39, pp. 439–446, 2012.

[14] C. Casavola, S. L. Campanelli, and C. Pappalettere, "Experimental analysis of residual stresses in the selective laser melting process," in *Proccedings of the XIth International Congress and Exposition, Orlando, Florida, USA*, 2008.

[15] J.-P. Kruth, J. Deckers, E. Yasa, and R. Wauthle, "Assessing and comparing influencing factors of residual stresses in selective laser melting using a novel analysis method," *Proc. Inst. Mech. Eng. Part B J. Eng. Manuf.*, vol. 226, no. 6, pp. 980–991, Jun. 2012.

[16] E. Brandl, U. Heckenberger, V. Holzinger, and et al, "Additive manufactured AlSi10Mg samples using Selective Laser Melting (SLM)," *Mater. Des.*, vol. 34, pp. 159–169, 2012.

[17] A.B. Spierings, T.L. Starr, and K. Wegener, "Fatigue performance of additive manufactured metallic parts," *Rapid Prototyp. J.*, vol. 19, no. 2, pp. 88–94, Mar. 2013.

[18] K. R. H. Gong, "Effect of defects on fatigue tests of as-built TI-6AL-4V parts fabricated by selective laser melting," *23rd Annu. Int. Solid Free. Fabr. Symp. - Addit. Manuf. Conf. SFF 2012*, pp. 499–506, 2012.

[19] A. S. Wu, D. W. Brown, M. Kumar, G. F. Gallegos, and W. E. King, "An Experimental Investigation into Additive Manufacturing-Induced Residual Stresses in 316L Stainless Steel," *Metall. Mater. Trans. A*, vol. 45, no. 13, pp. 6260–6270, Dec. 2014.

[20] K. Kunze, T. Etter, J. Grässlin, and V. Shklover, "Texture, anisotropy in microstructure and mechanical properties of IN738LC alloy processed by selective laser melting (SLM)," *Mater. Sci. Eng. A*, vol. 620, pp. 213–222, Jan. 2015.

[21] K. Kempen, B. Vrancken, S. Buls, L. Thijs, J. Van Humbeeck, and J.-P. Kruth, "Selective Laser Melting of Crack-Free High Density M2 High Speed Steel Parts by Baseplate Preheating," *J. Manuf. Sci. Eng.*, vol. 136, no. 6, p. 061026, Oct. 2014.

[22] D. Buchbinder, W. Meiners, N. Pirch, K. Wissenbach, and J. Schrage, "Investigation on reducing distortion by preheating during manufacture of aluminum components using selective laser melting," *J. Laser Appl.*, vol. 26, no. 1, p. 012004, 2014.

[23] A. V. Gusarov, M. Pavlov, and I. Smurov, "Residual Stresses at Laser Surface Remelting and Additive Manufacturing," *Phys. Procedia*, vol. 12, Part A, pp. 248–254, 2011.

[24] M. Shiomi, K. Osakada, K. Nakamura, T. Yamashita, and F. Abe, "Residual Stress within Metallic Model Made by Selective Laser Melting Process," *CIRP Ann. - Manuf. Technol.*, vol. 53, no. 1, pp. 195–198, 2004.

[25] Peter Mercelis and Jean-Pierre Kruth, "Residual stresses in selective laser sintering and selective laser melting," *Rapid Prototyp. J.*, vol. 12, no. 5, pp. 254–265, Oct. 2006.

[26] P. Peyre, R. Fabbro, P. Merrien, and H. P. Lieurade, "Laser shock processing of aluminium alloys. Application to high cycle fatigue behaviour," *Mater. Sci. Eng. A*, vol. 210, no. 1–2, pp. 102–113, Jun. 1996.

[27] T. W. Charles S. Montross, "Laser Shock Processing and its Effects on Microstructure and Properties of Metal Alloys: A Review," *Int. J. Fatigue*, vol. 24, no. 10, pp. 1021–1036, 2002.

[28] R. K. Nalla, I. Altenberger, U. Noster, G. Y. Liu, B. Scholtes, and R. O. Ritchie, "On the influence of mechanical surface treatments—deep rolling and laser shock peening—on the fatigue behavior of Ti–6Al–4V at ambient and elevated temperatures," *Mater. Sci. Eng. A*, vol. 355, no. 1–2, pp. 216–230, Aug. 2003.

[29] I. Nikitin, B. Scholtes, H. J. Maier, and I. Altenberger, "High temperature fatigue behavior and residual stress stability of laser-shock peened and deep rolled austenitic steel AISI 304," *Scr. Mater.*, vol. 50, no. 10, pp. 1345–1350, May 2004.

[30] U. Trdan, M. Skarba, and J. Grum, "Laser shock peening effect on the dislocation transitions and grain refinement of Al–Mg–Si alloy," *Mater. Charact.*, vol. 97, pp. 57–68, Nov. 2014.

[31] N. Kalentics, E. Boillat, P. Peyre, S. Ćirić-Kostić, N. Bogojević, and R. E. Logé, "Tailoring residual stress profile of Selective Laser Melted parts by Laser Shock Peening," *Addit. Manuf.*, May 2017.

[32] N. Kalentics, R. Logé, and E. Boillat, "Method and Device for Implementing Laser Shock Peening or Warm Laser Shock Peening During Selective Laser Melting," United States Patent Application 20170087670   Kind Code: A1, 30-Mar-2017.

[33] D. Lin, C. Ye, Y. Liao, S. Suslov, R. Liu, and G. J. Cheng, "Mechanism of fatigue performance enhancement in a laser sintered superhard nanoparticles reinforced nanocomposite followed by laser shock peening," *J. Appl. Phys.*, Apr. 2013.

[34] J. J. Ruschau, R. John, S. R. Thompson, and T. Nicholas, "Fatigue crack nucleation and growth rate behavior of laser shock peened titanium," *Int. J. Fatigue*, vol. 21, Supplement 1, pp. S199–S209, Sep. 1999.

[35] A. King, A. Steuwer, C. Woodward, and P. J. Withers, "Effects of fatigue and fretting on residual stresses introduced by laser shock peening," *Mater. Sci. Eng. A*, vol. 435–436, pp. 12–18, Nov. 2006.

[36] Y. K. Gao, "Improvement of fatigue property in 7050–T7451 aluminum alloy by laser peening and shot peening," *Mater. Sci. Eng. A*, vol. 528, no. 10–11, pp. 3823–3828, Apr. 2011.

[37] O. Hatamleh, "A comprehensive investigation on the effects of laser and shot peening on fatigue crack growth in friction stir welded AA 2195 joints," *Int. J. Fatigue*, vol. 31, no. 5, pp. 974–988, May 2009.

[38] C. A. Rodopoulos, J. S. Romero, S. A. Curtis, E. R. de los Rios, and P. Peyre, "Effect of controlled shot peening and laser shock peening on the fatigue performance of 2024-T351 aluminum alloy," *J. Mater. Eng. Perform.*, vol. 12, no. 4, pp. 414–419.

[39] A. K. Gujba and M. Medraj, "Laser Peening Process and Its Impact on Materials Properties in Comparison with Shot Peening and Ultrasonic Impact Peening," *Materials*, vol. 7, no. 12, pp. 7925–7974, 2014.

[40] D. Courapied *et al.*, "Laser adhesion test for thermal sprayed coatings on textured surface by laser," *J. Laser Appl.*, vol. 28, no. 2, p. 022509, May 2016.

[41] T. Schmidt-Uhlig, P. Karlitschek, M. Yoda, Y. Sano, and G. Marowsky, "Laser shock processing with 20 MW laser pulses delivered by optical fibers," *Eur. Phys. J. Appl. Phys.*, vol. 9, no. 3, pp. 235–238, Mar. 2000.

[42] D. Courapied, L. Berthe, P. Peyre, F. Coste, J.-P. Zou, and A.-M. Sautivet, "Laser-delayed double shock-wave generation in water-confinement regime," *J. Laser Appl.*, vol. 27, no. S2, p. S29101, Feb. 2015.

[43] C. Correa *et al.*, "Random-type scanning patterns in laser shock peening without absorbing coating in 2024-T351 Al alloy: A solution to reduce residual stress anisotropy," *Opt. Laser Technol.*, vol. 73, pp. 179–187, Oct. 2015.

[44] J. P. Nobre, M. Kornmeier, A. M. Dias, and B. Scholtes, "Use of the hole-drilling method for measuring residual stresses in highly stressed shot-peened surfaces," *Exp. Mech.*, vol. 40, no. 3, pp. 289–297, Sep. 2000.

[45] C. Rubio-González *et al.*, "Effect of laser shock processing on fatigue crack growth and fracture toughness of 6061-T6 aluminum alloy," *Mater. Sci. Eng. A*, vol. 386, no. 1–2, pp. 291–295, Nov. 2004.

[46] U. Trdan, J. A. Porro, J. L. Ocaña, and J. Grum, "Laser shock peening without absorbent coating (LSPwC) effect on 3D surface topography and mechanical properties of 6082-T651 Al alloy," *Surf. Coat. Technol.*, vol. 208, pp. 109–116, Sep. 2012.

[47] N. S. Rossini, M. Dassisti, K. Y. Benyounis, and A. G. Olabi, "Methods of measuring residual stresses in components," *Mater. Des.*, vol. 35, pp. 572–588, Mar. 2012.

[48] G. S. Schajer, "Relaxation Methods for Measuring Residual Stresses: Techniques and Opportunities," *Exp. Mech.*, vol. 50, no. 8, pp. 1117–1127, Jul. 2010.

[49] V. M. Measurements, "Measurement of residual stresses by the hole drilling strain gage method," Tech Note TN-503-6, 2007.

[50] F. Z. Dai, J. Z. Lu, Y. K. Zhang, D. P. Wen, X. D. Ren, and J. Z. Zhou, "Effect of laser spot size on the residual stress field of pure Al treated by laser shock processing: Simulations," *Appl. Surf. Sci.*, vol. 316, pp. 477–483, Oct. 2014.

[51] P. Peyre, R. Fabbro, L. Berthe, X. Scherpereel, and A. Le Cornec, "Laser shock processing with small impacts," 1996, vol. 2789, pp. 125–132.

[52] P. Peyre *et al.*, "Surface modifications induced in 316L steel by laser peening and shot-peening. Influence on pitting corrosion resistance," *Mater. Sci. Eng. A*, vol. 280, no. 2, pp. 294–302, Mar. 2000.

[53] P. Peyre, L. Berthe, X. Scherpereel, and R. Fabbro, "Laser-shock processing of aluminium-coated 55C1 steel in water-confinement regime, characterization and application to high-cycle fatigue behaviour," *J. Mater. Sci.*, vol. 33, no. 6, pp. 1421–1429, Mar. 1998.

Chapter 6

Laser Shock Peening: a promising tool for tailoring metallic microstructures in Selective Laser Melting

N. Kalentics[1,*], K. Huang[1, 2,*], M. Ortega[1], A. Burn[3], V. Romano[4], R. E. Logé[1]

1. Thermomechanical Metallurgy Laboratory – PX Group Chair, Ecole Polytechnique Fédérale de Lausanne (EPFL), CH-2002 Neuchâtel, Switzerland
2. State Key Laboratory for Manufacturing Systems Engineering, Xi'an Jiaotong University, Xi'an 710049, Shaanxi, People's Republic of China
3. Switzerland Innovation Park Biel/Bienne SIPBB, Swiss Advanced Manufacturing Center SAMC, Aarbergstrasse 46, 2503 Biel/Bienne, Switzerland
4. Bern University of Applied Sciences BUAS, Applied Laser-, Photonics- and Surface Technologies ALPS, Pestalozzistrasse 20, 3400 Burgdorf, Switzerland

Contribution:

Nikola Kalentics designed the experiment, did the Laser Shock Peening treatments, and assisted in making of the EBSD maps and microhardness measurements, interpretation of results and wrote the manuscript.

Abstract

Metallic parts made by Selective Laser Melting (SLM) are known for their heterogeneous microstructures in the as-built (AB) state. In this paper, Laser Shock Peening (LSP) was performed on a 316L stainless steel part fabricated by SLM. The LSP treatment increases the stored energy in the material but does not lead to measurable grain refinement. When subsequently annealed, the LSP treated sample undergoes recrystallization and transforms into a refined equiaxed structure, while this transformation is not activated yet for the AB sample. The LSP strategy therefore offers new routes for the selective 3D control of microstructures and mechanical properties of SLM parts.

1. Introduction

Selective Laser Melting (SLM) is a very well-known Additive Manufacturing process, in which the part is built in a layer-wise manner. A powder bed is deposited and selectively fused by a focused laser beam, and this sequence is repeated until completion of the part. SLM gives the ability to produce parts with increasingly complex geometries which are difficult or impossible to produce by conventional methods. However, the undesirable microstructure still presents an important limitation of the process. During the fabrication, due to the low thermal conductivity of the surrounding powder, the heat deposited by the laser beam is mostly extracted through the previously solidified layers, e.g. see Vilaro et al. (2012). This results in a thermal gradient along the building direction and directional solidification. Excellent studies made by Vrancken et al. (2012) as well as by Simonelli et al. (2012) demonstrate that, after solidification, the grain structure is most of the time columnar and grain size in the building direction can extend considerably, as a result of an "epitaxial" growth along a preferred crystallographic orientation, which is <100> in alloys with a cubic structure. The combination of a coarse grain structure with a strong crystallographic texture leads to non-optimal anisotropic mechanical properties of the parts made by SLM, which represents a known limitation of the SLM process.

Different methods have been used to tailor the microstructures of SLM samples. Since grain orientation and grain size are directly affected by the cooling rate and heat conduction during the solidification phase, attempts were made by Kruth et al. (2010) as well as by Song et al. (2012) to control the thermal exchanges and produce more appropriate fine and equiaxed microstructures. Even though the cooling rate can vary to a certain degree by tuning the SLM process parameters (e.g. laser scanning speed, laser power), the acceptable processing windows

are usually very narrow. An increase of the scanning speed leads to an unstable discontinuous melting track and the formation of pores, see for example Dadbakhsh and Hao (2014). This results in a detrimental decrease of the parts density which strongly affects the mechanical properties of the material. Low part density used to be one of the strongest limitations of the SLM process (and its predecessor, Selective Laser Sintering), which therefore limited its application to mostly prototyping purposes. Nowadays it is broadly accepted that an industrial use of SLM as a production method is only possible if part densities above 99 percent can be achieved. This is only possible in relatively small process windows, which in practice often excludes fine-tuning of the microstructure by varying process parameters such as power density, scanning velocity and hatching distance.

Laser Shock Peening (LSP) is a surface treatment method, which similarly to Shot Peening (SP) and Ultrasonic Shot Peening (USP) plastically deforms the surface region of the part, and introduces compressive residual stresses (CRS), see e.g. P. Peyre et al. (1996), and Cellard et al. (2012). Beneficial effects of LSP treatments include fatigue life increase, and improved resistance to stress corrosion cracking and fretting fatigue (Montross et al. (2002)). Nalla et al. (2003) demonstrate that these CRS can, depending on the treated material, reach a depth of more than one millimeter, therefore limiting partially or completely any applied tensile stress in the subsurface region.

Initial investigation made by Kalentics et al. (2017) on the effect of the LSP treatment on 316L SLM samples has shown that the tensile residual stresses (TRS) inherited from SLM processing can easily be converted to CRS. Also, a different study by Kalentics et al. (2017) showed that by periodically repeating the LSP treatment during the SLM building phase, deeper and more pronounced plastic deformation and CRS can be introduced near the external surface, with a further expected beneficial effect on fatigue life. This idea led to the concept of 3D LSP – a hybrid Additive Manufacturing process which combines LSP and SLM (patent US20170087670A1, 2017). However, to the best of knowledge of the authors, the detailed effect of LSP on SLM part microstructures has not been investigated until now. Since the main goal of the conventional LSP process is usually the increase of fatigue life, the corresponding analysis of microstructures is often very general. Limited investigations were made by Trdan et al. (2014) with Al-Mg-Si alloy and by Lu et al. (2017) with commercially pure (CP) titanium, and grain refinement was reported to occur within a shallow surface layer of several micrometers thickness. In contrast with these observations, some of the work done by Lu et al. on stainless steel (2010), aluminum (2010) and titanium (2017) report grain refinement up to 20, 529 and 500 microns depth, respectively. The present work will therefore clarify the depth of the LSP affected zone, in terms of microstructure change, focusing on 316L stainless steel.

2. Experimental procedure

2.1 Selective Laser Melting

316L SLM samples were produced with DIAMALLOY 1003 powders from Sulzer Metco, Switzerland. Selective Laser Melting was performed on a Concept M2 (Concept Laser GmbH, Germany) equipped with a fiber laser which was operated in a continuous mode and with a wavelength of 1070 nm. The geometry of the samples was a 20x20x7 mm^3 cuboid, as illustrated in Figure 1a. The operating SLM parameters, i.e. laser power, spot size, scanning speed, powder layer thickness and hatch distance were 125 W, 90 µm, 600 mm/s, 0.03 mm and 0.105 mm, respectively. Processing was done under nitrogen atmosphere and the oxygen content was maintained below 1 % during the process. These samples are hereafter referred to as SLM AB samples (AB = As Built).

2.2 Laser Shock Peening

Laser Shock Peening (LSP) treatments were applied on the top surface of the SLM AB samples (see Figure 1a). The laser source was a Nd:YAG SAGA HP - class laser from Thales Group with a pulse duration of 6.3 ns at 1064 nm wavelength and a "top-hat" beam spatial energy distribution. Based on previous results from Kalentics et al. (2017), a laser spot of 1 mm diameter with a laser energy of 0.4 J and a pulse frequency of 5 Hz were chosen. This gave a power density of 7.2 GW/cm^2. Using the empirical equation $P\ (GPa) = 1.75\ \sqrt{I_0}(\frac{GW}{cm^2})$ from Courapied et al. (2015), the pressure created at the surface of the part was estimated at 4.7 GPa. Three successive LSP treatments with a spot overlap of 80% were applied without a protective ablative layer. These samples are designated as SLM LSP samples.

2.3 Heat treatment

Some of the SLM AB and SLM LSP samples were further heat treated to illustrate LSP effects on microstructure evolution during high temperature annealing. Heating was conducted in a conventional furnace pre-heated to 1100 °C, with a duration of 10 min, followed by

immediate water quench. The microstructures of SLM AB and SLM LSP samples, as well as their heat treated counterparts, were characterized by Electron back-scatter diffraction (EBSD) in a FEI XLF-30 field emission gun scanning electron microscope (FEG-SEM). For the LSP treated samples, sections parallel to the front surface and containing the build direction were scanned, with the LSP treated zone on the right side, as indicated in Figure 1b. In order to make meaningful comparisons, microstructure characterizations were performed on the same location for samples with and without LSP treatment, using exactly the same scanning parameters (e.g. step size of 0.5 μm).
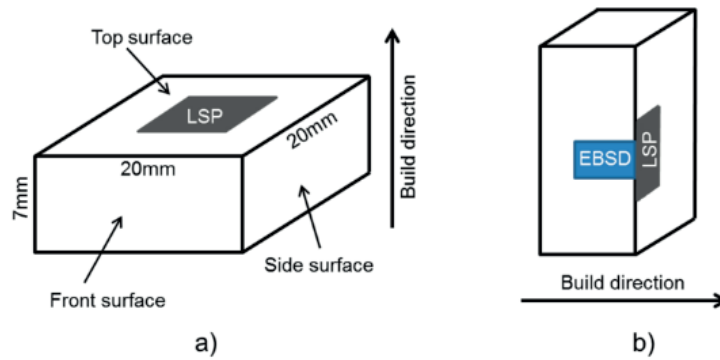
Fig. 1 a) Geometry of the SLM LSP sample; b) Area characterized by EBSD, with the build direction (BD) horizontal.

2.4 Microhardness tests

Vickers microhardness tests were conducted at room temperature using a 25 g load for a 12 s hold time, with a Q10A machine from Qness GmbH (Germany). As per ISO 6507-1 recommendations, and to avoid conflicting noise within the results, the distance in between two consecutive indentations was larger than 3 times the diagonal of the indented square. Microhardness tests were performed every 50 μm starting at 50 μm below the surface and going up to 750 μm in depth, following the ISO 6507-1 condition. The experiment was repeated 5 times and the average with their standard deviation was plotted.

3. Results and discussion

3.1 Microhardness

Microhardness measurements were done for SLM AB and SLM LSP, with results presented in Figure 2. We can observe an increase from 282 HV to 391 HV for the SLM AB and SLM LSP respectively, at a depth of 50 µm from the treated surface. Compared to the SLM AB hardness, this represents an increase of 38.65%, which can be attributed to the strain hardening effect, as already shown in previous studies by Wu et al. (2018) on titanium alloys. Moreover, the slope of the hardness curve vs depth for the SLM LSP sample is very pronounced, confirming that the LSP effect decreases with depth, as already reported in Kalentics et al. (2017). At a depth of ~400 µm from the treated surface the effect of LSP becomes negligible.

Fig. 2 Vickers microhardness results for SLM AB and SLM LSP samples.

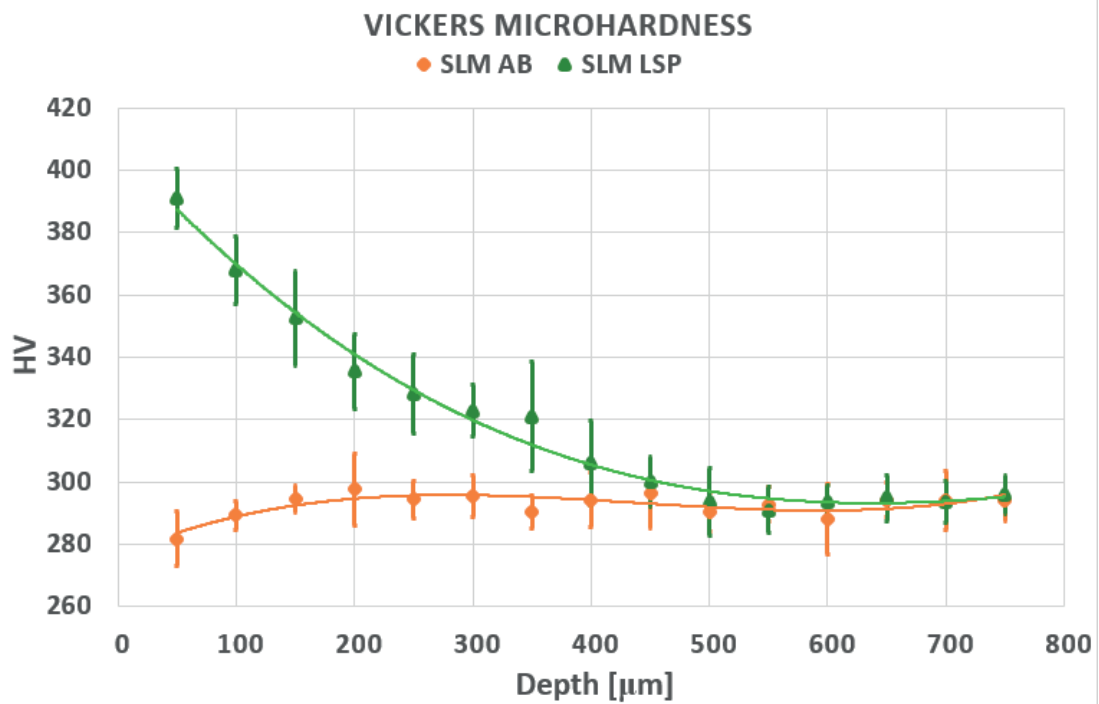In Figure 3, Vickers microhardness results are presented for the SLM AB and SLM LSP samples with and without a heat treatment, corresponding to the microstructures described in Figures 4 and 5. At 50µm from the surface, the heat treatment (~10 min at 1100°C) results in a

drastic decrease of hardness, up to 241 HV and 217 HV for the SLM AB and SLM LSP samples, respectively. Heat treated SLM LSP sample consistently has a lower hardness compared to SLM AB heat treated samples, up to a depth of ~400 μm from the surface. This depth corresponds exactly to the recrystallized region shown in Figure 5d. Beyond this depth, the hardness of heat treated samples can no longer be distinguished.
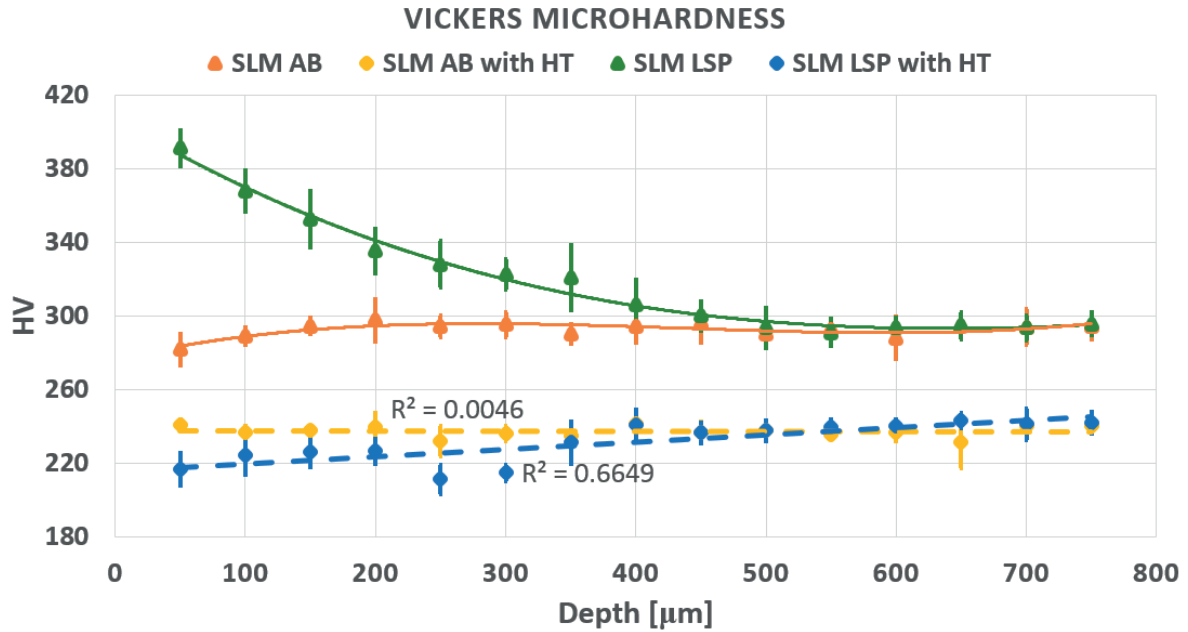
Fig. 3 Vickers microhardness results of SLM AB and SLM LSP samples before and after annealing.

3.2 Microstructure

The microstructures of the SLM AB and SLM LSP samples are shown in Figures 4a and 4b, respectively, with the same examined surface of 826 × 619 μm^2. The non-indexed points due to porosities are shown in black and can be observed in all figures, without any measurable effect of the LSP treatment on porosity size. The SLM microstructure is far from being equiaxed, it is dominated by coarse grains elongated along the (horizontal) build direction (Figure 4a). A similar grain structure is observed in the SLM LSP sample, as illustrated in Figure 4b. The grain refinement indicated by Lu et al. (2010) and Lu et al. (2017), is not achieved here, even close to the treated LSP surface, i.e. the very right side of the EBSD map in Figure 4b. Local crystallographic misorientation maps are provided in Figures 4c and 4d, with a scale between 0° and 3.5°, in agreement with Figure 7a. These maps measure the average misorientations between neighboring pixels, looking at regions extending up to it's the seventh nearest neighbor, excluding

misorientations beyond 5°. It appears that the SLM LSP sample does exhibit higher misorientation levels than the SLM AB one, as shown in Figures 4c and 4d.
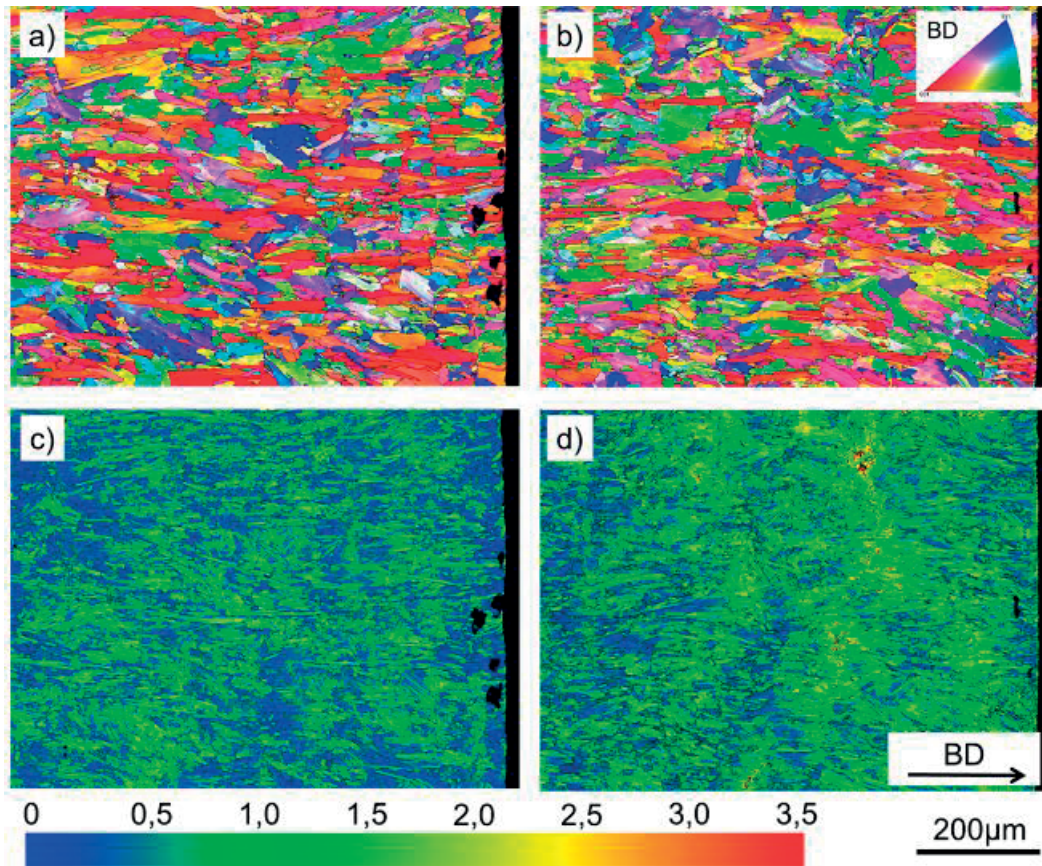
Fig. 4 EBSD maps of SLM AB and SLM LSP samples before heat treatment; a) Inverse pole figure map of the SLM AB sample; b) Inverse pole figure map of the SLM LSP sample; c) Local misorientation map of the SLM AB sample; d) Local misorientation map of the SLM LSP sample.

The SLM AB and SLM LSP samples were further heat treated at 1100°C for 10 min, the microstructures of which are shown in Figure 5. After this heat treatment, no recrystallization can be observed for the SLM AB sample, as can be seen in Figures 5a and 5c (looking at planes parallel to the front surface, see Figure 1a). This has also been confirmed by EBSD maps scanned parallel to the side surface. In contrast, significant recrystallization is achieved in the SLM LSP sample, as shown in Figures 5b and 5d. It is noticed that recrystallized grains are characterized by the presence of numerous annealing twins (represented by red lines in Figure 5b), and by very low internal local misorientations (<0.5°). Recrystallized grains are close to equiaxed, with sizes much smaller than the original elongated coarse grains. Recrystallization only dominates in the

region close to the LSP treated surface, with a penetration depth of ~400 µm, and only sparse recrystallized grains can be seen further below. Even though non-recrystallized grains still exist in the recrystallized zone, i.e. less than ~400 µm away from the surface, their sizes have decreased as a result of the nucleation and growth of recrystallized grains around them. Since the crystallographic texture of the AB sample is quite weak (~2.7 times random intensity), which is in full agreement with the study by Gray III et al. (2017) on the same material, recrystallization did not lead to significant randomization of texture.
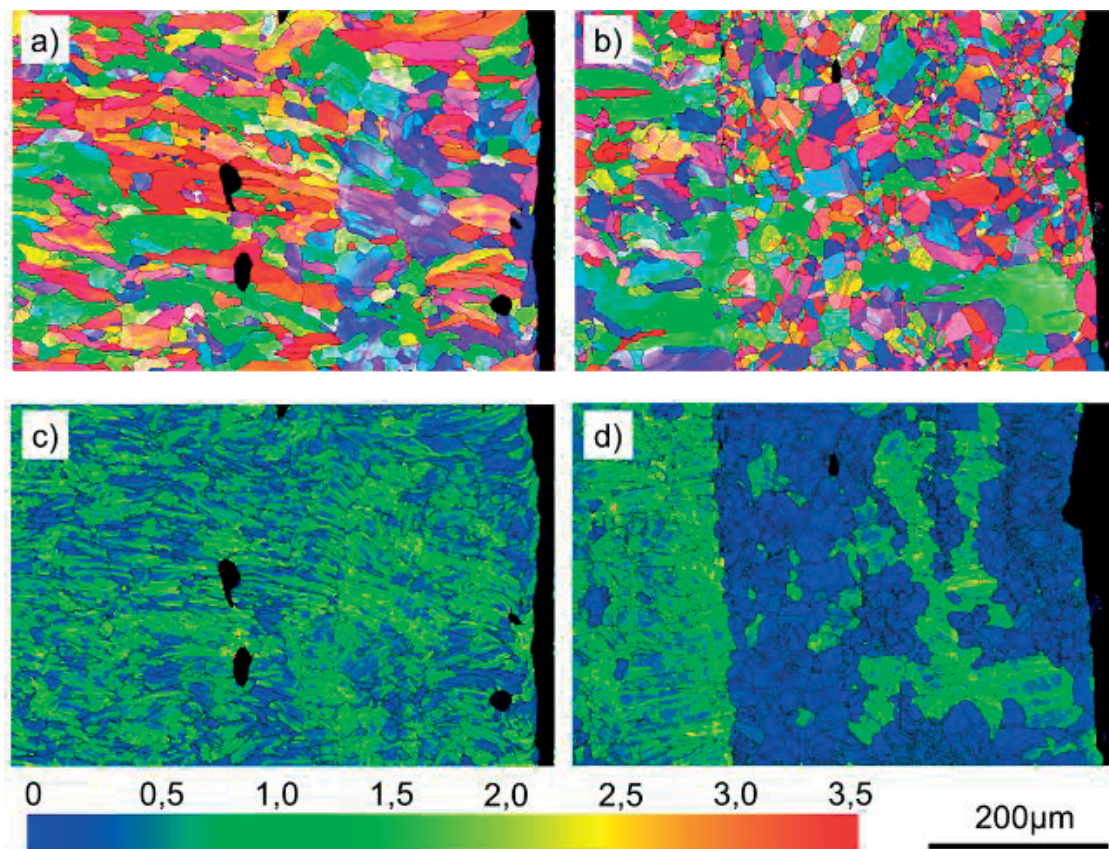
Fig. 5 EBSD maps of SLM AB and SLM LSP samples after heat treatment at 1100°C for 10 min; a) Inverse pole figure map of the SLM AB sample; b) Inverse pole figure map of the SLM LSP sample; c) Local misorientation map of the SLM AB sample; d) Local misorientation map of the SLM LSP sample.

Our studies also showed that recrystallization can still be completed for the SLM AB sample at 1100°C after a long annealing time of 2 h, however, this leads to a much coarser grain structure (Figure 6). For materials which recover faster than 316L stainless steel (e.g. materials of high stacking fault energy) during annealing, full recrystallization may however not be reached

by post-heat treatments even at very high temperature, as demonstrated by Kunze et al. (2015) and by Divya et al. (2016). In such cases, LSP might provide the needed additional driving force.
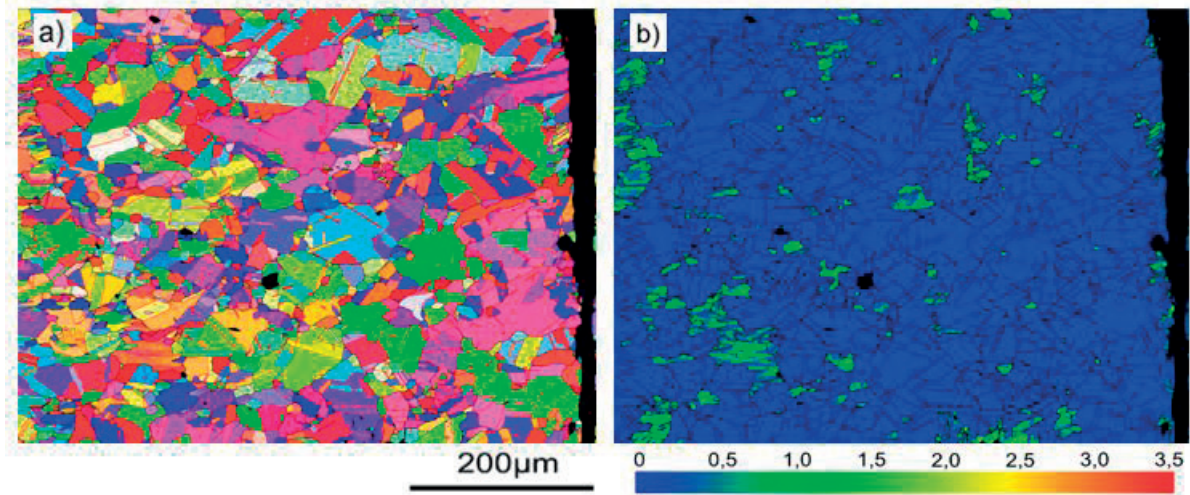
Fig. 6 EBSD maps of the SLM AB sample annealed at 1100°C for 2h; a) Inverse pole figure map showing the coarse recrystallized grain structure; b) Local misorientation map evidencing full recrystallization.

The higher local misorientation level after LSP treatment of the SLM LSP samples, as shown qualitatively in Figure 4, should be part of the reason for the larger recrystallization fraction in the SLM LSP sample after heat treatment. A quantitative comparison of local misorientation distributions for the SLM AB and SLM LSP samples is shown in Figure 7, corresponding to the EBSD maps given in Figure 4. The measured difference is surprisingly small compared to the large difference in recrystallized fraction. The higher driving force which leads to faster recrystallization for the SLM LSP samples therefore deserves some discussion.
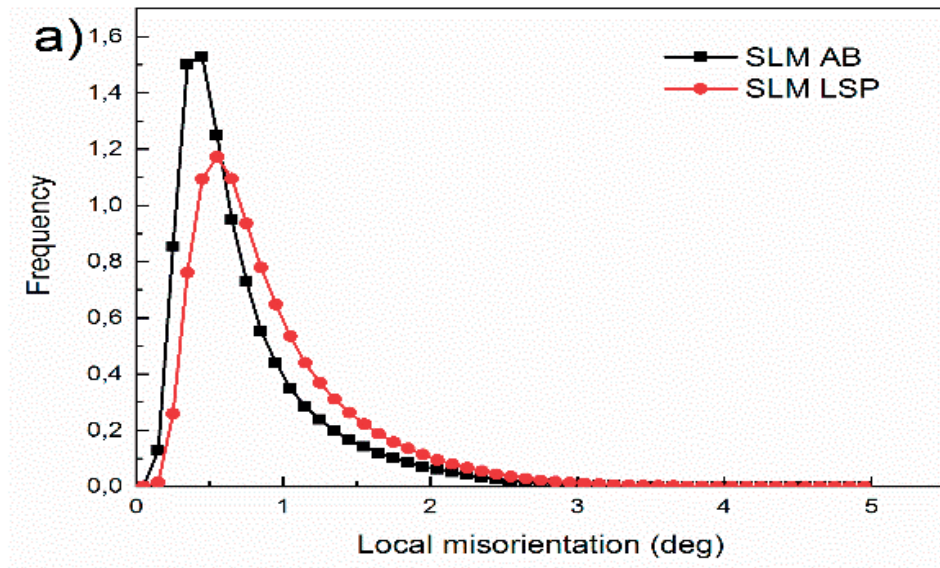
Fig.7 Local misorientation distributions of the SLM AB and SLM LSP samples.

4. Discussion

4.1 Recrystallization kinetics

First, even though the SLM AB samples exhibit tensile residual stresses, the compressive residual stresses in the SLM LSP samples are higher in magnitude, as demonstrated in our previous studies by Kalentics et al. (2017). The fact that higher residual stress could accelerate recrystallization was demonstrated by Toda-Caraballo et al. (2010) through simulation and by Liu et al. (2011) experimentally, for different types of materials. Second, it can be seen in Figure 8b that a large number of fine deformation twins were formed in the SLM LSP sample. As explained by Rollet et al. (2004), these deformation twins provide potential nucleation sites for recrystallization but are not taken into account by the local misorientation maps.

The fact that no deformation twins appear in the SLM AB sample, and that the magnified features shown in Figure 8b are indeed deformation twins is shown in Figure 8a and 8c, respectively.

Finally, only geometrically necessary dislocations (GNDs) are measured by the EBSD local misorientation measurements. Statistically stored dislocations (SSDs) in the SLM LSP sample

might be higher than those in the SLM AB sample due to the LSP process, but this would need confirmation by other dislocation characterization techniques.
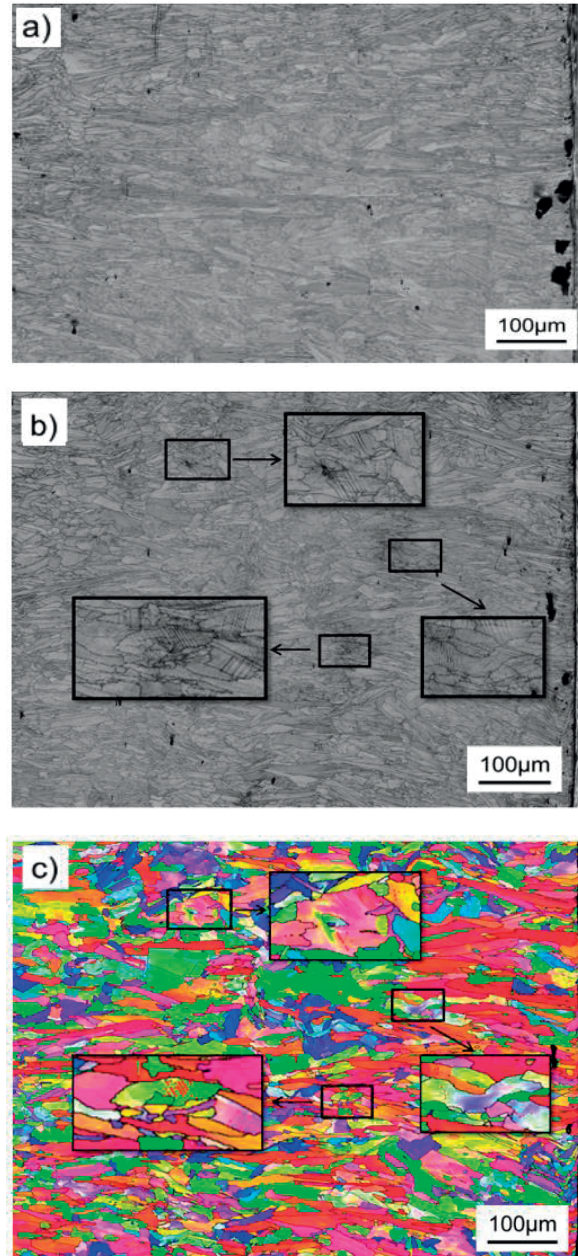
Fig. 8 a) EBSD band contrast map of the SLM AB sample showing no indication of deformation twins; b) EBSD band contrast maps showing the mechanical twins magnified in the SLM LSP sample; c) Inverse pole figure, deformation twin (60°<111> FCC twins) boundaries represented by red lines, noting that not all the deformation twin boundaries are resolved.

4.2 LSP treatment

LSP process parameters such as overlap rate, laser energy etc. can be further tuned to achieve larger penetration depth of plastic deformation. Moreover, it is envisaged that, if LSP treatment is performed repeatedly every few printed layers, i.e. if we use the 3D LSP technique, a fine equiaxed grain structure could be achieved in the entire volume of the part, with appropriate post heat treatment. The LSP process thus provides an important route to solve one of the bottlenecks of the SLM produced metallic parts, i.e. heterogeneous and textured microstructure, with its associated undesirable mechanical properties. With this approach it is then possible to decouple the search for optimal SLM process parameters, with the major objectives of increasing process efficiency and material density, from the microstructure design which operates by subsequent heat treatment. Such a heat treatment would evolve the microstructure differently in LSP treated zones and other non-treated zones, i.e. this would lead to selective microstructure control and therefore 3D microstructure design. Future work still needs to focus on the effect of LSP on crystallographic texture, and on mechanical properties of the post heat-treated SLM LSP samples.

5. Conclusions

In this paper, Laser Shock Peening treatments have been applied on SLM samples with the objective of analyzing the resulting microhardness and microstructure, both in the as – built state and after heat treatment. The following conclusions can be drawn:

- LSP significantly increases the microhardness of SLM AB parts in the near surface region but does not change grain size.
- In the LSP affected zone, recrystallization kinetics is strongly accelerated upon heat treatment, resulting in a refined, equiaxed grain structure, very different from the SLM AB microstructure.
- The combination of SLM with Laser Shock Peening offers a promising new route for the 3D control of microstructures and mechanical properties of SLM parts.

Data availability

The raw/processed data required to reproduce these findings cannot be shared at this time due to time limitations. However, data represented in the tables and graphs would be sufficient to reproduce the results.

References

Cellard, C., Retraint, D., François, M., Rouhaud, E., Le Saunier, D., 2012. Laser shock peening of Ti-17 titanium alloy: Influence of process parameters. Mater. Sci. Eng. A. 532, 362–372.

Courapied, D., Berthe, L., Peyre, P., Coste, F., Zou, J.P., Sautivet, A. M., 2015. Laser-delayed double shock-wave generation in water-confinement regime. J. Laser Appl. 27, S29101.

Dadbakhsh, S., Hao, L., 2014. Effect of Layer Thickness in Selective Laser Melting on Microstructure of Al/5 wt.%Fe2O3 Powder Consolidated Parts. J. Sci. World. 2014.

Divya, V.D., Muñoz-Moreno, R., Messé, O.M.D.M., Barnard, J.S., Baker, S., Illston, T., Stone., H.J., 2016. Microstructure of selective laser melted CM247LC nickel-based superalloy and its evolution through heat treatment. Mater. Charact. 114, 62–74.

Gray, G.T., Livescu, V., Rigg, P.A., Trujillo, C.P., Cady, C.M., Chen, S.R., Carpenter, J.S., Lienert, T.J., Fensin, S. J., 2017. Structure/property (constitutive and spallation response) of additively manufactured 316L stainless steel. Acta Mater. 138, 140–149.

Kalentics, N., Boillat, E., Peyre, P., Ćirić-Kostić, S., Bogojević, N., Logé, R.E., 2017. Tailoring residual stress profile of Selective Laser Melted parts by Laser Shock Peening. Addit. Manuf. 16, 90–97.

Kalentics, N., Boillat, E., Peyre, P., Gorny, C., Kenel, C., Leinenbach, C., Jhabvala, J., Logé., R.E., 2017. 3D Laser Shock Peening – A new method for the 3D control of residual stresses in Selective Laser Melting. Mater. Des. 130, 350–356.

Kalentics, N., Logé, R.E., Boillat, E., 2017. Method and Device for Implementing Laser Shock Peening or Warm Laser Shock Peening During Selective Laser Melting. US20170087670 A1.

Konijnenberg, P.J., Zaefferer, S., Raabe, D., 2015. Assessment of geometrically necessary dislocation levels derived by 3D EBSD. Acta Mater. 99, 402–414.

Kruth, J.P., Badrossamay, M., Yasa, E., Deckers, J., Thijs, L., Van Humbeeck, J., 2010. Part and material properties in selective laser melting of metals. Proceedings of the 16th International Symposium on Electromachining, Shanghai, China, pp. 1-12.

Kunze, K., Etter, T., Grässlin, J., Shklover, V., 2015. Texture anisotropy in microstructure and mechanical properties of IN738LC alloy processed by selective laser melting (SLM). Mater. Sci. Eng. A. 620, 213–222.

Liu, F., Lin, X., Yang, G., Song, M., Chen, J., Huang, W., 2011. Microstructure and residual stress of laser rapid formed Inconel 718 nickel-base superalloy. Opt. Laser Technol. 43, 208–213.

Lu, J.Z., Luo, K.Y., Zhang, Y.K., Sun, G.F., Gu, Y.Y., Zhou, J.Z., Ren, X.D., Zhang, X.C., Zhang, L.F., Chen, K.M., Cui, C.Y., Jiang, Y.F., Feng, A.X., Zhang L., 2010. Grain refinement mechanism of multiple laser shock processing impacts on ANSI 304 stainless steel. Acta Mater. 58, 16, 5354–5362.

Lu, J. Z., Luo, K.Y., Zhang, Y.K., Cui, C.Y., Sun, G.F., Zhou, J.Z., Zhang, L., You, J., Chen, K.M., Zhong, J.W., 2010. Grain refinement of LY2 aluminum alloy induced by ultra-high plastic strain during multiple laser shock processing impacts. Acta Mater. 58, 11, 3984–3994.

Lu, J. Z., Wu, L.J., Sun, G.F., Luo, K.Y., Zhang, Y.K., Cai, J., Cui, C.Y., Luo, X.M., 2017. Microstructural response and grain refinement mechanism of commercially pure titanium subjected to multiple laser shock peening impacts. Acta Mater. 127, 252–266.

Montross, C.S., Wei, T., Ye, L., Clark, G., Mai, Y.-W., 2002. Laser Shock Processing and its Effects on Microstructure and Properties of Metal Alloys: A Review. Int. J. Fatigue. 24, 10, 1021–1036.

Nalla, R.K., Altenberger, I., Noster, U., Liu, G.Y., Scholtes, B., Ritchie, R.O., 2003. On the influence of mechanical surface treatments—deep rolling and laser shock peening—on the fatigue behavior of Ti–6Al–4V at ambient and elevated temperatures. Mater. Sci. Eng. A. 355, 1–2, 216–230.

Peyre, P., Fabbro, R., Merrien, P., Lieurade, H.P., 1996. Laser shock processing of aluminium alloys. Application to high cycle fatigue behaviour. Mater. Sci. Eng. A. 210, 1–2, 102–113.

Rollett, A., Humphreys, F.J., Rohrer, G. S., Hatherly, M., 2004. Recrystallization and Related Annealing Phenomena, second ed. Elsevier, Oxford.

Simonelli, M., Tse, Y.Y., Tuck, C., 2012. Further Understanding of Ti6Al4V Selective Laser Melting using texture analysis. Proceedings of the 23rd Annual International Solid Freeform Fabrication Symposium, Austin TX, USA, pp. 480–491.

Song, B., Dong, S., Zhang, B., Liao, H., Coddet, C., 2012. Effects of processing parameters on microstructure and mechanical property of selective laser melted Ti6Al4V. Mater. Des. 35, 120–125.

Toda-Caraballo, I., Chao, J., Lindgren, L.E., Capdevila, C., 2010. Effect of residual stress on recrystallization behavior of mechanically alloyed steels. Scr. Mater. 62, 1, 41–44.

Trdan, U., Skarba, M., Grum, J., 2014. Laser shock peening effect on the dislocation transitions and grain refinement of Al–Mg–Si alloy. Mater. Charact. 97, 57–68.

Vilaro, T., Colin, C., Bartout, J.D., Nazé, L., Sennour, M., 2012. Microstructural and mechanical approaches of the selective laser melting process applied to a nickel-base superalloy. Mater. Sci. Eng. A. 534, 446–451.

Vrancken, B., Thijs, L., Kruth, J.-P., Van Humbeeck, J., 2012. Heat treatment of Ti6Al4V produced by Selective Laser Melting: microstructure and mechanical properties. J. Alloys Compd. 541, 177–185.

Wu, L.J., Luo, K.Y., Liu, Y., Cui, C. Y., Xue, W., Lu, J.Z., 2018. Effects of laser shock peening on the micro-hardness, tensile properties, and fracture morphologies of CP-Ti alloy at different temperatures. Appl. Surf. Sci., 431, 122–134.

Figure and Table Captions

Fig. 1 a) Geometry of the SLM LSP sample; b) Area characterized by EBSD, with the build direction (BD) horizontal.

Fig. 2 Vickers microhardness results for non-heat treated samples.

Fig. 3 Vickers microhardness results of SLM AB and SLM LSP samples before and after annealing.

Fig. 4 EBSD maps of SLM AB and SLM LSP samples before heat treatment. a) Inverse pole figure map of the SLM AB sample; b) Inverse pole figure map of the SLM LSP sample; c) Local misorientation map of the SLM AB sample; d) Local misorientation map of the SLM LSP sample.

Fig. 5 EBSD maps of SLM AB and SLM LSP samples after heat treatment at 1100°C for 10 min. a) Inverse pole figure map of the SLM AB sample; b) Inverse pole figure map of the SLM LSP sample; c) Local misorientation map of the SLM AB sample; d) Local misorientation map of the SLM LSP sample.

Fig. 6 EBSD maps of the SLM AB sample annealed at 1100°C for 2h. a) Inverse pole figure map showing the coarse recrystallized grain structure; b) Local misorientation map evidencing full recrystallization.

Fig.7 Local misorientation distributions of the SLM AB and SLM LSP samples.

Fig. 8 a) EBSD band contrast map of the SLM AB sample showing no indication of deformation twins; b) EBSD band contrast maps showing the mechanical twins magnified in the SLM LSP sample; c) Inverse pole figure, deformation twin (60°<111> FCC twins) boundaries represented by red lines, noting that not all the deformation twin boundaries are resolved.

92

Chapter 7

3D Laser Shock Peening as a way to improve geometrical accuracy in Selective Laser Melting

Nikola Kalentics[1,*], Andreas Burn[2], Michael Cloots[3], Roland E. Logé[1]

1. Thermomechanical Metallurgy Laboratory – PX Group Chair, Ecole Polytechnique Fédérale de Lausanne (EPFL), CH-2002 Neuchâtel, Switzerland
2. Switzerland Innovation Park Biel/Bienne SIPBB, Swiss Advanced Manufacturing Center SAMC, Aarbergstrasse 46, 2503 Biel/Bienne, Switzerland
3. Irpd AG, Lerchenfeldstrasse 3, 9014 St.Gallen, Switzerland

Corresponding author: nikola.kalentics@epfl.ch

Contribution:

Nikola Kalentics designed the experiment and the SLM sample geometry, did the Laser Shock Peening treatments, residual stress and distortion measurements, interpretation of results and wrote the manuscript.

Abstract

One of the major drawbacks of Selective Laser Melting (SLM) is the accumulation of tensile residual stresses (TRS) in the surface and subsurface zones of produced parts which can lead to cracking, delamination, geometrical distortions and a decrease in fatigue life. 3D Laser Shock Peening (3D LSP) is a novel hybrid method which introduces a repetitive Laser Shock Peening (LSP) treatment *during* the manufacturing phase of the Selective Laser Melting (SLM) process. In this paper, the ability of 3D LSP to convert TRS into beneficial compressive residual stresses and their subsequent effect on the geometrical accuracy of produced parts was investigated. Samples made of Ti6Al4V were manufactured with the 3D LSP process and treated with different processing parameters. Cuboidal samples were used for residual stress measurements and the evolution of residual stresses was investigated. Geometrical distortions were measured on bridge like samples and the influence on the final sample geometry was quantified. A significant improvement in geometrical accuracy resulting from reduced distortions was observed in all selected 3D LSP processing conditions.

1. Introduction

Selective Laser Melting (SLM) is one of the most widely researched Additive Manufacturing (AM) processes in which a part is built in a layer-wise method. SLM is known to be able to produce near net shape parts with very complex geometries, which are often very difficult or even impossible to manufacture with conventional methods. On the other hand, one of the major drawbacks of the process is the generation of tensile residual stresses (TRS) that accumulate near the surface during the building process and can cause significant distortion in the geometry of the part [1]–[4]. Accumulation of these stresses can even cause delamination and process failure during the building phase [1], [2], [5]. Different approaches addressing this problem were applied but with limited success. Baseplate preheating was used to decrease the thermal gradients during the building phase of the process, decreasing the TRS accumulation, however only a limited reduction of up to 40% was observed [6]. Baseplate preheating is usually applied with a maximum temperature of 200°C since higher chamber temperature will, while having a beneficial effect on the reduction of TRS, inevitably cause lower cooling rates. These reduced cooling rates can lead to undesirable mechanical properties, such as a reduction in yield strength and fatigue limit [7], [8]. Stress relieving by systematic laser rescanning of the previously solidified layer was also applied [6] and showed up to a 55% decrease of TRS. Although somewhat beneficial, laser rescanning of every layer significantly diminishes the productivity of the entire process, which is

94

contrary to the long lasting tendency of increasing the productivity by applying high power [9], [10] or using multiple lasers [11]. A heat treatment can be applied after the part is made and a reduction of up to 70% in RS can be achieved [6], but this approach cannot address the accumulation of TRS during the building phase which can cause part delamination and process failure. Also, all these approaches have shown the ability to decrease TRS, but none of them can introduce beneficial compressive residual stresses (CRS) into the near surface region of a part, which, if designed accurately, should improve its fatigue life without affecting the geometrical stability [12]–[14].

3D Laser Shock Peening (3D LSP) is a novel AM process patented by the Laboratory of Thermomechanical Metallurgy at EPFL [15]. It is a hybrid process which repeatedly applies Laser Shock Peening (LSP) *during* the building phase of the SLM process, thus giving additional degrees of freedom to adapt and control residual stresses in the part. This approach is applicable to all parts, including those with complex geometry, as long as they can be manufactured by the SLM process.

With the accumulation of tensile residual stresses in large SLM parts, geometrical distortion issues tend to rise. Also, part distortion represents a significant challenge for overhangs and thin wall structures which are often manufactured by SLM. One approach when dealing with distortions consists in producing parts with an increased volume, with the intention to remove the excess material by machining after the build job. Another approach is the use of more and more sophisticated supports which have a double function as mechanical fixation of the part and as additional heat extraction channels. These compensation strategies need to be taken into account at the design stage [16] and go along with an additional time consuming pre-processing step and a reduced buy-to-fly ratio. A post build machining can be time consuming as well and altogether reduces the near net - shape advantage of the SLM process. Furthermore, the machining step is limited only to the easily accessible zones of the part and cannot always be applied to the more complex typical SLM geometries involving internal structures.

Geometrical distortion can also cause an elevation in the previously solidified layer, especially while producing overhangs and other thin walled structures, which can damage the coater during subsequent powder bed deposition. A damaged (scratched) coater is then unable to further deposit an accurate and flat powder bed layer. This leads to defects and porosities in produced parts and usually requires abortion of the part production.

Our previous work has shown that conventional LSP can easily convert TRS into more desirable compressive residual stresses (CRS) [17]. It was also demonstrated that if applied repeatedly in 3D (as in 3D LSP), the process leads to an improved accumulation of CRS [18], both in magnitude and in depth, which is expected to further increase fatigue life compared to conventional LSP treated parts, or those in the as–built (AB) SLM state.

A recent publication [19] has shown that conventional LSP can be very successful as a post treatment process of 316L SLM parts in both increasing their fatigue life and reducing geometrical distortions. Due to the material shrinkage during cooling, SLM AB samples exhibit a concave distortion curvature angle on the top surface (an exaggerated image shown in Figure 1a). In [19] LSP was applied on one side of a 213 mm x 21.6 mm SLM made 3 mm thick bar, and a convex distortion was observed on the LSP treated side. With the increase in the number of LSP treatments on the surface, the distortion curvature radius increased and reached 1120 mm after three LSP treatments on the same side (as shown in Figure 1b). When three LSP treatments were applied on the opposite side, the bar returned to an almost flat state with an arc height of only 250 microns, thus showing the interest of applying LSP as a corrective distortion post treatment. One drawback of such an approach is that it is limited to thin parts where the effect of LSP as a post treatment is sufficient to correctively address the SLM distortion. It is also restricted to simple geometries where LSP can reach the external surfaces. Both limitations are of concern when considering SLM parts, which are rarely very thin or simple in shape. Furthermore, residual stresses developed *during* the SLM process can result in shape changes of the part which can inhibit further processing, e.g. elevation of overhangs above the powder coater level. There is therefore a strong interest in developing *in situ* methods for the correction of geometrical distortions which could be applied to *any* SLM part geometry.
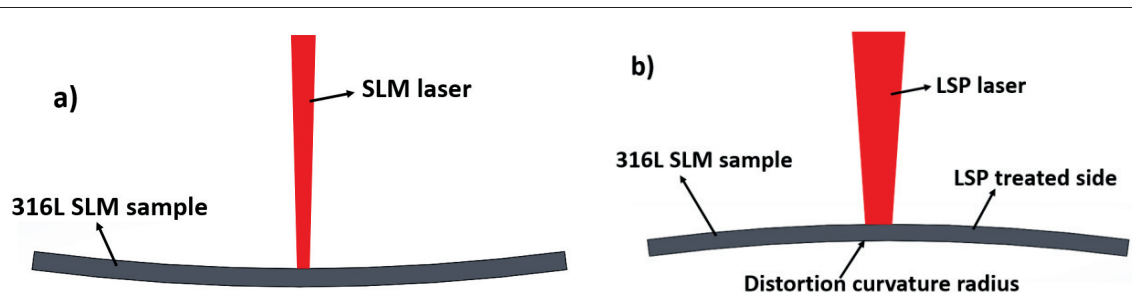
Fig. 1 a) exaggerated representation of an AB SLM sample with a concave distortion arc; b) LSP treated side of an SLM samples with a convex distortion arc of r =1120mm, modified from [19].

In this work, we show for the first time that the 3D LSP strategy can effectively reduce SLM geometrical distortions. Bridge type Ti6Al4V samples in the AB and LSP treated conditions are compared and contour accuracy is shown to be improved for all considered LSP processing conditions. Compared to previous approaches used to mitigate residual stress-based distortions, this one does not involve any heat treatment since LSP is a cold deformation process. This means that 3D LSP solves the residual stress problem with no detrimental effects on microstructure and mechanical properties.

2. Experimental setup

2.1 SLM parameters and sample geometry

Ti6Al4V was chosen since it is a widely studied SLM material with many applications in aerospace and medical fields [20]–[22]. The chemical composition is shown in Table 1. Samples were produced in a Concept Laser M2 machine equipped with a fiber laser which was operated in continuous mode. The laser has a wavelength of 1070 nm and a spot size of 150 microns. The SLM processing parameters were determined as follows: laser power of 190 W, scanning speed 950 mm/s, hatch distance 0.09 mm, and layer thickness of 0.03 mm. An island scanning strategy was selected such as to minimize TRS and associated geometrical distortion. Oxygen content in the chamber was set below 0.5 %. The Ti6Al4V powder was obtained from Concept Laser GmbH, Germany. Its commercial name is CL 41TI ELI.

	Al	V	Fe	C	O	N	H	Ti
Ti6Al4V	5.5 – 6.5	3.5- 4.5	0 - 0.25	0 - 0.008	0 - 0.13	0 - 0.05	0 - 0.012	Balance

Table 1 Chemical composition of Ti6Al4V (CL 41TI ELI), wt.% [23].

In the literature, different geometries have been used for evaluating distortion in SLM parts, most notably the cantilever [2], bridge-like [24] and three prong methods [25]. We have chosen here to produce thinner bridge-like samples in order to increase the number of samples on the baseplate. The sample geometry is shown in Figure 2 a,b, with dimensions 25mm x 10mm x 5mm, and an arc radius of 2.5mm. A total of 18 samples were produced, and the minimum thickness of the bridge overhang X (Figure 2a) was varied between 1, 2, and 3 mm. This gave a total of six samples for each group. While still attached to the baseplate, two samples from each group were treated with a conventional (surface) 2D LSP, two were left in the AB condition, and two were treated with 3D LSP. The two selected 3D LSP conditions considered either $n = 3$ or $n = 10$ SLM layers between two subsequent LSP treatments, respectively.
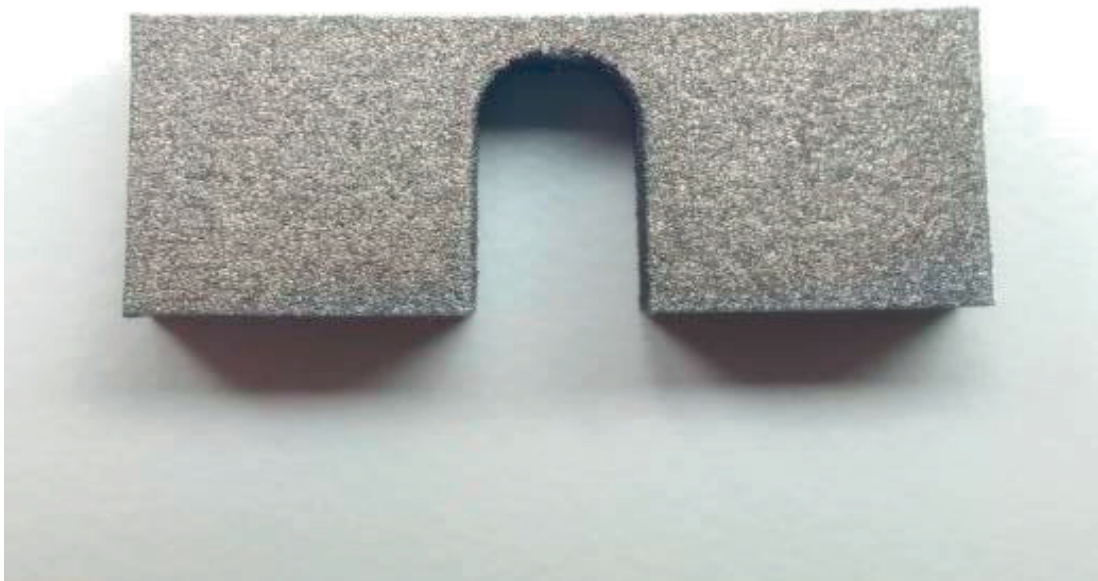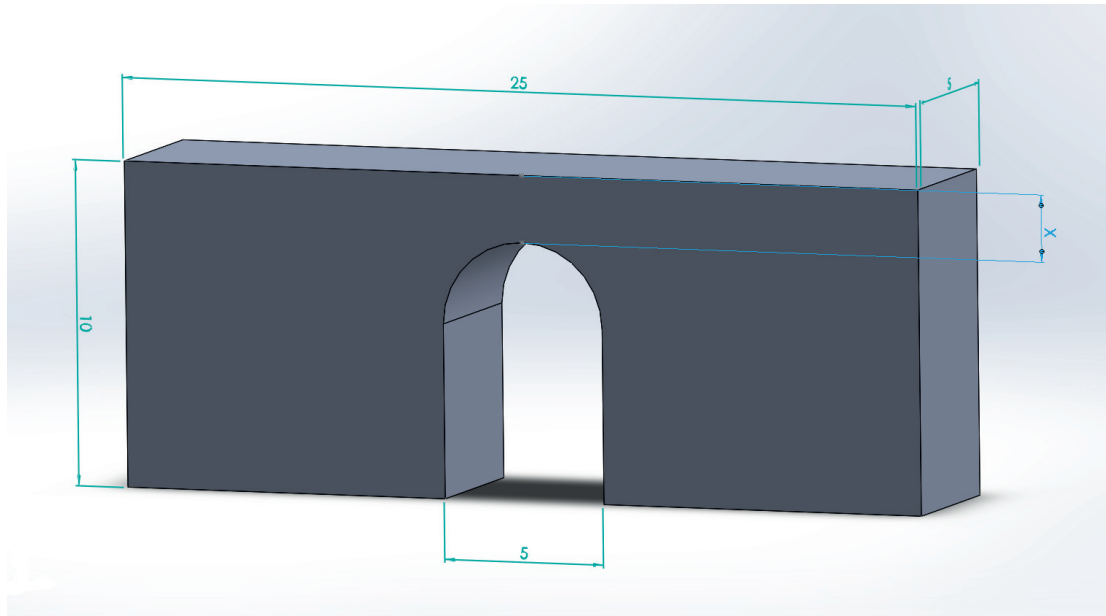
Fig. 2 a) CAD description of the miniature bridge - like sample; b) AB sample after detachment from the baseplate.

2.2 Laser Shock Peening setup

As in [18], the LSP treatment was done on a Nd:YAG SAGA HP - class laser from Thales company. For 3D LSP samples, the building phase was paused n layers before the end, and an LSP treatment was applied (see Figure 3). After the LSP treatment, the final n SLM layers were rebuilt and the LSP process was repeated. In this study, the investigated values of n were {3, 10}. For samples treated by conventional 2D LSP, only a final surface LSP treatment was performed (i.e. LSP was not applied during the SLM building process interruption). All LSP treatments were done while samples were attached to the baseplate. SLM AB samples received no LSP treatment. The LSP process parameters are given in Table 2, and the reader is directed to [18] for more information on the LSP setup.
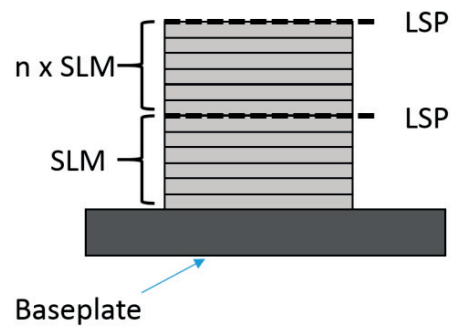
Fig. 3 Schematic of the 3D LSP process with the n number of layers between two subsequent LSP treatments.

Wavelength	1064nm
Pulse duration	6.3ns
Spot size diameter	1mm
Pulse energy	0.4J
Power density	7.2 GW/cm^2
Frequency	5Hz
Overlap value	80%

Table 2 LSP process parameters.

2.3 Residual stress measurements

Residual stresses measurements were performed on SLM samples made on the same baseplate and with the exact SLM and LSP processing parameters used for the bridge like distortion samples. The specimen geometry was a 20x20x5 mm3 cuboid and the measurements were made with the hole drilling method (HDM) on a RESTAN-MTS 3000 from SINT Technology in accordance to the ASTM standard E837 [26]. More information on the HDM measurements is provided in [17], [18].

2.4 Distortion measurements

Once sample fabrication and LSP treatments were done, the samples were removed from the baseplate by wire EDM. An alteration of the part geometry by mechanical forces during part removal can therefore be excluded. Upon removal, a distortion in their geometry was observed (Figure 4 a,b). Pictures of all samples were taken with a Hirox KH8700 digital microscope. The distortion angle α (Figure 4b) was measured using SolidWorks 2017 CAD software from Dassault Systemes.
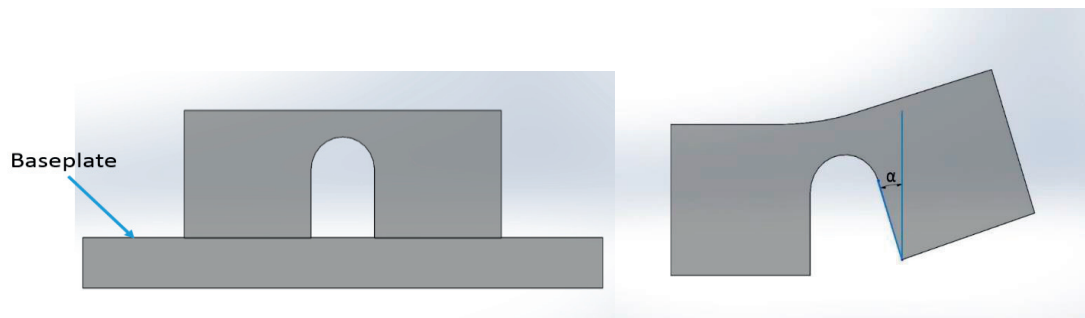
Fig. 4 a) SLM sample attached to the baseplate before removal; b) distorted sample after removal by wire EDM from the baseplate.

3. Results and discussion

Samples in this study were denoted as: "AB" for samples in the SLM as-built condition, "2D LSP" for samples that were treated only with a final LSP treatment on the top surface (as in conventional LSP), "3D LSP" for samples that were produced as explained in section 2.2. A further division was done into "3D LSP 3l" and "3D LSP 10l" indicating the value of n. In each of these 4 conditions, cuboidal samples for residual stress measurements as well as bridge like samples with a minimal overhang thickness of 1, 2 and 3mm for distortion measurements were produced.

3.1 Residual stresses

Residual stresses of Ti6Al4V samples in the AB, 2D LSP and 3D LSP 3l and 3D LSP 10l conditions are shown in Figure 5. It can be observed that in the AB SLM state, Ti6Al4V exhibits a tensile RS state with values of up to 422 MPa in the near surface region, and remain tensile throughout the depth of up to 1mm, which was the measurement limit for the HDM. In all 2D LSP and 3D LSP conditions, TRS are easily converted to CRS with similar values of around -400 MPa in the subsurface region. The significant difference is that the depth of the compressive stresses, and thus the total volume in the near surface zone, is increased when LSP is applied in the repetitive 3D LSP mode. In the case of 2D LSP post treatment, stresses remain compressive up to a depth of 523 microns, while an accumulation of CRS and an increase in their depth (up to 788 and 892 microns) is observed for 3D LSP 3l and 3D LSP 10l samples, respectively. This increase in the depth of CRS was observed in our previous studies [18] on 316L SLM samples, and is here confirmed on a different material. Due to the fast cooling rates operating during the rebuilding of subsequent n SLM layers (n being here either 3 or 10), the amount of introduced heat is insufficient to fully relax the introduced CRS. This explains why the following LSP treatment done on top of the rebuilt SLM layers connects well with the previously generated CRS profile; the connection being according to the present results more effective when choosing n = 10.
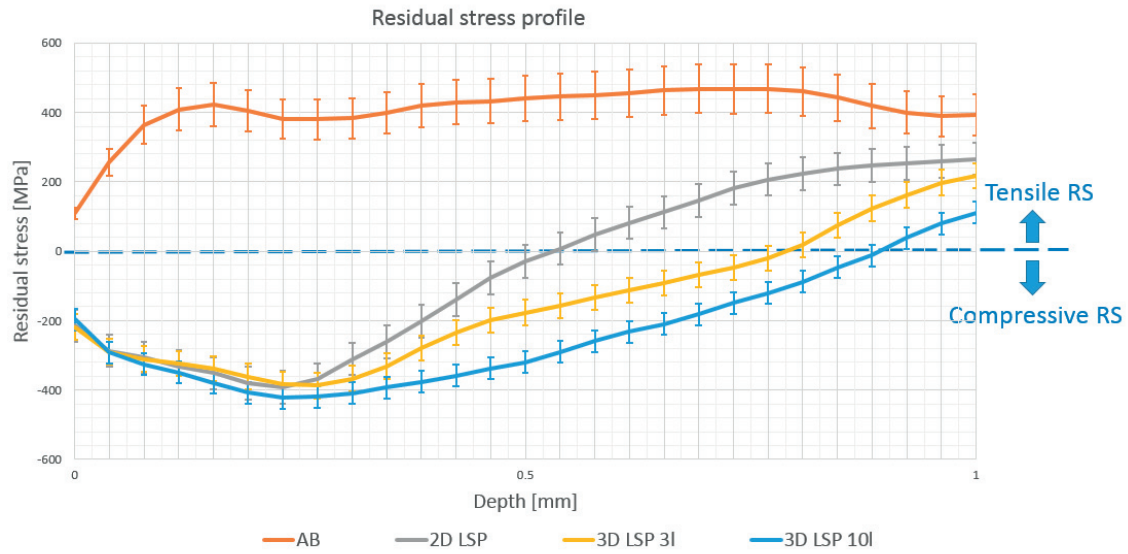
Fig. 5 Residual stress profile of Ti6Al4V samples in the AB, 2D LSP, 3D LSP 3l and 3D LSP 10l conditions.

3.2 Geometrical distortion

In the case of the AB and 2D LSP condition, for each overhang thickness two samples were made, and the average value of the distortion angle was taken. The α distortion angle was measured each time; it is reported in Table 3 and plotted in Figure 6.

3.2.1 As – built (AB) state

In the AB SLM state, high TRS accumulate close to the top surface of the part [17], [18], [24], [25]. These stresses create a curl–up distortion angle α [24]. For an overhang of 1mm thickness, the average value of this angle was measured at 2.21° ± 0.04°. As the overhang thickness increases to 2mm and 3mm, the distortion angle slightly decreases to 2.04° ± 0.05° and 1.92° ± 0.03° respectively. This was expected, as it is well known from the residual stress build-up in welded joints that as the thickness of the welded part is increased the geometrical distortions are decreasing [27]–[29].

3.2.2 2D LSP state

After a single LSP surface treatment, it can be observed (Table 3) that the distortion angle is significantly reduced. With the overhang thickness of 1mm, α is measured as 0.85° ± 0.04°, which represents a 62% improvement compare to the AB state. As the overhang thickness is increased to 2 and 3mm, α slightly increases to 0.94° ± 0.04° and 0.99° ± 0.02° respectively. Although conventional 2D LSP can easily convert TRS to Compressive RS [17], [18], this effect can be observed only up to a limited affected depth. The introduced CRS are therefore not sufficient to fully eliminate the geometrical distortion caused by the accumulated TRS throughout the overhang. With increasing thickness of the overhang, the effect of the LSP becomes comparably smaller, and the improvement on the distortion angle α is reduced.

3.2.3 3D LSP condition

3D LSP samples show a further decrease in the distortion angle α, and improvement in the geometrical accuracy compared to conventional 2D LSP and AB conditions. Looking at the 1 mm overhang, α is decreased to 0.64° and 0.56° for 3D LSP 3l and 3D LSP 10l respectively. These results present an improvement of 69 and 75% compared to the AB state, and 19 and 34% when compared to the conventional 2D LSP condition. This improvement can be correlated to the accumulation of CRS in the subsurface region shown in section 3.1. The observed increase in depth of CRS with the increase in the number n of SLM layers between two subsequent LSP treatments can explain the slightly better results achieved in the 3D LSP 10l condition.

Values from Table 3 were plotted in Figure 6 for better clarity. For the AB condition, a clear trend of increase in distortion angle with a decrease in the overhang thickness can be observed, while for the 2D LSP and 3D LSP conditions a reverse trend appears. 3D LSP leads to improved results in geometrical accuracy compared to conventional 2D LSP treatment. As the overhang thickness increases, the improvement is reduced.

Further improvement for thick geometries are expected with an increase of LSP treatments (> 2). In such cases, a hybrid automated 3D LSP machine - incorporating SLM and LSP processing units - is required to repeatedly apply LSP every n SLM layers and bring the part geometry inside the desired manufacturing tolerances.

Overhang	AB	2D LSP	3D LSP 3l	3D LSP 10l
1mm	2.21° ± 0.04°	0.85° ± 0.04°	0.64°	0.56°
2mm	2.04° ± 0.05°	0.94° ± 0.04°	0.73°	0.72°
3mm	1.92° ± 0.03°	0.99° ± 0.02°	0.93°	0.94°

Table 3 Values of the distortion angle α measured for samples in the AB, 2D LSP and 3D LSP conditions.
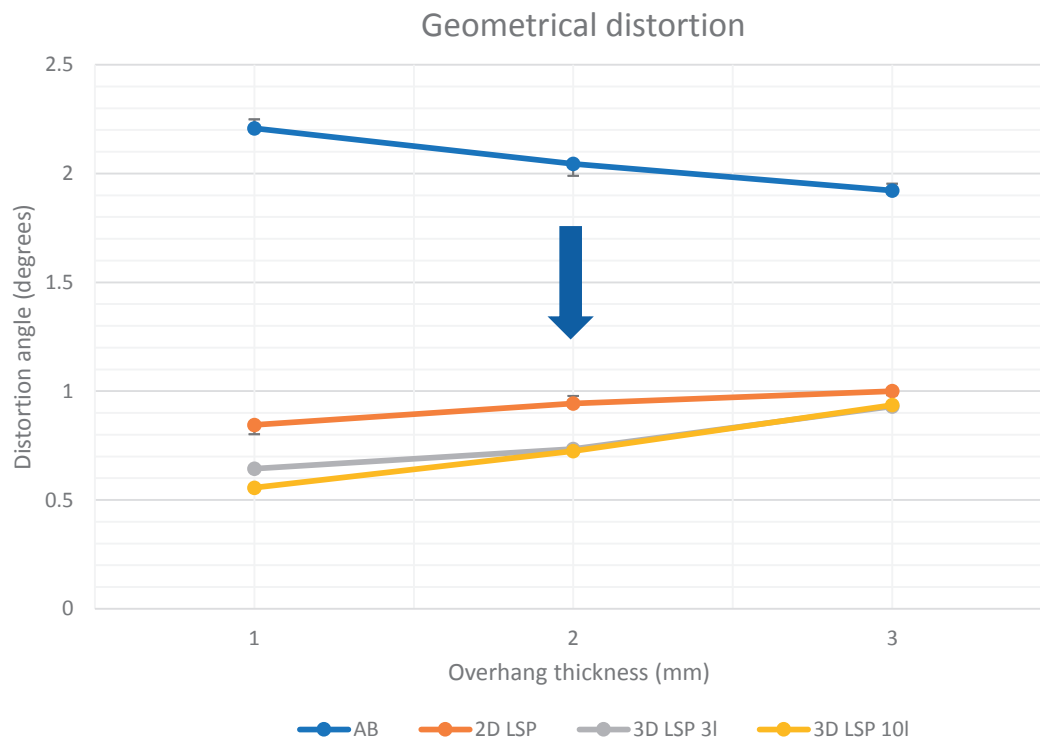
Fig. 6 Values of the distortion angle α measured for samples in the AB, 2D LSP and 3D LSP conditions for different overhang thicknesses.

4. Conclusions and future work

Residual stresses of SLM Ti6Al4V parts in the AB, 2D LSP post treatment and 3D LSP conditions were measured. A geometrical distortion angle α was quantified on bridge like samples with different overhang thicknesses (1, 2 and 3mm).

The following conclusion can be drawn:

- In the AB state, Ti6Al4V exhibits TRS up to the measured depth of 1mm;
- LSP easily converts TRS to CRS, and a cumulative effect on CRS is measured when processing by 3D LSP;
- In the AB state, a significant distortion above 2.2° can be observed, especially pronounced for thinner overhangs;
- With the increase of the overhang thickness the AB distortion angle slightly decreases;
- With the conventional surface 2D LSP treatment, a decrease in the distortion angle is observed, especially for the thinner overhang;
- 3D LSP shows a clear further improvement in the geometrical accuracy and a decrease in the distortion angle of up to 75% (in the current work) when compared to the AB and 2D LSP conditions;
- For thicker overhangs, an increased number of LSP treatments would need to be applied during SLM processing and would require a hybrid 3D LSP machine.

Further investigations on the influence of 3D LSP on thin overhangs (below 1mm) will be done. These thinner overhangs are very common in geometries of complex SLM parts, and further optimization of 3D LSP parameters for their treatment is planned.

Acknowledgments

References

[1] P. Mercelis and J.-P. Kruth, "Residual stresses in selective laser sintering and selective laser melting," *Rapid Prototyp. J.*, vol. 12, no. 5, pp. 254–265, Oct. 2006.

[2] M. F. Zaeh and G. Branner, "Investigations on residual stresses and deformations in selective laser melting," *Prod. Eng.*, vol. 4, no. 1, pp. 35–45, Feb. 2010.

[3] C. Li, C. H. Fu, Y. B. Guo, and F. Z. Fang, "Fast Prediction and Validation of Part Distortion in Selective Laser Melting," *Procedia Manuf.*, vol. 1, pp. 355–365, Jan. 2015.

[4] A. J. Dunbar *et al.*, "Development of experimental method for in situ distortion and temperature measurements during the laser powder bed fusion additive manufacturing process," *Addit. Manuf.*, vol. 12, pp. 25–30, Oct. 2016.

[5] K. Kempen, B. Vrancken, S. Buls, L. Thijs, J. Van Humbeeck, and J.-P. Kruth, "Selective Laser Melting of Crack-Free High Density M2 High Speed Steel Parts by Baseplate Preheating," *J. Manuf. Sci. Eng.*, vol. 136, no. 6, p. 061026, Oct. 2014.

[6] M. Shiomi, K. Osakada, K. Nakamura, T. Yamashita, and F. Abe, "Residual Stress within Metallic Model Made by Selective Laser Melting Process," *CIRP Ann. - Manuf. Technol.*, vol. 53, no. 1, pp. 195–198, 2004.

[7] H. K. Rafi, N. V. Karthik, H. Gong, T. L. Starr, and B. E. Stucker, "Microstructures and Mechanical Properties of Ti6Al4V Parts Fabricated by Selective Laser Melting and Electron Beam Melting," *J. Mater. Eng. Perform.*, vol. 22, no. 12, pp. 3872–3883, Dec. 2013.

[8] B. Vrancken, S. Buls, J.-P. Kruth, and J. Van Humbeeck, "Influence of preheating and oxygen content on Selective Laser Melting of Ti6Al4V," in *Proceedings of the 16th RAPDASA Conference*, 20151101.

[9] S. Bremen, W. Meiners, K. Wissenbach, and R. Poprawe, "Correlation of the High Power SLM Process with Resulting Material Properties for IN718," *BHM Berg- Hüttenmänn. Monatshefte*, vol. 162, no. 5, pp. 179–187, May 2017.

[10] T. Niendorf, S. Leuders, A. Riemer, H. A. Richard, T. Tröster, and D. Schwarze, "Highly Anisotropic Steel Processed by Selective Laser Melting," *Metall. Mater. Trans. B*, vol. 44, no. 4, pp. 794–796, May 2013.

[11] M. Masoomi, S. M. Thompson, and N. Shamsaei, "Quality part production via multi-laser additive manufacturing," *Manuf. Lett.*, vol. 13, pp. 15–20, Aug. 2017.

[12] X. C. Zhang, Y. K. Zhang, J. Z. Lu, F. Z. Xuan, Z. D. Wang, and S. T. Tu, "Improvement of fatigue life of Ti–6Al–4V alloy by laser shock peening," *Mater. Sci. Eng. A*, vol. 527, no. 15, pp. 3411–3415, Jun. 2010.

[13] M. Dorman, M. B. Toparli, N. Smyth, A. Cini, M. E. Fitzpatrick, and P. E. Irving, "Effect of laser shock peening on residual stress and fatigue life of clad 2024 aluminium sheet containing scribe defects," *Mater. Sci. Eng. A*, vol. 548, pp. 142–151, Jun. 2012.

[14] T. W. Charles S. Montross, "Laser Shock Processing and its Effects on Microstructure and Properties of Metal Alloys: A Review," *Int. J. Fatigue*, vol. 24, no. 10, pp. 1021–1036, 2002.

[15] N. Kalentics, R. Logé, and E. BOILLAT, "Method and Device for Implementing Laser Shock Peening or Warm Laser Shock Peening During Selective Laser Melting," US20170087670 A1, 30-Mar-2017.

[16] S. Afazov, W. A. D. Denmark, B. Lazaro Toralles, A. Holloway, and A. Yaghi, "Distortion prediction and compensation in selective laser melting," *Addit. Manuf.*, vol. 17, pp. 15–22, Oct. 2017.

[17] N. Kalentics, E. Boillat, P. Peyre, S. Ćirić-Kostić, N. Bogojević, and R. E. Logé, "Tailoring residual stress profile of Selective Laser Melted parts by Laser Shock Peening," *Addit. Manuf.*, vol. 16, pp. 90–97, Aug. 2017.

[18] N. Kalentics *et al.*, "3D Laser Shock Peening – A new method for the 3D control of residual stresses in Selective Laser Melting," *Mater. Des.*, vol. 130, pp. 350–356, Sep. 2017.

[19] L. Hackel, J. R. Rankin, A. Rubenchik, W. E. King, and M. Matthews, "Laser Peening: A Tool for Additive Manufacturing Post-processing," *Addit. Manuf.*, Sep. 2018.

[20] I. Yadroitsev, P. Krakhmalev, and I. Yadroitsava, "Selective laser melting of Ti6Al4V alloy for biomedical applications: Temperature monitoring and microstructural evolution," *J. Alloys Compd.*, vol. 583, pp. 404–409, Jan. 2014.

[21] A. A. Antonysamy, "Microstructure, Texture and Mechanical Property Evolution during Additive Manufacturing of Ti6Al4V Alloy for Aerospace Applications," *[Thesis]. Manchester, UK: The University of Manchester; 2012.*, 09-May-2012. [Online]. Available: https://www.escholar.manchester.ac.uk/uk-ac-man-scw:160535. [Accessed: 12-Apr-2018].

[22] S. L. Campanelli, N. Contuzzi, A. D. Ludovico, F. Caiazzo, F. Cardaropoli, and V. Sergi, "Manufacturing and Characterization of Ti6Al4V Lattice Components Manufactured by Selective Laser Melting," *Materials*, vol. 7, no. 6, pp. 4803–4822, Jun. 2014.

[23] "1709 CL 41TI ELI_layer.indd - Datasheet_CL_41TI_ELI.pdf." [Online]. Available: https://www.concept-laser.de/fileadmin//user_upload/Datasheet_CL_41TI_ELI.pdf. [Accessed: 12-Apr-2018].

[24] J.-P. Kruth, M. Badrossamay, E. Yasa, J. Deckers, L. Thijs, and J. Van Humbeeck, "Part and material properties in selective laser melting of metals," presented at the Proceedings of the 16th International Symposium on Electromachining, 2010.

[25] S. A. Sillars, C. J. Sutcliffe, A. M. Philo, S. G. R. Brown, J. Sienz, and N. P. Lavery, "The three-prong method: a novel assessment of residual stress in laser powder bed fusion," *Virtual Phys. Prototyp.*, vol. 13, no. 1, pp. 20–25, Jan. 2018.

[26] C. Casavola, S. L. Campanelli, and C. Pappalettere, "Experimental analysis of residual stresses in the selective laser melting process," in *Proccedings of the XIth International Congress and Exposition, Orlando, Florida, USA*, 2008.

[27] C. Renzi, D. Panari, and F. Leali, "Predicting tolerance on the welding distortion in a thin aluminum welded T-joint," *Int. J. Adv. Manuf. Technol.*, pp. 1–16, Feb. 2018.

[28] M. M. Mahapatra, G. L. Datta, B. Pradhan, and N. R. Mandal, "Three-dimensional finite element analysis to predict the effects of SAW process parameters on temperature distribution and angular distortions in single-pass butt joints with top and bottom reinforcements," *Int. J. Press. Vessels Pip.*, vol. 83, no. 10, pp. 721–729, Oct. 2006.

[29] D. Deng, W. Liang, and H. Murakawa, "Determination of welding deformation in fillet-welded joint by means of numerical simulation and comparison with experimental measurements," *J. Mater. Process. Technol.*, vol. 183, no. 2, pp. 219–225, Mar. 2007.

Chapter 8

Hybrid Additive Manufacturing of ultra-durable metal parts

(To be submitted)

Nikola Kalentics[1,*], Roland E. Logé[1]

1. Thermomechanical Metallurgy Laboratory – PX Group Chair, Ecole Polytechnique Fédérale de Lausanne (EPFL), CH-2002 Neuchâtel, Switzerland

Corresponding author: nikola.kalentics@epfl.ch

Contribution:

Nikola Kalentics designed the experiment and the SLM sample geometry, did the Laser Shock Peening treatments, fatigue tests, interpretation of results and wrote the manuscript.

Abstract

Additive manufacturing (AM) currently revolutionizes the way parts are designed and manufactured, with the ability to produce lightweight structures with unprecedented complex geometries. One well-known drawback of AM parts is that they can have a decreased fatigue life, compared to conventional manufacturing. 3D Laser Shock Peening is a new hybrid process adding a periodic Laser Shock Peening (LSP) treatment to the traditional Selective Laser Melting (SLM) AM method. LSP can be applied selectively in the 3D volume of metallic parts, and is shown here to drastically improve fatigue life. We report fatigue lives of 316L stainless steel multiplied by more than 15 times compared to standard SLM parts, and more than 57 times compared to conventional manufacturing.

Metal parts built to last!

Additive Manufacturing (better known as 3D printing) has seen a lot of media hype in the recent years. But besides the media hype, as some of the patents in the field are expiring, it is also experiencing a surge in the number of machine producers that have entered the field (from 97 companies in 2016 to 135 in 2017 [1]). This surge is driven by a clear and steady transition from Rapid Prototyping to Rapid Manufacturing applications. This trend can in particular be observed for metal Additive Manufacturing (AM) technologies, which showed an 80% increase in the number of sold machines in 2017 compared to the previous year, and 875% increase compared to 2012 [1]. As one of the most widely researched and mature AM technologies - Selective Laser Melting (SLM), a laser based powder bed process, has been at the forefront of this transition. With the constant improvements of the process over the last two decades, a clear increase in the process reliability, part density, production rates and range of materials processable by SLM can be observed. This context explains the surge in number of conferences, industrial exhibitions, trade fairs and workshops emerging in the SLM field, and the associated media coverage. It is also one of the fastest growing fields in industry at the moment, with many leading international companies (such as General Electric) investing billions in research and recent acquisitions (e.g. Concept Laser and Arcam [2], producers of metal Additive Manufacturing machines).

One of the well-known advantages of the SLM process is the ability to produce lightweight parts with extraordinary complex geometries, which are otherwise impossible to obtain with conventional manufacturing. On the other hand, one of the main drawback significantly limiting SLM current applications is the residual stress state inherited from the building phase of the

process. Tensile residual stresses (TRS) are known to significantly decrease fatigue life [3], increase part geometry distortions [4], promote cracks in materials (e.g. Ni-based superalloys) [5] and even cause delamination and process failure during the SLM building phase [6]–[8]. Geometrical distortions lead to an increased need for post process machining, while cracking in materials such as Ni-based superalloys significantly limits potential SLM applications. Hence, considerable effort has been put in multiple directions to cope with the residual stress issue, but so far with limited success. A post process heat treatment can be applied and a relief of ~70% of tensile residual stresses can be achieved [9], but this approach cannot address the problems of cracking and delamination during the building phase. Laser remelting of each layer can be applied as an in situ heat treatment to relieve the accumulation of TRS. However, although this approach can remove up to about 50% of TRS [9], rescanning every layer significantly increases processing time. This is in a sharp contrast with the long lasting trend to increase the productivity by either multiplying the number of lasers [10] or increasing the laser power [11], [12]. Baseplate preheating is another in situ process used to decrease thermal gradients and limit the accumulation of TRS. Here as well, only a limited effect of TRS reduction can be obtained (e.g. 40% in [9]). The baseplate temperature is usually limited to about 200°C in industrial applications since higher temperatures, with a positive effect on TRS, significantly reduce cooling rates and thereby decrease mechanical properties such as yield strength or fatigue limit [13], [14]. Hot Isostatic Pressing (HIP) is also commonly used for cast and SLM parts in order to remove residual stresses and close down any existing pores in order to improve fatigue life [15], [16]. However HIP remains limited to a post treatment, and can furthermore degrade the material microstructure, usually by excessive grain growth (often after a recrystallization step).

While all the above approaches have shown an ability to decrease TRS to a certain extent, none of them can introduce *compressive* residual stresses (CRS), although these are very beneficial to fatigue properties [17]–[19]. Expensive and time consuming surface treatments such as Laser Shock Peening (LSP), Shot Peening (SP) or Ultrasonic Shot Peening (USP) were precisely developed due to their ability to generate CRS (and increase hardness) in the near surface region, and improve fatigue life of treated parts [20]–[22]. These surface post treatments can be classified according to their affected depth, i.e. the depth to which CRS are being introduced into the part subsurface. The LSP process is the most effective one [19], [23] but also the most expensive due to the relative high cost and scarcity of the commercial equipment compared to SP and USP. An increase in the fatigue limit of 23.6% was observed when an LSP post treatment was applied on a titanium alloy (TC17) part manufactured by an AM blown powder method [24]. A recent publication on 316L SLM [25] shows that an SP post treatment improves the fatigue life by 2.7 times (compared to the AB state), whereas replacing SP by LSP provides a more than 20 times increase. However only two SP samples and three LSP samples were tested in these conditions. The SLM AB state also showed a nine times longer fatigue life compared to the softer

wrought conventional state. When applied as a post process, these surface treatments are restricted to accessible zones, and may therefore be ruled out for more complex geometries, typical of those produced by AM.

3D Laser Shock Peening (3D LSP) (Figure 1a) is a novel hybrid additive manufacturing process patented by the Laboratory of Thermomechanical Metallurgy at EPFL [26]. In essence, it consists of a repetitive application of LSP treatments *during* the SLM part building phase.

In previous work, we have shown that a conventional LSP post treatment can easily convert SLM induced TRS to more beneficial CRS, even when applied on a non – polished, rough SLM surface [27]. In further investigations preparing the ground for 3D LSP [28], it was shown that SLM layers built on an LSP treated surface do not erase the LSP induced CRS. On the contrary, it was observed that repetitive application of LSP on subsequent SLM layers leads to an accumulation and increase in magnitude of CRS, with the expected positive influence on the fatigue life of SLM parts. In this paper, we now investigate the fatigue life of 316L stainless steel SLM samples, by considering different processing steps: (i) the As-Built (AB) SLM state, (ii) the HIP post treatment, (iii) the conventional surface LSP (2D LSP) post treatment, and (iv) the 3D LSP process. Comparisons are also given with samples made by conventional manufacturing.

SLM samples made out of 316L stainless steel with a chemical composition given in Table S1 were produced. A miniature bridge like geometry (Figure 1b and 1c) was used to maximize the number of samples and produce 72 of them on the same baseplate, as shown in Figure S1. Fatigue life experiments were performed in bending, using a Rumul Cracktronic machine illustrated in Figure S2 and detailed in the supplementary material.
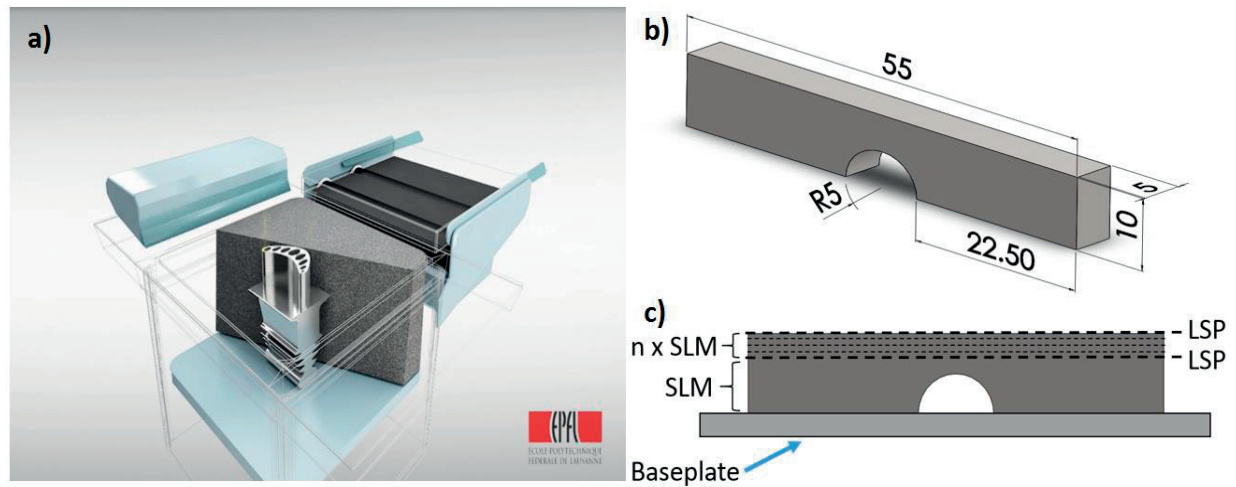
Fig. 1 a) Illustration of the 3D Laser shock peening process (3D LSP); b) Fatigue sample geometry and dimensions [29]; c) Schematic of the 3D LSP process with the n=10 number of layers between two subsequent LSP treatments.

Fatigue life measurement results for parts in the as-built (AB) SLM state, post-processed by Hot Isostatic Pressing (HIP), conventional 2D LSP post-treatment, and processed by 3D LSP, are shown in Figure 2. All samples were tested in fatigue with a non – machined (i.e. as-built) surface state, with an average roughness Ra of 12.3 microns. No measurable effect of the LSP process on the surface roughness was observed. Bending fatigue results were plotted and compared with "conventional 316L" samples made from wrought 316L material, with a chemical composition similar to that of the SLM powders (Table S1). These samples have been machined into the desired geometry, with an average surface roughness Ra of 0.53 microns.

A maximum number of 10 million cycles was considered in all fatigue experiments; samples reaching this stage without failure were marked as "runouts". Stress values at which runouts occurred were taken as the fatigue limit of the material, in the chosen bending conditions. The measured fatigue limit was 250 MPa in the AB state, and 300 MPa when post processed with 2D LSP. For the conventional 316L samples, a fatigue limit of 340 MPa was achieved which can be contributed to the significantly smoother machined surface. Surface roughness has an obvious detrimental effect on fatigue life since all valleys of the roughness profile act as stress concentration sites and nucleation points for crack initiation [30].

The achieved fatigue limit of 3D LSP samples was 360 MPa, which represents a modest increase compared to the conventional ones, however here again the surface state is very different. Samples processed by 3D LSP show a *drastic* increase of more than 15 times the fatigue life of AB samples, at a load of 360 MPa (Figure 2). They also have a substantially higher fatigue limit compared to the SLM AB state (44% increase). The increase in the fatigue life of 3D LSP samples

can be attributed to the accumulated compressive residual stresses in the subsurface region of the part [17], [19], [27], [28].

Fig. 2 Wöhler curves of non - machined 316L steel samples in the As-Built (AB) state, HIP treated, 2D LSP treated, 3D LSP processed, and comparison with machined wrought conventional samples. Runouts correspond to 10 million cycles without failure, and are marked by a black arrow.

Figure 3 compares fatigue lives of SLM AB, HIP post processed, 2D LSP post processed, 3D LSP processed, and conventionally made 316L samples, this time with all of them machined on the surface (Ra of 0.53 microns). The SLM AB condition outperforms the conventionally made 316L (4 times longer fatigue life at 480 MPa), the improvement increasing with the applied load. The SLM AB machined state shows a fatigue limit at 360 MPa, while a 2D LSP post treatment only improves it by 6%, reaching 380 MPa.

The 3D LSP condition again outperformed all other treatments and achieved a fatigue limit of 480 MPa, i.e. 26% higher than the 2D LSP post treatment case (380 MPa), and 33% higher than the SLM AB state (360 MPa). An impressive 41% increase is noticed in comparison with the conventional 316L samples (340 MPa). Looking at the increase in fatigue life, the benefits of LSP treatments are even more striking: for example, at 480 MPa, the 3D LSP fatigue life is more than 14 times that of the AB state, and more than 57 times that of the conventionally made 316L. Again, the increase in fatigue life should be related to the previously demonstrated introduction

[27] and accumulation [28] of CRS in the subsurface region of the 316L SLM sample, which are very effective in delaying the onset of cracking.

Figure 3 also shows different slopes of fatigue curves depending on the processing steps. This can be especially observed for the HIP, AB and conventional 316L curves which have a similar fatigue limit, but behave very differently at higher stresses. With the increase in applied stress, softer HIPed samples experience a more drastic decrease in fatigue life which lowers the slope of the fatigue curve compared to the steeper SLM AB state curve. The beneficial effects of the 2D and 3D LSP process are more pronounced in the lower stress zone, where the accumulated CRS have the most significant role [19], [23]. This also reduces the slope of their fatigue curves (compared to the AB state), with fatigue lives remaining significantly increased in most of the investigated stress range.
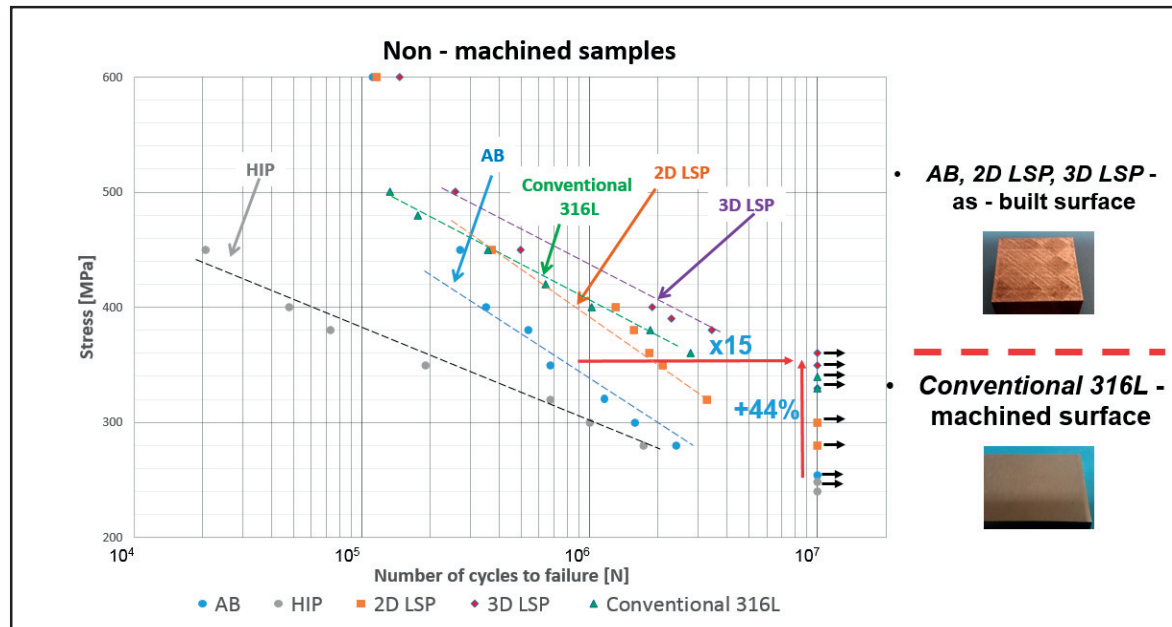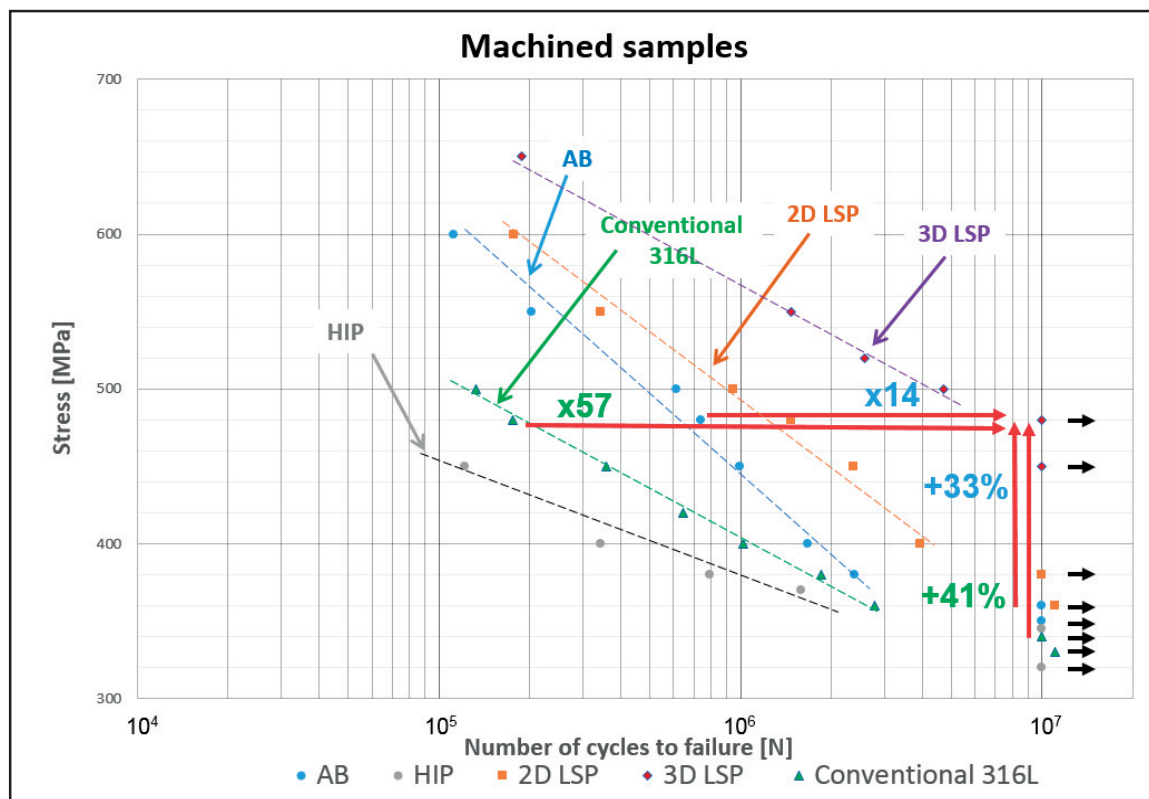

Fig. 3 Wöhler curves of machined 316L steel samples in the As-Built (AB) state, HIP treated, 2D LSP treated, 3D LSP processed, and comparison with wrought conventional samples. Runouts correspond to 10 million cycles without failure, and are marked by a black arrow.

The HIP treated samples showed an overall lower performance, even worse than the AB samples, in both non – machined and machined conditions. It was already observed in literature that for 316L samples, due to the high temperatures used in the HIP process, recrystallization and grain growth occur, leading to an increase in grain size, a decrease in dislocation density, and therefore a decrease in yield strength [31]–[33], which reduces fatigue life [32].

To better understand the effect of the HIP treatment and the comparison with the conventional 316L samples, Vickers microhardness measurements were performed, as shown in Figure 4 and Table S3. At a depth of 50 microns, the AB state achieves 236HV, while 2D LSP and 3D LSP lead to a strain-hardening, quantified by 281 HV and 322 HV, respectively. The increase in strain hardening of the material when going from 2D to 3D LSP is due to the plastic strain accumulation in latter case [27], [28], which relates as well to the accumulation of CRS. Wrought conventionally produced 316L is significantly softer, 212 HV, while the HIP treatment leads to an increase in grain size [33] and to the lowest microhardness (200 HV). The associated low yield strength explains the decrease in fatigue life, especially in the higher stress load regime.
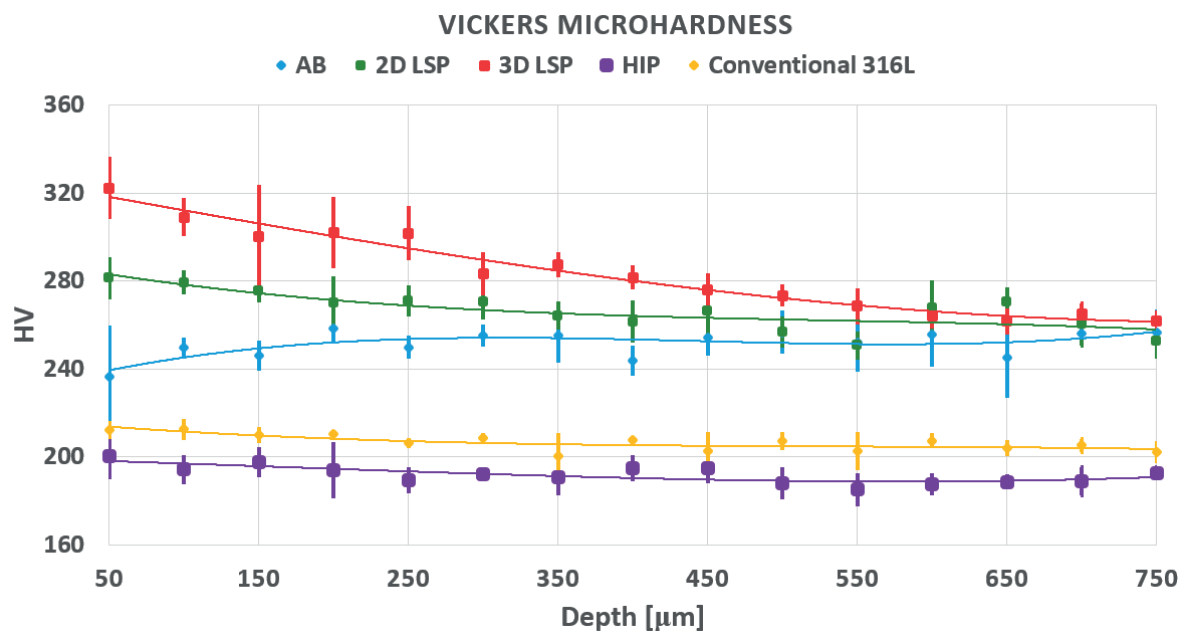
Fig. 4 Microhardness profiles for samples in the AB, 2D LSP, 3D LSP, HIPed condition and made by wrought Conventional 316L.

It was shown that by producing SLM parts in a 3D LSP manner, residual stresses can be effectively tailored [27], [28] in the extent that cannot be reached by any other in situ or post treatment

116

alike. The ability to convert these TRS to neutral or CRS will have a beneficial effect on the decrease in part geometry distortion as well as a decrease in the amount of cracks caused by the accumulation of TRS during the building process.

In this work we have shown that the ability to accumulate compressive residual stresses has an important beneficial effect on fatigue life and fatigue limit of the produced part. A dramatic increase of more than 15 times in fatigue life, together with a 44% improvement in fatigue limit was achieved, for a non - machined 3D LSP sample compared to an equivalent as-built SLM sample. The improvement is even more remarkable in the case of machined surface states, where the 3D LSP sample showed an increase in fatigue life of more than 14 times that of the AB state and more than 57 times that of the conventionally produced 316L. In the latter machined surface state, the fatigue limit increased by 33% compared to the AB state, and 41% compared to the conventional 316L.

These substantial improvements in the fatigue life and fatigue limit of parts made by the 3D LSP process will further contribute to the ability to optimize geometry and produce light weight and highly engineered parts, a main driving force of the whole metal Additive Manufacturing field.

References

[1] "Wohlers Associates Publishes 23rd Edition of Its 3D Printing and Additive Manufacturing Industry Report | Wohlers Associates." [Online]. Available: https://wohlersassociates.com/press74.html. [Accessed: 14-May-2018].

[2] "GE Agrees to Purchase Controlling Shares of Arcam AB," *GE Newsroom*, 15-Nov-2016. [Online]. Available: http://www.genewsroom.com/press-releases/ge-agrees-purchase-controlling-shares-arcam-ab-283443. [Accessed: 14-May-2018].

[3] H. Stoffregen, K. Butterweck, and E. Abele, "Fatigue Analysis in Selective Laser Melting: Review and Investigation of Thin-walled Actuator Housings," presented at the 25th Solid Freeform Fabrication Symposium 2014, Austin, Texas, 2014, pp. 635–650.

[4] J.-P. Kruth, M. Badrossamay, E. Yasa, J. Deckers, L. Thijs, and J. Van Humbeeck, "Part and material properties in selective laser melting of metals," presented at the Proceedings of the 16th International Symposium on Electromachining, 2010.

[5] L. N. Carter, C. Martin, P. J. Withers, and M. M. Attallah, "The influence of the laser scan strategy on grain structure and cracking behaviour in SLM powder-bed fabricated nickel superalloy," *J. Alloys Compd.*, vol. 615, pp. 338–347, 2014.

[6] P. Mercelis and J.-P. Kruth, "Residual stresses in selective laser sintering and selective laser melting," *Rapid Prototyp. J.*, vol. 12, no. 5, pp. 254–265, Oct. 2006.

[7] K. Kempen, B. Vrancken, S. Buls, L. Thijs, J. Van Humbeeck, and J.-P. Kruth, "Selective Laser Melting of Crack-Free High Density M2 High Speed Steel Parts by Baseplate Preheating," *J. Manuf. Sci. Eng.*, vol. 136, no. 6, p. 061026, Oct. 2014.

[8] M. F. Zaeh and G. Branner, "Investigations on residual stresses and deformations in selective laser melting," *Prod. Eng.*, vol. 4, no. 1, pp. 35–45, Feb. 2010.

[9] M. Shiomi, K. Osakada, K. Nakamura, T. Yamashita, and F. Abe, "Residual Stress within Metallic Model Made by Selective Laser Melting Process," *CIRP Ann. - Manuf. Technol.*, vol. 53, no. 1, pp. 195–198, 2004.

[10] M. Masoomi, S. M. Thompson, and N. Shamsaei, "Quality part production via multi-laser additive manufacturing," *Manuf. Lett.*, vol. 13, pp. 15–20, Aug. 2017.

[11] S. Bremen, W. Meiners, K. Wissenbach, and R. Poprawe, "Correlation of the High Power SLM Process with Resulting Material Properties for IN718," *BHM Berg- Hüttenmänn. Monatshefte*, vol. 162, no. 5, pp. 179–187, May 2017.

[12] T. Niendorf, S. Leuders, A. Riemer, H. A. Richard, T. Tröster, and D. Schwarze, "Highly Anisotropic Steel Processed by Selective Laser Melting," *Metall. Mater. Trans. B*, vol. 44, no. 4, pp. 794–796, May 2013.

[13] H. Ali, L. Ma, H. Ghadbeigi, and K. Mumtaz, "In-situ residual stress reduction, martensitic decomposition and mechanical properties enhancement through high temperature powder bed pre-heating of Selective Laser Melted Ti6Al4V," *Mater. Sci. Eng. A*, vol. 695, pp. 211–220, May 2017.

[14] H. K. Rafi, T. L. Starr, and B. E. Stucker, "A comparison of the tensile, fatigue, and fracture behavior of Ti–6Al–4V and 15-5 PH stainless steel parts made by selective laser melting," *Int. J. Adv. Manuf. Technol.*, vol. 69, no. 5–8, pp. 1299–1309, Jun. 2013.

[15] S. Leuders *et al.*, "On the mechanical behaviour of titanium alloy TiAl6V4 manufactured by selective laser melting: Fatigue resistance and crack growth performance," *Int. J. Fatigue*, vol. 48, pp. 300–307, Mar. 2013.

[16] G. Kasperovich and J. Hausmann, "Improvement of fatigue resistance and ductility of TiAl6V4 processed by selective laser melting," *J. Mater. Process. Technol.*, vol. 220, pp. 202–214, Jun. 2015.

[17] X. C. Zhang, Y. K. Zhang, J. Z. Lu, F. Z. Xuan, Z. D. Wang, and S. T. Tu, "Improvement of fatigue life of Ti–6Al–4V alloy by laser shock peening," *Mater. Sci. Eng. A*, vol. 527, no. 15, pp. 3411–3415, Jun. 2010.

[18] M. Dorman, M. B. Toparli, N. Smyth, A. Cini, M. E. Fitzpatrick, and P. E. Irving, "Effect of laser shock peening on residual stress and fatigue life of clad 2024 aluminium sheet containing scribe defects," *Mater. Sci. Eng. A*, vol. 548, pp. 142–151, Jun. 2012.

[19] T. W. Charles S. Montross, "Laser Shock Processing and its Effects on Microstructure and Properties of Metal Alloys: A Review," *Int. J. Fatigue*, vol. 24, no. 10, pp. 1021–1036, 2002.

[20] M. Sugavaneswaran, A. V. Jebaraj, M. D. B. Kumar, K. Lokesh, and A. J. Rajan, "Enhancement of surface characteristics of direct metal laser sintered stainless steel 316L by shot peening," *Surf. Interfaces*, vol. 12, pp. 31–40, Sep. 2018.

[21] B. AlMangour and J.-M. Yang, "Improving the surface quality and mechanical properties by shot-peening of 17-4 stainless steel fabricated by additive manufacturing," *Mater. Des.*, vol. 110, pp. 914–924, Nov. 2016.

[22] A. Amanov, S. Sasaki, I.-S. Cho, Y. Suzuki, H.-J. Kim, and D.-E. Kim, "An investigation of the tribological and nano-scratch behaviors of Fe–Ni–Cr alloy sintered by direct metal laser sintering," *Mater. Des.*, vol. 47, pp. 386–394, May 2013.

[23] A. K. Gujba and M. Medraj, "Laser Peening Process and Its Impact on Materials Properties in Comparison with Shot Peening and Ultrasonic Impact Peening," *Materials*, vol. 7, no. 12, pp. 7925–7974, 2014.

[24] S. Luo, W. He, K. Chen, X. Nie, L. Zhou, and Y. Li, "Regain the fatigue strength of laser additive manufactured Ti alloy via laser shock peening," *J. Alloys Compd.*, vol. 750, pp. 626–635, Jun. 2018.

[25] L. Hackel, J. R. Rankin, A. Rubenchik, W. E. King, and M. Matthews, "Laser Peening: A Tool for Additive Manufacturing Post-processing," *Addit. Manuf.*, Sep. 2018.

[26] N. Kalentics, R. Logé, and E. BOILLAT, "Method and Device for Implementing Laser Shock Peening or Warm Laser Shock Peening During Selective Laser Melting," US20170087670 A1, 30-Mar-2017.

[27] N. Kalentics, E. Boillat, P. Peyre, S. Ćirić-Kostić, N. Bogojević, and R. E. Logé, "Tailoring residual stress profile of Selective Laser Melted parts by Laser Shock Peening," *Addit. Manuf.*, vol. 16, pp. 90–97, Aug. 2017.

[28] N. Kalentics *et al.*, "3D Laser Shock Peening – A new method for the 3D control of residual stresses in Selective Laser Melting," *Mater. Des.*, vol. 130, pp. 350–356, Sep. 2017.

[29] G. Nicoletto, "Anisotropic high cycle fatigue behavior of Ti–6Al–4V obtained by powder bed laser fusion," *Int. J. Fatigue*, vol. 94, pp. 255–262, Jan. 2017.

[30] C. D. D. Greitemeier, "Effect of surface roughness on fatigue performance of additive manufactured Ti–6Al–4V," *Mater. Sci. Technol.*, p. 1743284715Y.000, 2015.

[31] N. P. Lavery *et al.*, "Effects of hot isostatic pressing on the elastic modulus and tensile properties of 316L parts made by powder bed laser fusion," *Mater. Sci. Eng. A*, vol. 693, pp. 186–213, May 2017.

[32] S. Leuders, T. Lieneke, S. Lammers, T. Tröster, and T. Niendorf, "On the fatigue properties of metals manufactured by selective laser melting – The role of ductility," *J. Mater. Res.*, vol. 29, no. 17, pp. 1911–1919, Sep. 2014.

[33] A. Riemer, S. Leuders, M. Thöne, H. A. Richard, T. Tröster, and T. Niendorf, "On the fatigue crack growth behavior in 316L stainless steel manufactured by selective laser melting," *Eng. Fract. Mech.*, vol. 120, pp. 15–25, Apr. 2014.

Authors contributions

Nikola Kalentics had a lead task in design and interpretation of the reported experiments and results. He participated in the acquisition and analysis of data related to the fatigue life and microhardness. He had a lead role in drafting the manuscript.

Roland E. Logé had a contributed role in design and interpretation of the reported experiments and results. He participated in the analysis of data related to the fatigue life and microhardness. He had a lead role in the supervision of the work and in revising the manuscript.

Competing interests

Authors declare that they have no competing interests or affiliations besides the one declared above.

Data and materials availability

All data is available in the manuscript or the supplementary materials.

Supplementary Materials

Materials and Methods

Tables S1 – S3

Figures S1 – S2

Methods and materials – supplement

1. Material and SLM parameters

Samples were made out of well-investigated and widely used austenitic stainless steel 316L. The chemical composition is shown in Table S1, and the used powder was DIAMALLOY 1003 obtained from Sulzer Metco, Switzerland. Samples were manufactured on a Concept M2 machine (Concept Laser GmbH, Germany) equipped with a fiber laser operated in continuous mode. The laser has a wavelength of 1070 nm and a spot size of 90 microns. A total of 72 fatigue samples were made (Figure S1). The processing parameters, i.e. laser power, scanning speed, hatch distance and powder layer thickness were 125 W, 500 mm/s, 0.105 mm and 0.03 mm, respectively. An island scanning strategy was applied. Samples were produced under N_2 atmosphere and the O_2 content was kept below 1 % during the process.

	Cr	Ni	Si	Mo	C	Fe
316L (Sulzer Metco)	17	12	2.3	2.5	0.03	Balance
Conventional 316L (PX)	17-19	12.5-15	<1	2.5-3	<0.03	Balance

Table S1 Chemical composition of 316L stainless steel, wt. %.

Samples designated as "conventional 316L" were machined out of 316L **1.4435** acquired from PX Precimet SA (Switzerland) with a chemical composition given in Table S1.

Fig. S1 Baseplate with 72 miniature fatigue samples made out of 316L.

2. Laser Shock Peening setup

The LSP treatment was done on a Nd:YAG SAGA HP - class laser from Thales company with a "top-hat" beam spatial energy distribution and a near – Gaussian pulse shape. LSP parameters are given in Table S2. 3D LSP processing consisted in applying the LSP treatments twice, the first time at a depth of 10 SLM layers below the top surface, and the second time on the top surface itself (see Figure 1c). All LSP treatments were done while samples were still attached to the baseplate. Samples designated as SLM AB received no LSP treatment.

Wavelength	1064nm
Pulse duration	6.3ns
Spot size diameter	1mm
Pulse energy	0.4J
Power density	7.2 GW/cm^2
Frequency	5Hz
Overlap value	80%

Table S2 LSP process parameters.

3. Hot Isostatic Pressing (HIP)

Hot Isostatic Pressing (HIP) treatments were done on an ABRA *Shirp8/16-200-2000* (Abra Fluid AG, Switzerland) machine under a protective Argon atmosphere. A pressure of 100 bar, and a temperature of 1150°C were applied for a duration of 4h.

4. Fatigue life experiments

The specimen geometry was a bridge like structure shown in Figure 1b with dimension of 55x10x5 mm^3, an arc of 5mm diameter such that the cross section of the specimen was 5x5mm^2. Samples were built on support structures of 3 mm height, and were removed from the baseplate by EDM.

Fatigue tests were done on a Rumul Cracktronic (Switzerland) machine shown in Figure S2, under pure bending load. Tensile stresses were applied on the specimen top surface, with a stress ratio R=0. The applied load frequency was 120 Hz.
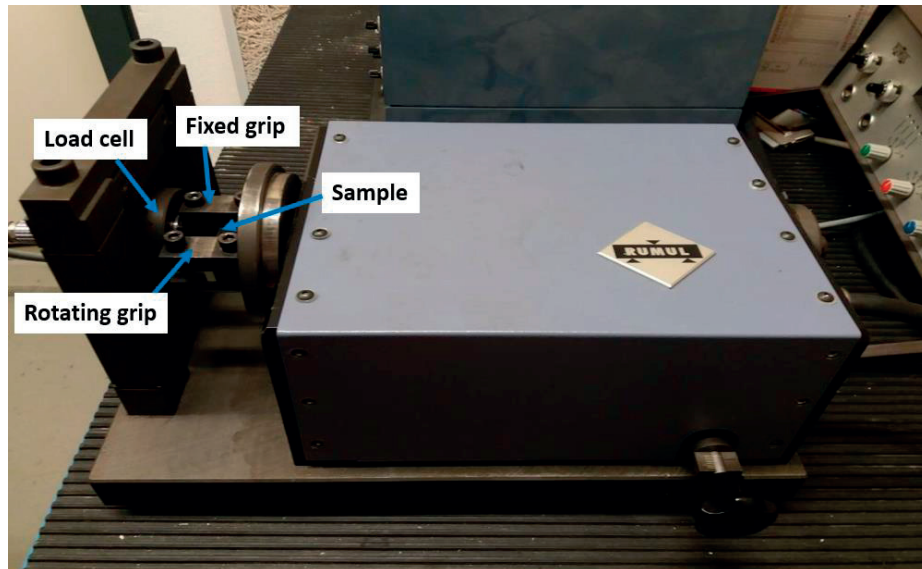
Fig. S2 Rumul Cracktronic fatigue machine.

5. Microhardness measurements

Vickers microhardness measurements were done using a 25 g load and a 12 s hold time at room temperature, on a Q10A machine from Qness GmbH (Germany). As recommended by ISO 6507-1, the distance between two consecutive indentations was larger than 3 times the diagonal of the indented square. 5 parallel rows of 15 indentations separated by 50 μm gaps were made along the samples depth, with the first indentation placed at 50 μm from the free edge of the top surface, following the ISO 6507-1 recommendation. The mean microhardness and its standard deviation were plotted by considering the 5 measurements at each depth level (Figure 4). Numerical values are given in Table S3.

Depth (μm)	Microhardness value (HV)				
	AB	2D LSP	3D LSP	HIP	Conventional 316L
50	236.4	281.4	322.3	200.3	212.3
100	250.0	279.4	309.1	194.3	212.7
150	246.0	275.4	300.2	197.7	210.0
200	258.6	270.0	302.2	194.0	210.7
250	250.0	271.0	301.8	189.5	206.3
300	255.2	270.4	283.4	192.3	208.7
350	255.2	264.4	287.6	191.0	200.3
400	243.8	261.6	281.6	195.0	207.7
450	254.4	266.6	276.1	194.8	202.7
500	256.8	257.0	273.4	188.0	207.3
550	252.0	250.8	268.5	185.3	202.7
600	255.6	268.0	264.1	187.8	207.3
650	245.4	270.6	261.7	188.8	204.0
700	256.2	260.4	264.9	189.0	205.3
750	256.8	252.6	261.9	192.8	202.3

Table S3 Mean values of microhardness measurements for samples in the AB, HIP, 2D LSP, 3D LSP conditions, and comparison with wrought conventional 316L.

Chapter 9

Reducing crack density in Selective Laser Melting by 3D Laser Shock Peening

<div align="center">(To be submitted)</div>

Nikola Kalentics[1,*], Navid Sohrabi[1], Hossein Ghasemi Tabasi[1], Jamasp Jhabvala[1], Andreas Burn[2], Roland E. Logé[1]

1. Thermomechanical Metallurgy Laboratory – PX Group Chair, Ecole Polytechnique Fédérale de Lausanne (EPFL), CH-2002 Neuchâtel, Switzerland
2. Switzerland Innovation Park Biel/Bienne SIPBB, Swiss Advanced Manufacturing Center SAMC, Aarbergstrasse 46, 2503 Biel/Bienne, Switzerland

Corresponding author: nikola.kalentics@epfl.ch

Contribution:

Nikola Kalentics designed the experiment, did the Laser Shock Peening treatments, interpretation of results and wrote the manuscript.

Abstract

Selective Laser Melting (SLM) of Ni-based superalloys such as CM247LC is prone to weld-cracking. This paper investigates how the cracking behavior of the alloy can be improved by repeatedly applying Laser Shock Peening (LSP) during the building phase of SLM. Samples made of CM247LC were processed with different LSP parameters, and the influence on bulk crack density has been quantified. It was observed that for all chosen conditions, a significant decrease of up to 95% could be achieved, demonstrating the potential of the new hybrid 3D LSP method in improving SLM processing of alloys sensitive to cracking.

1. Introduction

Selective Laser Melting (SLM) is a laser based powder bed process considered to be one of the most accurate and widely researched Additive Manufacturing (AM) processes [1], [2]. AM is known for a number of advantages over conventional manufacturing methods, such as the possibility to build parts with complex geometries, low lead time, mass customization, minimal waste, and the ability to process materials which are difficult or impossible to manufacture with conventional manufacturing methods. SLM is however very sensitive to the accumulation of tensile residual stresses (TRS), which can lead to cracking and warping. If not released after processing, these TRS also usually result in a significant decrease in fatigue life [3]–[5].

Ni-based superalloys have a major importance in industries dealing with high temperature applications, such as gas and jet turbine engines. Among these, CM247LC has demonstrated excellent creep and corrosion resistance at elevated temperatures [6], which places this alloy in ideal position for production of turbine blades designed for demanding conditions such as high pressures and high temperatures [7], [8]. The as-fabricated CM247LC alloy is strengthened by a high-amount of γ´ ordered secondary phase [8], and is well-known to be prone to weld-cracking [9], [10]. Both fusion welding and Selective Laser Melting processes therefore lead to the formation of cracks. Four potential mechanisms have been discussed so far in Ni-based superalloys, and could apply to CM247LC:

1) Solidification Cracking (Hot-Tearing) happens where the material is in a partially solid state (solidifying melt pool or mushy zone) as a result of entrapment of remained liquid in the interdendritic regions [10]. Due to presence of tensile residual stresses induced by solidification, the entrapped liquid regions can act as crack initiation sites [11], [12].

2) Liquation Cracking mostly occurs in the Heat Affected Zone (HAZ), and some research studies have identified it as the main reason of cracking in lower-energy welding conditions [13]. In the HAZ, phases with low melting point, such as γ-γ' eutectic or zones with chemical segregation, form a liquid film along the grain boundaries. Since the liquid film cannot withstand solidification shrinkage (TRS due to shrinkage), it serves as crack initiation site.

3) Strain-age cracking (SAC) is correlated with post weld heat treatment (PWHT) of Ni-based superalloys. SAC may occur during reheating of the welded material in the aging region [10]. The mechanism of SAC is explained by two competing actions. First, residual stresses relax slowly during PWHT. One the other hand, γ' keeps precipitating which makes the alloy less ductile and induces additional residual stresses. If the resulting residual stresses induce strain beyond the ductility limit, cracks form at grain boundaries along carbides. In SLM, reheating repeatedly occurs after deposition of each new layer, which is the equivalent of post weld reheating [10], [14].

4) Ductility-dip cracking (DDC) is a 'creep-like' mechanism which occurs at elevated temperature, not high enough for dynamic recrystallization, but sufficient for grain boundary sliding [15]. The latter can induce stress concentration at triple grain boundary junctions, and lead to void formation, or cracking.

SLM of Ni-superalloys has been largely studied [9], [16]–[19]. Strategies for reducing crack density include optimizing SLM parameters [9], [18], [19], applying Hot Isostatic Pressing (HIP) [9] and tuning the chemical composition [9], [18]. The HIP process usually leads to grain coarsening [20], [21] which has detrimental consequences on mechanical properties. Carter et al. [9] stated that the cracking mechanism in CM247LC is DDC, due to presence of high angle grain boundaries near the cracks. Liquation cracking is also reported in SLM of IN738LC [22] (another γ´-strengthened Ni superalloy). The dendritic structure at the crack surfaces, and the presence of low melting point alloying components are two solid evidences for this cracking mechanism [22].

Although cracking mechanisms in γ´strengthened Ni superalloys are still a matter of debate, all of them require a TRS field which acts as a crack driving force.

3D Laser Shock Peening (3D LSP) is a hybrid Additive Manufacturing process which repeatedly applies Laser Shock Peening (LSP), a well-known surface treatment [23], [24], during the building phase of SLM. It was developed and patented by the Laboratory of Thermomechanical Metallurgy at EPFL [25]. Initial investigations have shown that LSP can convert the SLM induced TRS into compressive residual stresses (CRS) [26]. When LSP is repeatedly applied every few SLM layers, CRS can accumulate, i.e. both their magnitude and their penetration depth from the free surface can increase [27].

γ´ strengthened Ni-based superalloys are susceptible to cracking when subjected to welding or SLM conditions. Cracking is always promoted by TRS, regardless of the particular mechanism. From an industrial point of view, any part that contains excessive cracks should be rejected and thus, removing cracks is of a high importance. In this paper, we show for the first time that the 3D LSP approach can significantly reduce the amount of cracks in the SLM CM247LC samples. Samples in the AB and 3D LSP treated conditions are compared and the measured cracks density is significantly reduced for all considered 3D LSP processing conditions.

2. Experimental setup

2.1 SLM parameters and sample geometry

The chemical composition of CM247LC powders is shown in Table 1.

Cr	Co	Ta	Ti	Al	W	Hf	Mo	C	B	Zr	Ni
8.1	9.2	3.2	0.7	5.6	8.5	1.4	0.5	0.05	0.015	0.015	balance

Table 1 Chemical composition of CM247LC powders, wt.% [6].

SLM processing was performed on a laboratory machine equipped with an Ytterbium fiber laser operated in continuous mode at a wavelength of 1070 nm and a spot size of 90 microns. The chosen SLM processing parameters were: laser power 200 W, scanning speed 1300 mm/s, hatching distance 0.090 mm, and layer thickness 0.03 mm, with a bi-directional scanning (90° alternating). The oxygen content in the SLM chamber was around 0.5%. Twelve samples with dimensions of 10x10x10 mm^3 were manufactured (Figure 1 a,b).
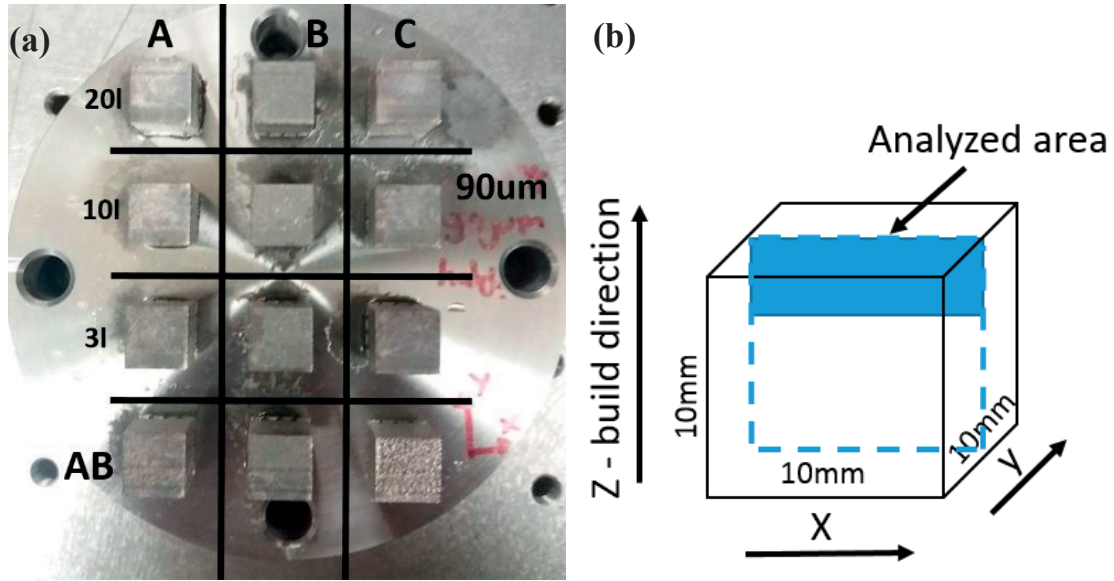
Fig. 1 a) Samples attached to the baseplate; b) sample geometry with the build direction vertical (Z).

2.2 Laser Shock Peening setup

While still being attached to the baseplate, 9 out of the 12 samples in Figure 1a were treated with different LSP parameters: three samples for each set of parameters A, B and C. The last three samples were left in the as-built (AB) condition. After LSP treatment, samples were brought back to the SLM station and n additional SLM layers were rebuilt (Figure 2). The chosen numbers of layers n were {3, 10, 20}, as shown in Figure 1a.

Similarly to previous work [27], the LSP treatment was done on a Nd:YAG SAGA HP laser from Thales company. The LSP process parameters were kept constant with the exception of the overlap rate (Table 2). The chosen overlap rate was 80% for samples A, 40% for samples B, and two times 80% (two treatments with 80% coverage each) for samples C (Figure 1a). The ratio of number of LSP shots between 80% overlap and 40% overlap is 9. The reader is directed to [26], [27] for more information on the LSP setup.
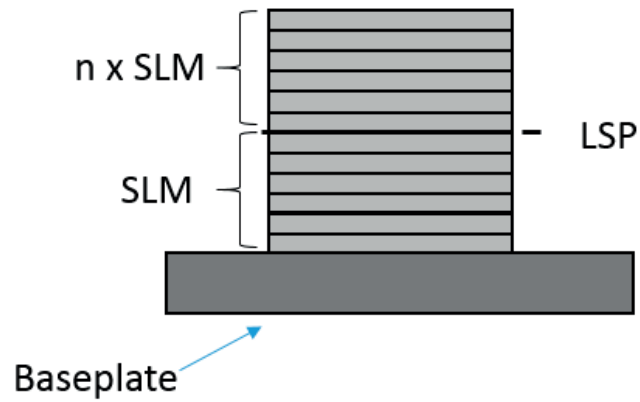
Fig. 2 Schematic view of the 3D LSP process with the *n* number of rebuilt SLM layers after the LSP treatment.

Wavelength	1064nm
Pulse duration	6.3ns
Spot size diameter	1mm
Pulse energy	0.4J
Power density	7.2 GW/cm^2
Frequency	5Hz

Table 2 LSP process parameters.

2.3 Crack density measurements

Samples were cut according to Figure 1b, ground with sand papers (down to 2500), then polished with suspension of alumina particles until 0.04 µm, and images of the XZ plane were taken on an optical microscope Leica DM6000M with a magnification of 200. Micrographs were analyzed with the ImageJ software, and a plugin [28] was used to quantify the crack density values.

2.4 Heat treatment

A stress relieve heat treatment was done on some of the 3D LSP samples in order to assess the influence of residual stresses on the measured crack density. Samples were heat treated at $1250°C$ in a Borel FP 1400 furnace for 3 hours, and cooled down to room temperature with a flow of compressed argon gas.

2.5 Chemical etching

Chemical etching was done with the Kalling's reagent (2.5 g CuCl2 + 50 mL HCl + 50 mL water). Samples were immersed for 5 seconds in the etching solution. Similarly to the heat treatment, chemical etching was used to evaluate if cracks in the material were barely closed due to the LSP induced CRS and/or smeared due to grinding and polishing, or instead if they were completely removed.

3. Results and discussion

Samples were denoted as "AB" in the SLM as-built condition, and 3D LSP "A", "B" or "C" when LSP treated with 80% overlap, 40% or two times 80% respectively. As explained in section 2.2 the number *n* of rebuilt layers after the LSP treatment varied between 3, 10 and 20.

3.1 As–built (AB) state

An image of an AB SLM sample is shown in Figures 3 and 4c. It can be observed that, as reported in [9], [29], there is a significant crack density in these samples, with cracks mostly oriented along the vertical build direction. Crack density measurements were made in an area of $8.0 \times 0.5\ mm^2$ and at a depth of 600 μm below the top surface (thus keeping the zone comparable to the 3D LSP measured zones in Figure 4). An average from three measurements was taken and a crack density of $2.16\ \frac{mm}{mm^2}$ was obtained with a relatively small standard deviation of $0.27\frac{mm}{mm^2}$.

Fig. 3 CM247LC sample in the SLM AB condition.

3.2 3D LSP state

As shown in Figure 1a, there were nine unique 3D LSP conditions with different overlap rates and numbers of rebuilt layers n={3, 10, 20}. The rebuilding of additional SLM layers used a misalignment step (i.e. the rebuilt SLM layers were offset) so that the zone of the LSP treated layer could be easily observed (Figure 4a). Below the LSP treated layer, an LSP affected zone with a reduced crack density can be distinguished. The crack density was measured for all samples at different distances below the LSP line. For each measurement, a rectangle was considered, made of the LSP line and the defined distance below it (Figure 4a). Table 3 shows measured crack densities obtained with rectangles extending at 200 microns below the LSP line. Sample A with n = 20 has the lowest crack density ($0.12 \frac{mm}{mm^2}$), which represents a drastic reduction of almost 95% compared to the AB condition ($2.16 \frac{mm}{mm^2}$). This significant improvement is attributed to the removal of TRS and the introduction of CRS by the 3D LSP treatment. As previously stated [9], [16]–[18] the presence of TRS is the main cause of crack generation in critical areas. 3D LSP does not only remove the detrimental TRS which tend to initiate damage and cracks, but introduces CRS which have the opposite effect.

A micrograph of this sample is shown in Figure 4. A reduced crack density zone can clearly be distinguished below the LSP treated layer (Figure 4b). At increased depth, a gradual change occurs, finally reaching the AB state (Figure 4c). The estimated LSP affected zone extended over 500 microns in depth, while only a marginal improvement of crack density was observed *above* the LSP line. This can be understood from the usual SLM induced (tensile) stresses which, in this case, were generated during the SLM rebuilding step.

132
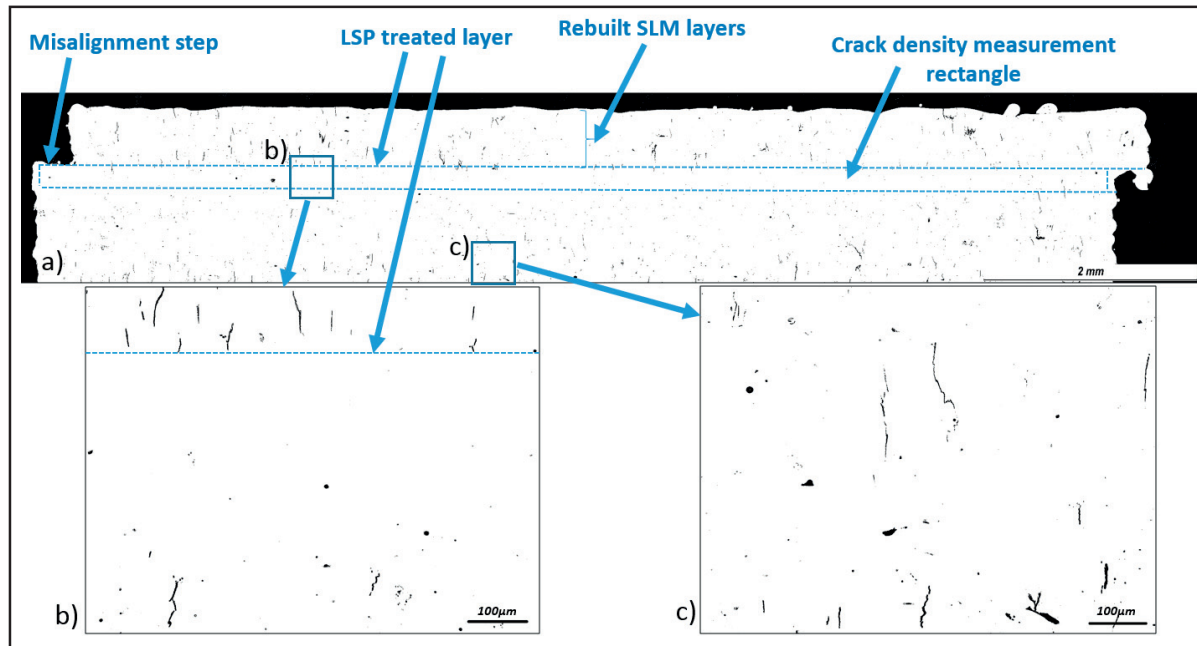
Fig. 4 Micrograph of the A1 sample (80% LSP overlap and 20 rebuilt SLM layers): a) illustration of the rebuilding misalignment step, LSP treated layer, rebuilt SLM layers and the crack density measurement rectangle below the LSP treated layer; b) enlarged LSP affected zone; c) enlarged as –built SLM zone.

Overlap rate	Crack density ($\frac{mm}{mm^2}$)		
	$n = 3$	$n = 10$	$n = 20$
A = 80%	0.28	0.41	0.12
B= 40%	0.2	0.36	1.39
C= 2x80%	0.23	0.66	0.48
AB	2.16		

Table 3 Crack density values in the rectangular area from the LSP line up to 200 microns below.

From Table 3, it can be observed that except for the B sample with n= 20 (with crack density of 1.39 $\frac{mm}{mm^2}$), all other conditions had a fairly similar effect with an average crack density of 0.34 $\frac{mm}{mm^2}$. The particular value of the B 20l sample is difficult to explain, and should probably be related to improper LSP confinement or disturbance in the laser energy. B LSP processing conditions with only 40% overlap are more likely to be sensitive to such variations, due to the lower number of shots per unit area (divided by 9 and 18 compared to A and C respectively). Reversely, B conditions are much more productive compared to A and C.

By changing the vertical size of the rectangle from which the crack density is calculated, the depth of the LSP affected zone can be quantified. Figure 5 shows this analysis for A samples *n* = 3 (A3l), 10 (A10l) and 20 (A20l) and the AB state. The performance of the different samples remains in line with the values given in Table 3. A typical LSP affected depth of 500 microns can be concluded for all A conditions (A3l, A10l, A20l). Below this depth, the average crack density starts increasing.
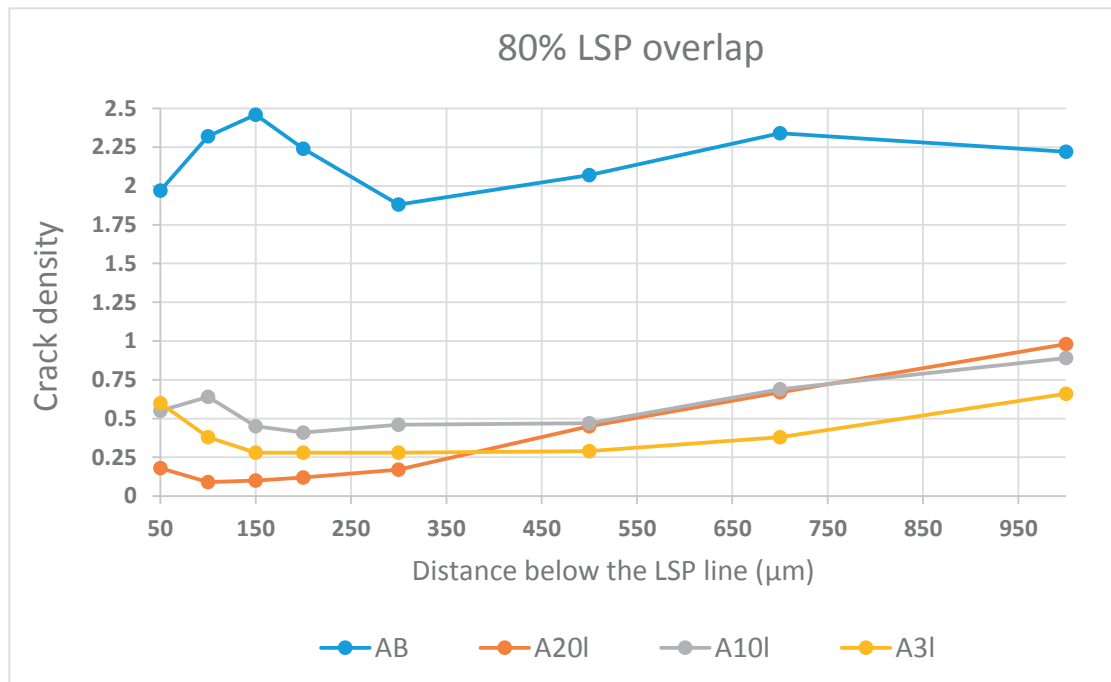
Fig. 5 Average crack density values up to 1000 microns below the LSP line for A samples and the as-built state.

Figure 5 and Table 3 also indicate that the most reliable results (for any overlap rate) are achieved with *n* = 3 (0.2 - 0.28 $\frac{mm}{mm^2}$), i.e. when the least amount of TRS are reintroduced into the sample during the rebuilding phase. These values still represent a significant reduction in crack density of approximately 90% compared to the AB SLM state. An in depth comparison of samples with *n* = 3 is given in Figure 6. All curves follow a similar trend up to 300 to 500 microns, followed by an increase in crack density. In the B condition, this increase starts earlier, around 300 microns, which is consistent with a decreased LSP affected depth related to the decreased number of LSP shots per surface area [26], [27].

One can conclude from the above that if LSP is applied often enough (e.g. every 3 layers) the effect of the number of shots per unit area becomes low. Although higher overlap rates do increase the magnitude and depth of CRS, this effect is limited (and eventually saturates), and

does not strongly influence crack density. In the investigated range of overlap, one can conclude here that lower overlaps can be selected, especially if processing time (productivity) is of concern.
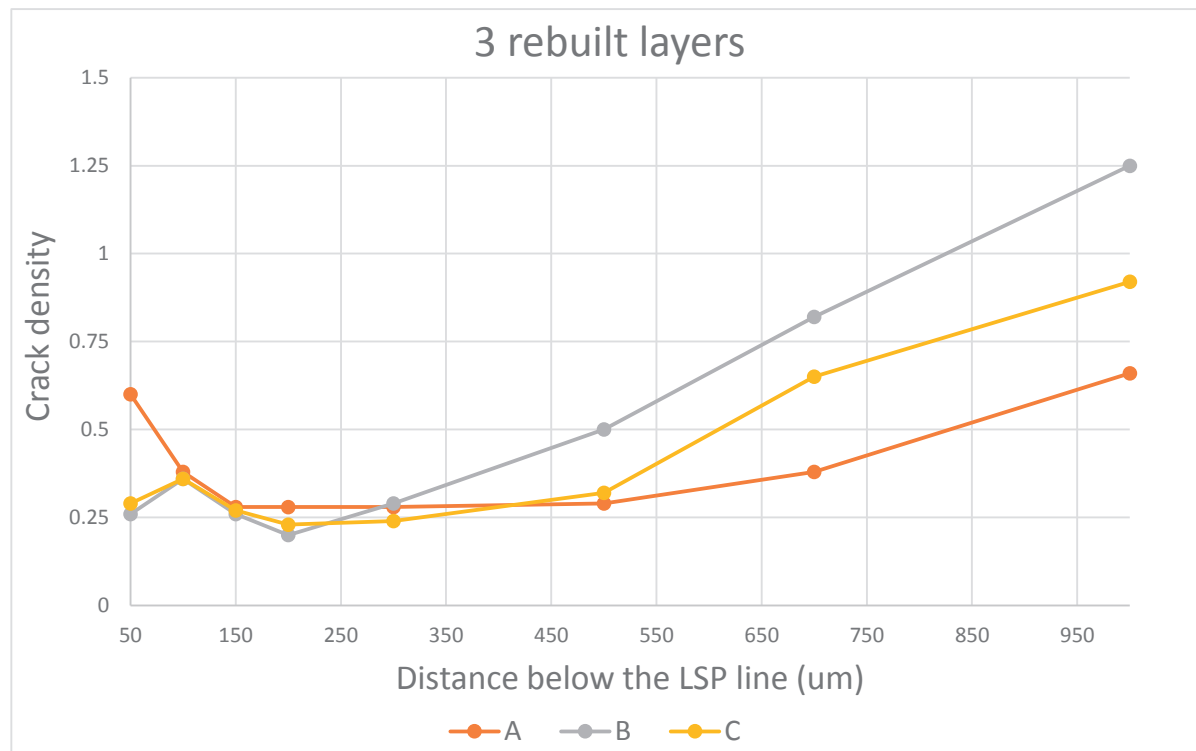
Fig. 6 Crack density values up to 1000 microns below the LSP line for A, B and C samples and *n* = 3.

3.3 Crack closure mechanism

As compressive residual stresses and/or surface preparation can lead to potential artefacts in the accurate measurement of crack density, both stress relieve heat treatment and chemical etching were performed on some of the samples. The stress relieve heat treatment was meant to remove LSP induced CRS to check if cracks would reopen. Chemical etching was used to better reveal grain boundaries and cracks on the sample surface.

Figure 7 shows optical micrographs of the SLM AB condition, and of the 3D LSP treated case with A condition and *n* = 20. In the latter, heat treatment, chemical etching, and polishing steps were considered. The improvement in crack density previously shown in Figures 3, 4, 5, and Table 3 is confirmed (Figures 7a and 7b), with no significant difference when heat treatment or chemical etching is being used (Figures 7c and 7d). This further strengthens the ability of the 3D LSP process

to effectively remove SLM induced cracks, and indicates that many of these cracks form well below the external surface of the material, during SLM processing. This finding may have consequences on the current debates related to the various cracking mechanisms operating in SLM processing of CM247LC.
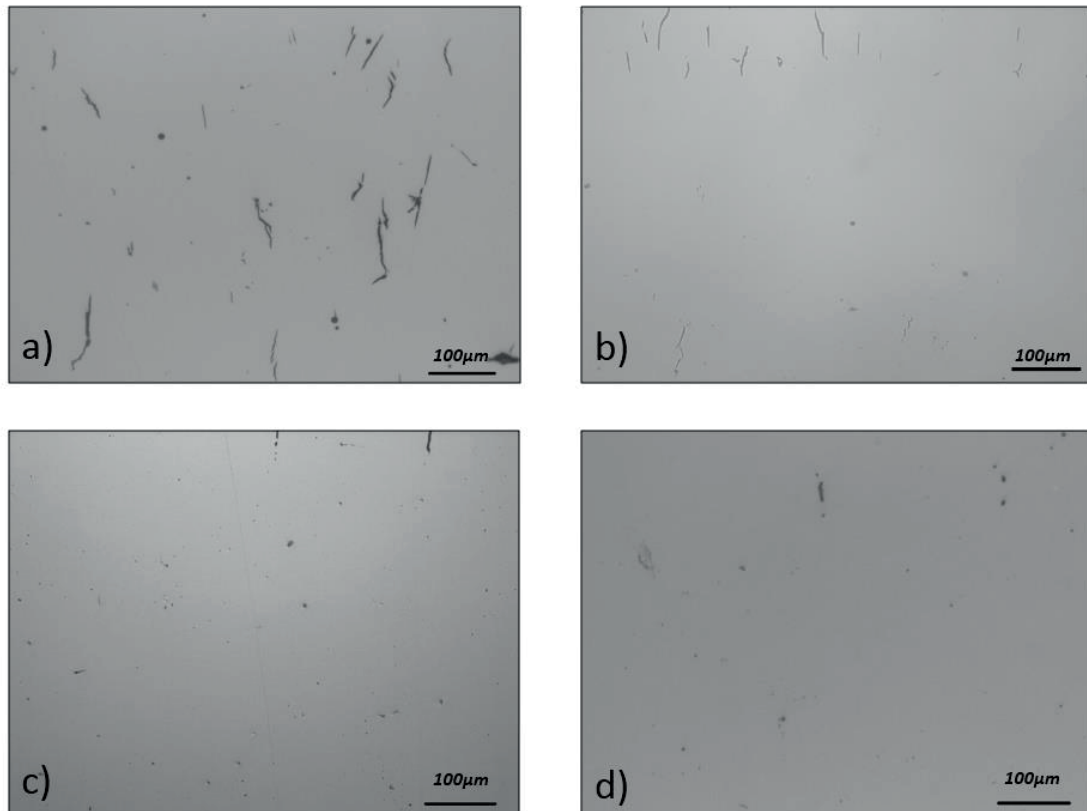
Fig. 7 a) micrograph of the polished SLM AB condition; b) polished 3D LSP A sample with *n* = 20; c) 3D LSP A sample with *n* = 20, heat treated and polished; d) 3D LSP A sample with *n* = 20, heat treated, chemically etched and polished.

Although, as shown in the introduction, the cracking mechanism of γ´ strengthened Ni-based superalloys is still a controversial debate, all proposed cracking mechanisms have tensile residual stresses as a common driving force encouraging crack nucleation and/or growth along the build direction. Consequently the observed decrease in crack density (Figures 3, 4 and 7) and the proposed 3D LSP crack closure mechanism (Figure 8) can be attributed to the removal of existing TRS and the introduction of a compressive stress field in the plane perpendicular to the build direction. In the AB state, tensile residual stresses tend to open up and enhance crack creation (Figure 8a). By applying 3D LSP on the surface of a CM247LC sample (Figure 8b), TRS are replaced

136

by CRS in the near surface region. In the newly introduced CRS zone, vertical cracks are compressed and closed (Figure 8c). The subsequent SLM rebuilding step melts additional layers on top of the CRS zone (Figure 8d), which introduces heat into the underlying layers which promotes diffusion in the closed cracks, and eventually leads to complete healing and bonding. This process produces crack free areas in the 3D LSP affected zone (Figure 4 a,b). As demonstrated, cracks do not reappear upon CRS removal by post heat treatment, or after chemical etching. Further investigations on the kinetics and quality of the crack healing mechanism are planned in the future.
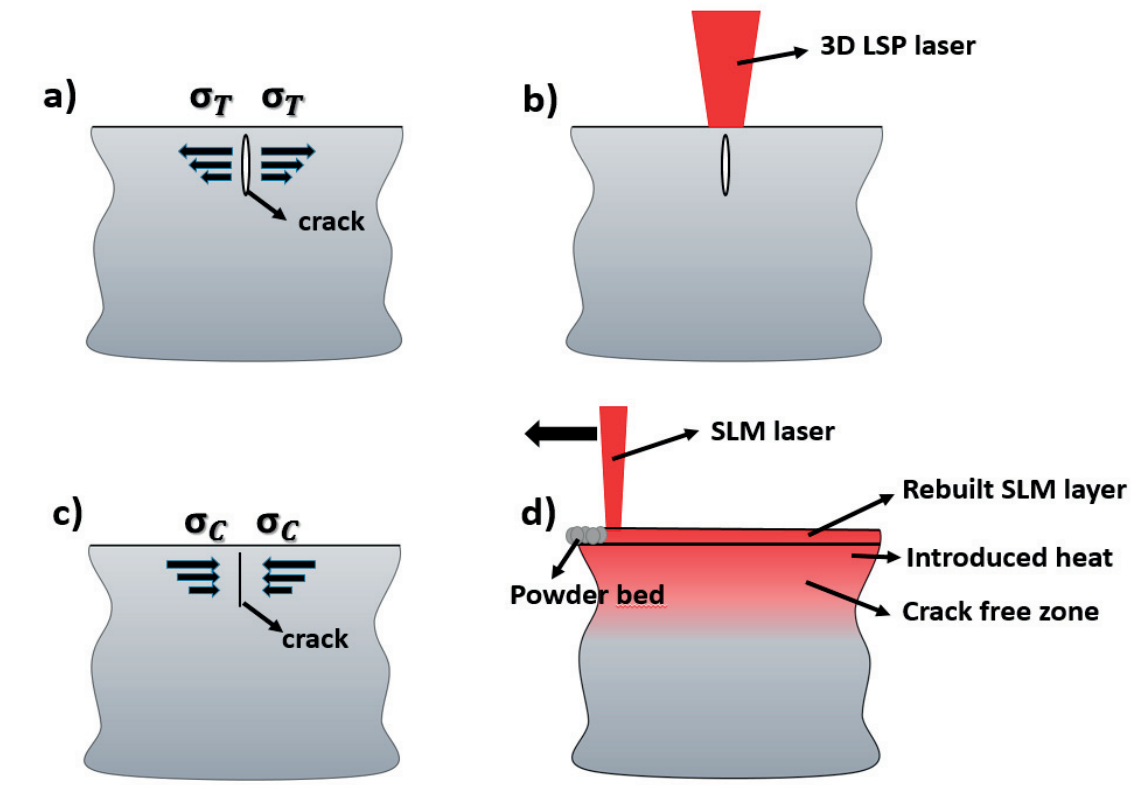
Fig. 8 3D LSP crack closure mechanism: a) tensile residual stresses with one crack in the material in the SLM AB state; b) 3D LSP treatment; c) sample after 3D LSP with introduced compressive residual stresses and closed cracks; d) additional SLM layers and crack healing due to the introduced heat.

4. Conclusions and future work

Crack density was measured for CM247LC SLM samples, either in the as-built (AB) SLM state or after 3D LSP processing using nine different operating conditions. The LSP overlap rate varied

between 40%, 80% and 2x80%, and the number of SLM rebuilt layers after LSP treatment was n ={3, 10, 20}.

The following conclusions can be drawn:

- In the AB state, a substantial and homogeneous crack density of 2.16 $\frac{mm}{mm^2}$ was measured.
- For all nine 3D LSP operating conditions, a significant improvement in crack density was measured.
- The best results were obtained with the 80% LSP overlap rate, where a crack density of 0.12 $\frac{mm}{mm^2}$ up to a depth of 200 microns below the LSP treated line was measured. This represents a decrease of almost 95% compared to the SLM AB state.
- If the LSP treatment is applied often enough (every 3 layers), there is no significant effect of the overlap rate, thus giving the motivation of selecting faster 3D LSP conditions, with lower overlap and enhanced productivity.
- Heat treatment and chemical etching did not induce crack reopening, which confirms the effectiveness of the crack closure mechanism.

Further investigations and optimization of 3D LSP parameters and their effect on crack density in Ni-based alloys will be performed. Lower LSP overlap rates will be tested, together with increased periodicity (e.g. after 1 rebuilt SLM layer). The effect of 3D LSP on crack density above the LSP treated layer needs to be evaluated in more details, such as to conclude better on the operating cracking mechanisms. Finally, larger samples with more complex geometries will be produced on a hybrid (automated) 3D LSP machine, in order to study the control of cracks in a more systematic way, and for different materials.

References

[1] C. Y. Yap *et al.*, "Review of selective laser melting: Materials and applications," *Appl. Phys. Rev.*, Dec. 2015.

138

[2] "Wohlers Associates." [Online]. Available: https://wohlersassociates.com/2018report.htm. [Accessed: 07-Jul-2018].

[3] J.-P. Kruth, J. Deckers, E. Yasa, and R. Wauthlé, "Assessing and comparing influencing factors of residual stresses in selective laser melting using a novel analysis method," *Proc. Inst. Mech. Eng. Part B J. Eng. Manuf.*, vol. 226, no. 6, pp. 980–991, 2012.

[4] K. Kempen, B. Vrancken, S. Buls, L. Thijs, J. Van Humbeeck, and J.-P. Kruth, "Selective Laser Melting of Crack-Free High Density M2 High Speed Steel Parts by Baseplate Preheating," *J. Manuf. Sci. Eng.*, vol. 136, no. 6, p. 061026, Oct. 2014.

[5] S. Afazov, W. A. D. Denmark, B. Lazaro Toralles, A. Holloway, and A. Yaghi, "Distortion prediction and compensation in selective laser melting," *Addit. Manuf.*, vol. 17, pp. 15–22, Oct. 2017.

[6] I. Gurrappa, "Hot Corrosion Behavior of CM 247 LC Alloy in Na2SO4 and NaCl Environments," *Oxid. Met.*, vol. 51, no. 5–6, pp. 353–382, Jun. 1999.

[7] K. Harris, G. L. Erickson, and R. E. Schwer, "Mar M 247 Derivations - Cm 247 Lc Ds Alloy Cmsx Single Crystal Alloys Properties & Performance," *Superalloys 1984*, pp. 221–230, 1984.

[8] O. A. Ojo, N. L. Richards, and M. C. Chaturvedi, "Study of the fusion zone and heat-affected zone microstructures in tungsten inert gas-welded INCONEL 738LC superalloy," *Metall. Mater. Trans. Phys. Metall. Mater. Sci.*, vol. 37, no. 2, pp. 421–433, 2006.

[9] L. N. Carter, C. Martin, P. J. Withers, and M. M. Attallah, "The influence of the laser scan strategy on grain structure and cracking behaviour in SLM powder-bed fabricated nickel superalloy," *J. Alloys Compd.*, vol. 615, pp. 338–347, 2014.

[10] M. J. Donachie and S. J. Donachie, *Superalloys A Technical Guide*. 2002.

[11] J. E. Doherty, B. H. Kea, and A. F. Giamei, "On the origin of the ductility enhancement in Hf-doped Mar-M200," *JOM*, vol. 23, no. 11, pp. 59–62, Nov. 1971.

[12] J. Zhang and R. F. Singer, "Effect of Grain-Boundary Characteristics on Castability of Nickel-Base Superalloys," *Metall. Mater. Trans. Phys. Metall. Mater. Sci.*, vol. 35 A, no. 3, pp. 939–946, 2004.

[13] D. Dye, O. Hunziker, and R. C. Reed, "Numerical analysis of the weldability of superalloys," *Acta Mater.*, vol. 49, no. 4, pp. 683–697, 2001.

[14] M. B. Henderson, D. Arrell, R. Larsson, M. Heobel, and G. Marchant, "Nickel based superalloy welding practices for industrial gas turbine applications," *Sci. Technol. Weld. Join.*, vol. 9, no. 1, pp. 13–21, 2004.

[15] A. J. Ramirez and J. C. Lippold, "High temperature behavior of Ni-base weld metal Part II - Insight into the mechanism for ductility dip cracking," *Mater. Sci. Eng. A*, vol. 380, no. 1, pp. 245–258, 2004.

[16] P. Kanagarajah, F. Brenne, T. Niendorf, and H. J. Maier, "Inconel 939 processed by selective laser melting: Effect of microstructure and temperature on the mechanical properties under static and cyclic loading," *Mater. Sci. Eng. A*, vol. 588, pp. 188–195, Dec. 2013.

[17] F. Liu, X. Lin, G. Yang, M. Song, J. Chen, and W. Huang, "Microstructure and residual stress of laser rapid formed Inconel 718 nickel-base superalloy," *Opt. Laser Technol.*, vol. 43, no. 1, pp. 208–213, Feb. 2011.

[18] N. J. Harrison, I. Todd, and K. Mumtaz, "Reduction of micro-cracking in nickel superalloys processed by Selective Laser Melting: A fundamental alloy design approach," *Acta Mater.*, vol. 94, pp. 59–68, Aug. 2015.

[19] S. Catchpole-Smith, N. Aboulkhair, L. Parry, C. Tuck, I. A. Ashcroft, and A. Clare, "Fractal scan strategies for selective laser melting of 'unweldable' nickel superalloys," *Addit. Manuf.*, vol. 15, pp. 113–122, May 2017.

[20] R. W. E. P.W. Davies, "The contribution of voids to the tertiary creep of gold," *Acta Met.*, vol. 13, no. 3, pp. 353–361, 1965.

[21] A. Baldan, "Rejuvenation procedures to recover creep properties of nickel-base superalloys by heat treatment and hot isostatic pressing techniques - A review," *J. Mater. Sci.*, vol. 26, no. 13, pp. 3409–3421, 1991.

[22] M. Cloots, P. J. Uggowitzer, and K. Wegener, "Investigations on the microstructure and crack formation of IN738LC samples processed by selective laser melting using Gaussian and doughnut profiles," *Mater. Des.*, vol. 89, pp. 770–784, 2016.

[23] C. S. Montross, V. Florea, and M. V. Swain, "The influence of coatings on subsurface mechanical properties of laser peened 2011-T3 aluminum," *J. Mater. Sci.*, vol. 36, no. 7, pp. 1801–1807, Apr. 2001.

[24] A. K. Gujba and M. Medraj, "Laser Peening Process and Its Impact on Materials Properties in Comparison with Shot Peening and Ultrasonic Impact Peening," *Materials*, vol. 7, no. 12, pp. 7925–7974, 2014.

[25] N. Kalentics, R. Logé, and E. BOILLAT, "Method and Device for Implementing Laser Shock Peening or Warm Laser Shock Peening During Selective Laser Melting," US20170087670 A1, 30-Mar-2017.

[26] N. Kalentics, E. Boillat, P. Peyre, S. Ćirić-Kostić, N. Bogojević, and R. E. Logé, "Tailoring residual stress profile of Selective Laser Melted parts by Laser Shock Peening," *Addit. Manuf.*, vol. 16, pp. 90–97, Aug. 2017.

[27] N. Kalentics *et al.*, "3D Laser Shock Peening – A new method for the 3D control of residual stresses in Selective Laser Melting," *Mater. Des.*, vol. 130, pp. 350–356, Sep. 2017.

[28] R. Engeli, "Selective laser melting & heat treatment of γ´ strengthened Ni-base superalloys for high temperature applications," Doctoral Thesis, ETH Zurich, 2017.

[29] V. D. Divya *et al.*, "Microstructure of selective laser melted CM247LC nickel-based superalloy and its evolution through heat treatment," *Mater. Charact.*, vol. 114, pp. 62–74, 2016.

Chapter 10. Conclusions

10.1 Achieved results

Over the course of this thesis we have tried to present the effects of 3D LSP: a hybrid Additive Manufacturing process which combines Laser Shock Peening with Selective Laser Melting. In this novel field we have focused on the issues related to the anisotropic microstructure and the accumulation of tensile residual stresses (TRS) in SLM parts, and the new degrees of freedom provided by LSP for a better control of residual stresses, microstructures, geometric distortions, crack density and fatigue life. The manuscript proposes a paper on each of these topics.

In this chapter we will summarize and briefly present the results achieved in the different sections of this thesis.

In Chapter 4, we have shown the capability of LSP treatment to alter the residual stresses of SLM parts even when applied on their rough as – built surface state, which was initially not clear due to the lack of prior art on such applications. Samples made out of the martensitic PH1 and austenitic 316L stainless steels were treated with various LSP processing parameters and the following conclusions could be made:

- LSP treatment of parts with high surface roughness such as the SLM as – built surface state is feasible, and the well-known high tensile residual stresses in the near-surface region are easily converted to compressive residual stresses (CRS).
- A smaller spot size (1 mm diameter) applied during the LSP treatment leads to larger values of introduced CRS compared to larger spots such as 2 and 5 mm. These trends were observed in both coating conditions, i.e. with and without an ablative coating.
- A larger spot size leads to a deeper profile of CRS.
- Ablative coatings lead to larger and deeper CRS.
- Higher overlap rates (80%) lead to higher and deeper CRS due to the increased number of shots per surface area, but require longer processing times compared to smaller overlap rates (40%), thus affecting the productivity of the process.

Our work on the effect of 3D LSP process on the residual stress state of 316L stainless steel samples was detailed in Chapter 5 and brought the following contributions:

- 3D LSP accumulates and increases CRS both in magnitude and depth compared to conventional surface 2D LSP. This was observed for various processing parameters.
- 3D LSP with a smaller spot size and thus a reduced pulse energy (keeping the same energy density) can create deeper CRS compared to conventional LSP treatment with a larger spot size and pulse energy. This was observed for different overlap rates (40 and 80% overlap), and highlights the interest of using a smaller spot size which can be provided by lasers with lower pulse energies but at significantly higher repetition rates. Such lasers are readily available on the market and are substantially cheaper compared to higher energy lasers needed for LSP with larger spot sizes. Another benefit is that they are also smaller in size and can be coupled to a fiber beam delivery which are all important advantages when thinking of applying such lasers to a hybrid 3D LSP machine.

In Chapter 6, our work on the effect of LSP treatments on the microstructure and microhardness of 316L SLM samples was presented. The following conclusions could be drawn:

- Laser Shock Peening significantly increases the microhardness of SLM AB samples but does not affect the grain size in the as – treated LSP state (i.e. without a subsequent heat treatment).
- In the zone affected by the LSP process, recrystallization kinetics are strongly accelerated upon heat treatment. This results in a refined, equiaxed grain structure which is very different from the SLM AB microstructure. Thus, 3D LSP offers a very promising new route for 3D control and tailoring of microstructures and mechanical properties of SLM parts. It is also a way of reducing or eliminating the mechanical anisotropy related to crystallographic textures, which are often very strong in SLM parts, and cannot always be changed by conventional heat treatments.

Our investigation of the geometrical accuracy of bridge like SLM parts made out of Ti6Al4V and the improvements brought by 3D LSP were presented in Chapter 7. It provided the following contributions:

- In the SLM AB state, a significant distortion angle above 2.2° can be observed, particularly pronounced for SLM parts with thinner overhangs.
- The increase in overhang thickness slightly reduces the distortion in SLM AB parts.
- 2D LSP treatment is able to reduce the distortion angle, especially for thinner overhangs. As the thickness of parts increases, the beneficial effect of a 2D LSP post treatment is less pronounced.
- 3D LSP brings a clear improvement in the geometrical accuracy and a decrease in distortion of up to 75% compared to the AB state (in the current work with only 2 LSP treatments during the SLM process). A further improvement and complete reduction of

geometrical distortions is expected by increasing the number and frequency of LSP treatments during the 3D LSP process.

In Chapter 8, we have investigated the microhardness and fatigue life of 316L stainless steel parts considering different processing steps: (i) the AB SLM state, (ii) the HIP post treatment, (iii) the conventional surface LSP post treatment (2D LSP), (iv) the 3D LSP process. These were also compared with conventional wrought samples. The study considered samples with both non – machined and machined surface state. The following conclusions could be drawn:

- An exceptional 15 times increase in fatigue life and 44% improvement in fatigue limit of a non – machined 3D LSP sample compared to the AB SLM state was achieved.
- In the machined surface state, an even more remarkable improvement of more than 57 times compared to the conventionally made 316L and more than 14 times compared to the AB state was observed. The fatigue limit was increased by 33% compared to the AB state and 41% compared to the conventionally made 316L.

Finally in Chapter 9, we have addressed the issue of crack generation in a Ni-based superalloy, CM247LC. Crack density was measured in samples in the SLM AB state as well as processed by various 3D LSP processing parameters. The work can be summarized as follows:

- In the AB state, a significant crack density of 2.16 $\frac{mm}{mm^2}$ was measured.
- All 3D LSP processing conditions brought significant improvements and decreased the crack density.
- The best results were obtained with an 80% LSP overlap rate which resulted in a crack density of 0.12 $\frac{mm}{mm^2}$. This represents a decrease of 95% compared to the SLM AB state.
- A stress relieving heat treatment and chemical etching of the surface did not reveal additional cracks in the 3D LSP treated samples. This confirms the stability of the proposed 3D LSP crack closing mechanism.

10.2 Future developments

The goal of this PhD work was to show the feasibility of a novel hybrid 3D LSP process, and the interest in further research on the new degrees of freedom provided by the method. Since this has been an initial study, we have tried to cover a broad range of improvements that this process achieves and to bring forward experimental results which show the beneficial effects on various issues of the SLM process such as the inadequate microstructure, detrimental residual stresses,

distortions, decreased fatigue life and high crack density of SLM processed parts. By taking such an approach of addressing a number of SLM related issues we wanted to address an audience from both academia and industry. This would likely intensify future research activities in the field of 3D LSP and would decrease the time needed for such hybrid machines to enter the commercial market. But such an approach has, besides attracting interest, opened interesting research questions on many of the addressed topics which leave significant room for future academic work.

Similarly to the SLM field, development of material specific 3D LSP processing parameters is needed to achieve optimal results. Additionally, 3D LSP parameters are also dependent on the intended improvements of the process such as microstructure design, distortion decrease, fatigue life improvement, crack density decrease, and should be fine-tuned accordingly. Special interest should be addressed to:

- More accurate investigation of the effects of the number n of rebuilt SLM layers between two subsequent LSP treatments.
- Fine tuning of the laser spot size, and evaluating the potential of using a larger spot size for the inner part of the treated surface and a smaller spot for the outer part (shell – core approach).
- Further investigation of the effects of 3D LSP on the distortion of parts with complex geometries.
- Evaluation of the influence of 3D LSP on parts with thin overhangs (below 1mm).
- Further investigation of the effect on the fatigue life at elevated temperatures (temperature stability of internal stresses).
- Investigation on 3D LSP effects on cracking mechanisms in different materials, and assessment on the competition between overlap rate and periodicity of LSP treatments (number n).
- Evaluation of the optimal laser pulse energy for various materials as a function of the repetition rate and with the goal of achieving optimal productivity. E.g. softer aluminum alloys might require lower energy per pulse which in return can be achieved at higher repetition rates and improved productivity.

Last but not least, to fully understand the evolution of residual stresses in parts produced by 3D LSP and their effect on the geometrical distortions, fatigue life and crack density, extensive efforts in modeling and simulation of 3D residual stresses of both SLM and LSP processes are crucial. Significant efforts in modeling of residual stresses have been made by various groups around the world [187]–[192]. This will help to better predict the residual stress state after the hybrid 3D LSP process and optimize the processing parameters which are best suited for each of these 3D LSP applications.

144

Bibliography

[1] "What is Additive Manufacturing? | Wohlers Associates." [Online]. Available: https://wohlersassociates.com/additive-manufacturing.html. [Accessed: 31-Jul-2018].

[2] T. Wohlers and T. Gornet, "History of additive manufacturing," p. 34, 2014.

[3] "Wohlers Associates." [Online]. Available: https://wohlersassociates.com/2018report.htm. [Accessed: 07-Jul-2018].

[4] A. Bandyopadhyay and B. Heer, "Additive manufacturing of multi-material structures," *Mater. Sci. Eng. R Rep.*, vol. 129, pp. 1–16, Jul. 2018.

[5] M. Vaezi, S. Chianrabutra, B. Mellor, and S. Yang, "Multiple material additive manufacturing – Part 1: a review," *Virtual Phys. Prototyp.*, vol. 8, no. 1, pp. 19–50, Mar. 2013.

[6] Siemens, "Breakthrough with 3D printed gas turbine blades." [Online]. Available: https://www.siemens.com/innovation/en/home/pictures-of-the-future/industry-and-automation/additive-manufacturing-3d-printed-gas-turbine-blades.html. [Accessed: 30-Jul-2018].

[7] B. Boen, "3-D Printed Rocket Parts Rival Traditionally Manufactured Parts," *NASA*, 02-Mar-2015. [Online]. Available: http://www.nasa.gov/exploration/systems/sls/3dprinting.html. [Accessed: 30-Jul-2018].

[8] "Wohlers Associates Publishes 23rd Edition of Its 3D Printing and Additive Manufacturing Industry Report | Wohlers Associates." [Online]. Available: https://wohlersassociates.com/press74.html. [Accessed: 14-May-2018].

[9] K.-U. Bletzinger and E. Ramm, "Structural optimization and form finding of light weight structures," *Comput. Struct.*, vol. 79, no. 22, pp. 2053–2062, Sep. 2001.

[10] "Printing the future: Airbus expands its applications of the revolutionary additive layer manufacturing process," *Airbus*. [Online]. Available: http://www.airbus.com/newsroom/news/en/2014/03/printing-the-future-airbus-expands-its-applications-of-the-revolutionary-additive-layer-manufacturing-process.html. [Accessed: 07-Jul-2018].

[11] "GE buys Germany's Concept Laser after SLM bid fails," *Reuters*, 27-Oct-2016.

[12] "GE Agrees to Purchase Controlling Shares of Arcam AB," *GE Additive*. [Online]. Available: https://www.ge.com/additive/press-releases/ge-agrees-purchase-controlling-shares-arcam-ab. [Accessed: 08-Jul-2018].

[13] T. Kellner, "How 3D Printing Will Change Manufacturing," *GE Reports*, 13-Nov-2017. [Online]. Available: https://www.ge.com/reports/epiphany-disruption-ge-additive-chief-explains-3d-printing-will-upend-manufacturing/. [Accessed: 08-Jul-2018].

[14] "GE's new aviation plant in the heart of Europe will build engines with 3D printed parts for next-gen Cessna Denali," *GE Additive*. [Online]. Available: https://www.ge.com/additive/case-study/ges-new-aviation-plant-heart-europe-will-build-engines-3d-printed-parts-next-gen-cessna. [Accessed: 08-Jul-2018].

[15] "Additive manufacturing at GE Aviation." [Online]. Available: https://www.industrial-lasers.com/articles/print/volume-28/issue-6/features/additive-manufacturing-at-ge-aviation.html. [Accessed: 15-Jul-2018].

[16] W. Meiners, K. D. Wissenbach, and A. D. Gasser, "Verfahren zur Herstellung eines Formkörpers," DE19649865C1, 12-Feb-1998.

[17] K. Kempen, E. Yasa, L. Thijs, J.-P. Kruth, and J. Van Humbeeck, "Microstructure and mechanical properties of Selective Laser Melted 18Ni-300 steel," *Phys. Procedia*, vol. 12, Part A, pp. 255–263, 2011.

[18] "Heavy metal," *The Economist*, 03-May-2014.

[19] "Airbus puts its faith in 3D printed parts." [Online]. Available: http://www.materialsforengineering.co.uk/engineering-materials-news/airbus-puts-its-faith-in-3d-printed-parts/62218/. [Accessed: 08-Jul-2018].

[20] C. Y. Yap *et al.*, "Review of selective laser melting: Materials and applications," *Appl. Phys. Rev.*, Dec. 2015.

[21] "Additive Manufacturing," *Fraunhofer-Gesellschaft*. [Online]. Available: https://www.fraunhofer.de/en/research/current-research/additive-manufacturing.html. [Accessed: 30-Jul-2018].

[22] "Dental Laboratory Services." [Online]. Available: http://bavaria-medical.ro/en/services.html. [Accessed: 30-Jul-2018].

[23] "LZN - Technologien." [Online]. Available: http://www.lzn-hamburg.de/technologien.html. [Accessed: 30-Jul-2018].

[24] R. plc, "Renishaw: Industries," *Renishaw*. [Online]. Available: http://www.renishaw.com/en/industrial-applications-of-renishaw-metal-additive-manufacturing-technology--15256. [Accessed: 30-Jul-2018].

[25] Randall Desmond, "Proto Labs Acquires 3D Printing Company FineLine Prototyping Inc.," *3DPrint.com | The Voice of 3D Printing / Additive Manufacturing*, 25-Apr-2014. .

[26] W. E. Frazier, "Metal Additive Manufacturing: A Review," *J. Mater. Eng. Perform.*, vol. 23, no. 6, pp. 1917–1928, Jun. 2014.

[27] L Thijs, J Van Humbeeck, K Kempen, E Yasa, JP Kruth, and M Rombouts, "Investigation on the inclusions in maraging steel produced by Selective Laser Melting," in *Innovative Developments in Virtual and Physical Prototyping*, 0 vols., CRC Press, 2011, pp. 297–304.

[28] H. Stoffregen, K. Butterweck, and E. Abele, "Fatigue Analysis in Selective Laser Melting: Review and Investigation of Thin-walled Actuator Housings," presented at the 25th Solid Freeform Fabrication Symposium 2014, Austin, Texas, 2014, pp. 635–650.

[29] T. H. Becker, M. Beck, and C. Scheffer, "MICROSTRUCTURE AND MECHANICAL PROPERTIES OF DIRECT METAL LASER SINTERED TI-6AL-4V," *South Afr. J. Ind. Eng.*, vol. 26, no. 1, pp. 1–10, Mar. 2015.

[30] L. T. B. Vrancken, "Microstructure and mechanical properties of a novel β titanium metallic composite by selective laser melting," *Acta Mater.*, vol. 68, no. 15, pp. 150–158, 2014.

146

[31] E. Sallica-Leva, A. L. Jardini, and J. B. Fogagnolo, "Microstructure and mechanical behavior of porous Ti–6Al–4V parts obtained by selective laser melting," *J. Mech. Behav. Biomed. Mater.*, vol. 26, pp. 98–108, Oct. 2013.

[32] H. K. Rafi, D. Pal, N. Patil, T. L. Starr, and B. E. Stucker, "Microstructure and Mechanical Behavior of 17-4 Precipitation Hardenable Steel Processed by Selective Laser Melting," *J. Mater. Eng. Perform.*, vol. 23, no. 12, pp. 4421–4428, Sep. 2014.

[33] J.-P. Kruth, M. Badrossamay, E. Yasa, J. Deckers, L. Thijs, and J. Van Humbeeck, "Part and material properties in selective laser melting of metals," presented at the Proceedings of the 16th International Symposium on Electromachining, 2010.

[34] K. Kempen, L. Thijs, J. Van Humbeeck, and J.-P. Kruth, "Mechanical Properties of AlSi10Mg Produced by Selective Laser Melting," *Phys. Procedia*, vol. 39, pp. 439–446, 2012.

[35] T. Vilaro, C. Colin, J. D. Bartout, L. Nazé, and M. Sennour, "Microstructural and mechanical approaches of the selective laser melting process applied to a nickel-base superalloy," *Mater. Sci. Eng. A*, vol. 534, pp. 446–451, Feb. 2012.

[36] B. Vrancken, L. Thijs, J.-P. Kruth, and J. Van Humbeeck, "Heat treatment of Ti6Al4V produced by Selective Laser Melting: Microstructure and mechanical properties," *J. Alloys Compd.*, vol. 541, pp. 177–185, Nov. 2012.

[37] K. Kunze, T. Etter, J. Grässlin, and V. Shklover, "Texture, anisotropy in microstructure and mechanical properties of IN738LC alloy processed by selective laser melting (SLM)," *Mater. Sci. Eng. A*, vol. 620, pp. 213–222, Jan. 2015.

[38] P. Kanagarajah, F. Brenne, T. Niendorf, and H. J. Maier, "Inconel 939 processed by selective laser melting: Effect of microstructure and temperature on the mechanical properties under static and cyclic loading," *Mater. Sci. Eng. A*, vol. 588, pp. 188–195, Dec. 2013.

[39] T. E. L. Rickenbacher, "High temperature material properties of IN738LC processed by selective laser melting (SLM) technology," *Rapid Prototyp. J.*, vol. 19, no. 4, 2013.

[40] M. Simonelli, Y. Y. Tse, and C. Tuck, "Further Understanding of Ti6Al4V Selective Laser Melting Using Texture Analysis," *Proc. 23rd Annu. Int. Solid Free. Fabr. Symp. Austin TX*, 2012.

[41] L. Thijs *et al.*, "Strong morphological and crystallographic texture and resulting yield strength anisotropy in Selective Laser Melted tantalum," *Acta Mater.*, vol. 61, no. 12, pp. 4657–4668, Jul. 2013.

[42] S. Sarkar, C. Siva Kumar, and A. Kumar Nath, "Effect of mean stresses on mode of failures and fatigue life of selective laser melted stainless steel," *Mater. Sci. Eng. A*, vol. 700, pp. 92–106, Jul. 2017.

[43] C. Casavola, S. L. Campanelli, and C. Pappalettere, "Experimental analysis of residual stresses in the selective laser melting process," in *Proccedings of the XIth International Congress and Exposition, Orlando, Florida, USA*, 2008.

[44] J.-P. Kruth, J. Deckers, E. Yasa, and R. Wauthle, "Assessing and comparing influencing factors of residual stresses in selective laser melting using a novel analysis method," *Proc. Inst. Mech. Eng. Part B J. Eng. Manuf.*, vol. 226, no. 6, pp. 980–991, Jun. 2012.

[45] A. S. Wu, D. W. Brown, M. Kumar, G. F. Gallegos, and W. E. King, "An Experimental Investigation into Additive Manufacturing-Induced Residual Stresses in 316L Stainless Steel," *Metall. Mater. Trans. A*, vol. 45, no. 13, pp. 6260–6270, Dec. 2014.

[46] K. Kempen, B. Vrancken, S. Buls, L. Thijs, J. Van Humbeeck, and J.-P. Kruth, "Selective Laser Melting of Crack-Free High Density M2 High Speed Steel Parts by Baseplate Preheating," *J. Manuf. Sci. Eng.*, vol. 136, no. 6, p. 061026, Oct. 2014.

[47] I. Yadroitsava, S. Grewar, D. G. Hattingh, and I. Yadroitsev, "Residual Stress in SLM Ti6Al4V Alloy Specimens," *Mater. Sci. Forum*, vol. 828–829, pp. 305–310, Aug. 2015.

[48] F. Liu, X. Lin, G. Yang, M. Song, J. Chen, and W. Huang, "Microstructure and residual stress of laser rapid formed Inconel 718 nickel-base superalloy," *Opt. Laser Technol.*, vol. 43, no. 1, pp. 208–213, Feb. 2011.

[49] L. N. Carter, C. Martin, P. J. Withers, and M. M. Attallah, "The influence of the laser scan strategy on grain structure and cracking behaviour in SLM powder-bed fabricated nickel superalloy," *J. Alloys Compd.*, vol. 615, pp. 338–347, 2014.

[50] G. Kasperovich, J. Haubrich, J. Gussone, and G. Requena, "Correlation between porosity and processing parameters in TiAl6V4 produced by selective laser melting," *Mater. Des.*, vol. 105, pp. 160–170, Sep. 2016.

[51] L. Thijs, F. Verhaeghe, T. Craeghs, J. V. Humbeeck, and J.-P. Kruth, "A study of the microstructural evolution during selective laser melting of Ti–6Al–4V," *Acta Mater.*, vol. 58, no. 9, pp. 3303–3312, May 2010.

[52] K. R. H. Gong, "Effect of defects on fatigue tests of as-built TI-6AL-4V parts fabricated by selective laser melting," *23rd Annu. Int. Solid Free. Fabr. Symp. - Addit. Manuf. Conf. SFF 2012*, pp. 499–506, 2012.

[53] R. Li, J. Liu, Y. Shi, L. Wang, and W. Jiang, "Balling behavior of stainless steel and nickel powder during selective laser melting process," *Int. J. Adv. Manuf. Technol.*, vol. 59, no. 9–12, pp. 1025–1035, Apr. 2012.

[54] L. Thijs, K. Kempen, J.-P. Kruth, and J. Van Humbeeck, "Fine-structured aluminium products with controllable texture by selective laser melting of pre-alloyed AlSi10Mg powder," *Acta Mater.*, vol. 61, no. 5, pp. 1809–1819, Mar. 2013.

[55] T. Niendorf, S. Leuders, A. Riemer, H. A. Richard, T. Tröster, and D. Schwarze, "Highly Anisotropic Steel Processed by Selective Laser Melting," *Metall. Mater. Trans. B*, vol. 44, no. 4, pp. 794–796, May 2013.

[56] K. Kunze, T. Etter, J. Grässlin, and V. Shklover, "Texture, anisotropy in microstructure and mechanical properties of IN738LC alloy processed by selective laser melting (SLM)," *Mater. Sci. Eng. A*, vol. 620, pp. 213–222, Jan. 2015.

[57] P. Kanagarajah, F. Brenne, T. Niendorf, and H. J. Maier, "Inconel 939 processed by selective laser melting: Effect of microstructure and temperature on the mechanical properties under static and cyclic loading," *Mater. Sci. Eng. A*, vol. 588, pp. 188–195, Dec. 2013.

[58] T. E. L. Rickenbacher, "High temperature material properties of IN738LC processed by selective laser melting (SLM) technology," *Rapid Prototyp. J.*, vol. 19, no. 4, 2013.

[59] M. Simonelli, Y. Y. Tse, and C. Tuck, "Further Understanding of Ti6Al4V Selective Laser Melting Using Texture Analysis," *Proc. 23rd Annu. Int. Solid Free. Fabr. Symp. Austin TX*, 2012.

[60] L. Thijs *et al.*, "Strong morphological and crystallographic texture and resulting yield strength anisotropy in Selective Laser Melted tantalum," *Acta Mater.*, vol. 61, no. 12, pp. 4657–4668, Jul. 2013.

[61] J.-P. Kruth, M. Badrossamay, E. Yasa, J. Deckers, L. Thijs, and J. Van Humbeeck, "Part and material properties in selective laser melting of metals," presented at the Proceedings of the 16th International Symposium on Electromachining, 2010.

[62] B. Song, S. Dong, B. Zhang, H. Liao, and C. Coddet, "Effects of processing parameters on microstructure and mechanical property of selective laser melted Ti6Al4V," *Mater. Des.*, vol. 35, pp. 120–125, Mar. 2012.

[63] K. P. Monroy, J. Delgado, L. Sereno, J. Ciurana, and N. J. Hendrichs, "Effects of the Selective Laser Melting manufacturing process on the properties of CoCrMo single tracks," *Met. Mater. Int.*, vol. 20, no. 5, pp. 873–884, Sep. 2014.

[64] N. T. Aboulkhair, N. M. Everitt, I. Ashcroft, and C. Tuck, "Reducing porosity in AlSi10Mg parts processed by selective laser melting," *Addit. Manuf.*, vol. 1–4, pp. 77–86, Oct. 2014.

[65] J. A. Cherry, H. M. Davies, S. Mehmood, N. P. Lavery, S. G. R. Brown, and J. Sienz, "Investigation into the effect of process parameters on microstructural and physical properties of 316L stainless steel parts by selective laser melting," *Int. J. Adv. Manuf. Technol.*, vol. 76, no. 5, pp. 869–879, Feb. 2015.

[66] Peter Mercelis and Jean-Pierre Kruth, "Residual stresses in selective laser sintering and selective laser melting," *Rapid Prototyp. J.*, vol. 12, no. 5, pp. 254–265, Oct. 2006.

[67] D. Buchbinder, W. Meiners, N. Pirch, K. Wissenbach, and J. Schrage, "Investigation on reducing distortion by preheating during manufacture of aluminum components using selective laser melting," *J. Laser Appl.*, vol. 26, no. 1, p. 012004, 2014.

[68] A. V. Gusarov, M. Pavlov, and I. Smurov, "Residual Stresses at Laser Surface Remelting and Additive Manufacturing," *Phys. Procedia*, vol. 12, Part A, pp. 248–254, 2011.

[69] M. Shiomi, K. Osakada, K. Nakamura, T. Yamashita, and F. Abe, "Residual Stress within Metallic Model Made by Selective Laser Melting Process," *CIRP Ann. - Manuf. Technol.*, vol. 53, no. 1, pp. 195–198, 2004.

[70] E. R. Denlinger and P. Michaleris, "Effect of stress relaxation on distortion in additive manufacturing process modeling," *Addit. Manuf.*, vol. 12, pp. 51–59, Oct. 2016.

[71] M. B. Henderson, D. Arrell, R. Larsson, M. Heobel, and G. Marchant, "Nickel based superalloy welding practices for industrial gas turbine applications," *Sci. Technol. Weld. Join.*, vol. 9, no. 1, pp. 13–21, 2004.

[72] M. J. Donachie and S. J. Donachie, *Superalloys A Technical Guide*. 2002.

[73] D. Dye, O. Hunziker, and R. C. Reed, "Numerical analysis of the weldability of superalloys," *Acta Mater.*, vol. 49, no. 4, pp. 683–697, 2001.

[74] A. J. J. M. G. A. YOUNG, T. E. CAPOBIANCO, M. A. PENIK, B. W. MORRIS, "The Mechanism of Ductility Dip Cracking in Nickel-Chromium Alloys," *Weld. J.*, no. February, pp. 31–43, 2008.

[75] K. Harris, G. L. Erickson, and R. E. Schwer, "Mar M 247 Derivations - Cm 247 Lc Ds Alloy Cmsx Single Crystal Alloys Properties & Performance," *Superalloys 1984*, pp. 221–230, 1984.

[76] O. A. Ojo, N. L. Richards, and M. C. Chaturvedi, "Study of the fusion zone and heat-affected zone microstructures in tungsten inert gas-welded INCONEL 738LC superalloy," *Metall. Mater. Trans. Phys. Metall. Mater. Sci.*, vol. 37, no. 2, pp. 421–433, 2006.

[77] I. Gurrappa, "Hot Corrosion Behavior of CM 247 LC Alloy in Na2SO4 and NaCl Environments," *Oxid. Met.*, vol. 51, no. 5–6, pp. 353–382, Jun. 1999.

[78] T. W. Charles S. Montross, "Laser Shock Processing and its Effects on Microstructure and Properties of Metal Alloys: A Review," *Int. J. Fatigue*, vol. 24, no. 10, pp. 1021–1036, 2002.

[79] R. K. Nalla, I. Altenberger, U. Noster, G. Y. Liu, B. Scholtes, and R. O. Ritchie, "On the influence of mechanical surface treatments—deep rolling and laser shock peening—on the fatigue behavior of Ti–6Al–4V at ambient and elevated temperatures," *Mater. Sci. Eng. A*, vol. 355, no. 1–2, pp. 216–230, Aug. 2003.

[80] I. Nikitin, B. Scholtes, H. J. Maier, and I. Altenberger, "High temperature fatigue behavior and residual stress stability of laser-shock peened and deep rolled austenitic steel AISI 304," *Scr. Mater.*, vol. 50, no. 10, pp. 1345–1350, May 2004.

[81] P. Peyre, R. Fabbro, P. Merrien, and H. P. Lieurade, "Laser shock processing of aluminium alloys. Application to high cycle fatigue behaviour," *Mater. Sci. Eng. A*, vol. 210, no. 1–2, pp. 102–113, Jun. 1996.

[82] U. Trdan, M. Skarba, and J. Grum, "Laser shock peening effect on the dislocation transitions and grain refinement of Al–Mg–Si alloy," *Mater. Charact.*, vol. 97, pp. 57–68, Nov. 2014.

[83] Y. K. Gao, "Improvement of fatigue property in 7050–T7451 aluminum alloy by laser peening and shot peening," *Mater. Sci. Eng. A*, vol. 528, no. 10–11, pp. 3823–3828, Apr. 2011.

[84] M. Dorman, M. B. Toparli, N. Smyth, A. Cini, M. E. Fitzpatrick, and P. E. Irving, "Effect of laser shock peening on residual stress and fatigue life of clad 2024 aluminium sheet containing scribe defects," *Mater. Sci. Eng. A*, vol. 548, pp. 142–151, Jun. 2012.

[85] J. J. Ruschau, R. John, S. R. Thompson, and T. Nicholas, "Fatigue crack nucleation and growth rate behavior of laser shock peened titanium," *Int. J. Fatigue*, vol. 21, Supplement 1, pp. S199–S209, Sep. 1999.

[86] E. Maawad, H.-G. Brokmeier, L. Wagner, Y. Sano, and C. Genzel, "Investigation on the surface and near-surface characteristics of Ti–2.5Cu after various mechanical surface treatments," *Surf. Coat. Technol.*, vol. 12, no. 205, pp. 3644–3650, 2011.

[87] A. S. Gill, A. Telang, and V. K. Vasudevan, "Characteristics of surface layers formed on inconel 718 by laser shock peening with and without a protective coating," *J. Mater. Process. Technol.*, vol. 225, pp. 463–472, Nov. 2015.

[88] D. Karthik and S. Swaroop, "Laser shock peening enhanced corrosion properties in a nickel based Inconel 600 superalloy," *J. Alloys Compd.*, vol. 694, pp. 1309–1319, Feb. 2017.

[89] Y. Li *et al.*, "The strengthening mechanism of a nickel-based alloy after laser shock processing at high temperatures," *Sci. Technol. Adv. Mater.*, vol. 14, no. 5, p. 055010, Oct. 2013.

[90] "Metal Improvement | Laser Peening Benefits." [Online]. Available: http://www.metalimprovement.com/laser_peening_benefits.php. [Accessed: 08-Oct-2015].

150

[91] A. K. Gujba and M. Medraj, "Laser Peening Process and Its Impact on Materials Properties in Comparison with Shot Peening and Ultrasonic Impact Peening," *Materials*, vol. 7, no. 12, pp. 7925–7974, 2014.

[92] P. Peyre and R. Fabbro, "Laser shock processing: a review of the physics and applications," *Opt. Quantum Electron.*, vol. 27, no. 12, pp. 1213–1229, Dec. 1995.

[93] X. C. Zhang, Y. K. Zhang, J. Z. Lu, F. Z. Xuan, Z. D. Wang, and S. T. Tu, "Improvement of fatigue life of Ti–6Al–4V alloy by laser shock peening," *Mater. Sci. Eng. A*, vol. 527, no. 15, pp. 3411–3415, Jun. 2010.

[94] Y. B. Guo and R. Caslaru, "Fabrication and characterization of micro dent arrays produced by laser shock peening on titanium Ti–6Al–4V surfaces," *J. Mater. Process. Technol.*, vol. 211, no. 4, pp. 729–736, Apr. 2011.

[95] C. Rubio-Gonzalez *et al.*, "Effect of an absorbent overlay on the residual stress field induced by laser shock processing on aluminum samples," *Appl. Surf. Sci.*, vol. 252, no. 18, pp. 6201–6205, 2006.

[96] K. Ding and L. Ye, *Laser shock peening Performance and process simulation*. CRC Press, 2006.

[97] P. Peyre *et al.*, "Surface modifications induced in 316L steel by laser peening and shot-peening. Influence on pitting corrosion resistance," *Mater. Sci. Eng. A*, vol. 280, no. 2, pp. 294–302, Mar. 2000.

[98] X. C. Zhang, Y. K. Zhang, J. Z. Lu, F. Z. Xuan, Z. D. Wang, and S. T. Tu, "Improvement of fatigue life of Ti–6Al–4V alloy by laser shock peening," *Mater. Sci. Eng. A*, vol. 527, no. 15, pp. 3411–3415, Jun. 2010.

[99] S. Srinivasan, D. B. Garcia, M. C. Gean, H. Murthy, and T. N. Farris, "Fretting fatigue of laser shock peened Ti–6Al–4V," *Tribol. Int.*, vol. 42, no. 9, pp. 1324–1329, Sep. 2009.

[100] P. Peyre, R. Fabbro, P. Merrien, and H. P. Lieurade, "Laser shock processing of aluminium alloys. Application to high cycle fatigue behaviour," *Mater. Sci. Eng. A*, vol. 210, no. 1–2, pp. 102–113, Jun. 1996.

[101] O. Hatamleh, "A comprehensive investigation on the effects of laser and shot peening on fatigue crack growth in friction stir welded AA 2195 joints," *Int. J. Fatigue*, vol. 31, no. 5, pp. 974–988, May 2009.

[102] O. Hatamleh and A. DeWald, "An investigation of the peening effects on the residual stresses in friction stir welded 2195 and 7075 aluminum alloy joints," *J. Mater. Process. Technol.*, vol. 209, no. 10, pp. 4822–4829, Jun. 2009.

[103] C. S. Montross, V. Florea, and M. V. Swain, "The influence of coatings on subsurface mechanical properties of laser peened 2011-T3 aluminum," *J. Mater. Sci.*, vol. 36, no. 7, pp. 1801–1807, Apr. 2001.

[104] G. Cheng and M. Shehadeh, "Dislocation behavior in silicon crystal induced by laser shock peening: A multiscale simulation approach," *Scr. Mater.*, vol. 53, pp. 1013–1018, Nov. 2005.

[105] A. H. Clauer, B. P. Fairand, and B. A. Wilcox, "Pulsed laser induced deformation in an Fe-3 Wt Pct Si alloy," *Metall. Trans. A*, vol. 8, no. 1, pp. 119–125, Jan. 1977.

[106] X. Hong *et al.*, "Confining medium and absorptive overlay: Their effects on a laser-induced shock wave," *Opt. Lasers Eng.*, vol. 29, no. 6, pp. 447–455, Jun. 1998.

[107]   Z. Zhou *et al.*, "Thermal relaxation of residual stress in laser shock peened Ti–6Al–4V alloy," *Surf. Coat. Technol.*, vol. 206, no. 22, pp. 4619–4627, Jun. 2012.

[108]   Y. Cao, Y. C. Shin, and B. Wu, "Parametric Study on Single Shot and Overlapping Laser Shock Peening on Various Metals via Modeling and Experiments," *J. Manuf. Sci. Eng.*, vol. 132, no. 6, pp. 061010–061010–10, Nov. 2010.

[109]   T. W. Charles S. Montross, "Laser Shock Processing and its Effects on Microstructure and Properties of Metal Alloys: A Review," *Int. J. Fatigue*, vol. 24, no. 10, pp. 1021–1036, 2002.

[110]   J. J. Ruschau, R. John, S. R. Thompson, and T. Nicholas, "Fatigue crack nucleation and growth rate behavior of laser shock peened titanium," *Int. J. Fatigue*, vol. 21, Supplement 1, pp. S199–S209, Sep. 1999.

[111]   Y. Sano *et al.*, "Retardation of crack initiation and growth in austenitic stainless steels by laser peening without protective coating," *Mater. Sci. Eng. A*, vol. 417, no. 1–2, pp. 334–340, Feb. 2006.

[112]   U. Trdan, J. A. Porro, J. L. Ocaña, and J. Grum, "Laser shock peening without absorbent coating (LSPwC) effect on 3D surface topography and mechanical properties of 6082-T651 Al alloy," *Surf. Coat. Technol.*, vol. 208, pp. 109–116, Sep. 2012.

[113]   S. Kalainathan, S. Sathyajith, and S. Swaroop, "Effect of laser shot peening without coating on the surface properties and corrosion behavior of 316L steel," *Opt. Lasers Eng.*, vol. 50, no. 12, pp. 1740–1745, Dec. 2012.

[114]   R. Fabbro, J. Fournier, P. Ballard, D. Devaux, and J. Virmont, "Physical study of laser-produced plasma in confined geometry," *J. Appl. Phys.*, vol. 68, pp. 775–784, Jul. 1990.

[115]   S. Couturier, T. de Rességuier, M. Hallouin, J. P. Romain, and F. Bauer, "Shock profile induced by short laser pulses," *J. Appl. Phys.*, vol. 79, pp. 9338–9342, Jun. 1996.

[116]   X. Ling, W. Peng, and G. Ma, "Influence of Laser Peening Parameters on Residual Stress Field of 304 Stainless Steel," *J. Press. Vessel Technol.*, vol. 130, no. 2, pp. 021201–021201–8, Mar. 2008.

[117]   C. Ye, S. Suslov, B. J. Kim, E. A. Stach, and G. J. Cheng, "Fatigue performance improvement in AISI 4140 steel by dynamic strain aging and dynamic precipitation during warm laser shock peening," *Acta Mater.*, vol. 59, no. 3, pp. 1014–1025, Feb. 2011.

[118]   A. H. Clauer and B. P. Fairand, "INTERACTION OF LASER-INDUCED STRESS WAVES WITH METALS," p. 22.

[119]   R. K. Thareja and S. Shukla, "Synthesis and characterization of zinc oxide nanoparticles by laser ablation of zinc in liquid," *Appl. Surf. Sci.*, vol. 253, pp. 8889–8895, Sep. 2007.

[120]   A. Kruusing, "Underwater and water-assisted laser processing: Part 1—general features, steam cleaning and shock processing," *Opt. Lasers Eng.*, vol. 41, no. 2, pp. 307–327, Feb. 2004.

[121]   Z. Hong and Y. Chengye, "Laser shock processing of 2024-T62 aluminum alloy," *Mater. Sci. Eng. A*, vol. 257, no. 2, pp. 322–327, Dec. 1998.

[122]   Y. Zhang, J. You, J. Lu, C. Cui, Y. Jiang, and X. Ren, "Effects of laser shock processing on stress corrosion cracking susceptibility of AZ31B magnesium alloy," *Surf. Coat. Technol.*, vol. 204, no. 24, pp. 3947–3953, Sep. 2010.

[123]   Y. C. H. J. -M. Yang, "Laser shock peening on fatigue behavior of 2024-T3 Al alloy with fastener holes and stopholes," *Mater. Sci. Eng. A*, vol. 298, no. 1–2, pp. 296–299, 2001.

[124]   E. Hombergsmeier, V. Holzinger, W. von Bestenbostel, and U. C. Heckenberger, "Laser shock peening to improve the fatigue resistance of AA7050 components," *Int. J. Struct. Integr.*, vol. 2, no. 1, pp. 22–33, Mar. 2011.

[125]   A. Chahardehi, F. P. Brennan, and A. Steuwer, "The effect of residual stresses arising from laser shock peening on fatigue crack growth," *Eng. Fract. Mech.*, vol. 77, no. 11, pp. 2033–2039, Jul. 2010.

[126]   Gulshan Singh, Miguel Cortina, Harry Millwater, and Allan Clauer, "Probabilistic sensitivity analysis of a laser peening fatigue life enhancement processnull," *Int. J. Struct. Integr.*, vol. 3, no. 3, pp. 210–235, Aug. 2012.

[127]   Z. CAO, H. XU, S. ZOU, and Z. CHE, "Investigation of Surface Integrity on TC17 Titanium Alloy Treated by Square-spot Laser Shock Peening," *Chin. J. Aeronaut.*, vol. 25, no. 4, pp. 650–656, Aug. 2012.

[128]   J. l. Ocaña *et al.*, "Laser Shock Processing: an emerging technique for the enhancement of surface properties and fatigue life of high-strength metal alloys," *Int. J. Microstruct. Mater. Prop.*, vol. 8, no. 1/2, pp. 38–52, Jan. 2013.

[129]   Uroš Trdan, Sebastjan Žagar, Janez Grum, and José Luis Ocan˜a, "Surface modification of laser- and shot-peened 6082 aluminium alloy: Laser peening effect to pitting corrosion," *Int. J. Struct. Integr.*, vol. 2, no. 1, pp. 9–21, Mar. 2011.

[130]   H. Lee, D. Kim, J. Jung, Y. Pyoun, and K. Shin, "Influence of peening on the corrosion properties of AISI 304 stainless steel," *Corros. Sci.*, vol. 51, no. 12, pp. 2826–2830, Dec. 2009.

[131]   O. Hatamleh, P. M. Singh, and H. Garmestani, "Stress Corrosion Cracking Behavior of Peened Friction Stir Welded 2195 Aluminum Alloy Joints," *J. Mater. Eng. Perform.*, vol. 18, no. 4, p. 406, Jun. 2009.

[132]   S. A. Martinez, S. Sathish, M. P. Blodgett, and M. J. Shepard, "Residual stress distribution on surface-treated Ti-6Al-4V by X-ray diffraction," *Exp. Mech.*, vol. 43, no. 2, pp. 141–147, Jun. 2003.

[133]   Y. Zhao, "Effects of Laser Shock Peening on Residual Stress, Texture and Deformation Microstructure of Ti-6Al-4V Alloy," University of Cincinnati, 2012.

[134]   B. Rouleau, P. Peyre, J. Breuils, H. Pelletier, T. Baudin, and F. Brisset, "Characterization at a local scale of a laser-shock peened aluminum alloy surface," *Appl. Surf. Sci.*, vol. 257, no. 16, pp. 7195–7203, Jun. 2011.

[135]   A. T. DeWald, J. E. Rankin, M. R. Hill, M. J. Lee, and H.-L. Chen, "Assessment of Tensile Residual Stress Mitigation in Alloy 22 Welds Due to Laser Peening," *J. Eng. Mater. Technol.*, vol. 126, no. 4, pp. 465–473, Nov. 2004.

[136]   U. Sánchez-Santana *et al.*, "Wear and friction of 6061-T6 aluminum alloy treated by laser shock processing," *Wear*, vol. 260, no. 7, pp. 847–854, Apr. 2006.

[137]   K. Y. Luo *et al.*, "Effects of laser shock processing on mechanical properties and micro-structure of ANSI 304 austenitic stainless steel," *Mater. Sci. Eng. A*, vol. 528, no. 13, pp. 4783–4788, May 2011.

[138]   J. P. Chu, J. M. Rigsbee, G. Banaś, and H. E. Elsayed-Ali, "Laser-shock processing effects on surface microstructure and mechanical properties of low carbon steel," *Mater. Sci. Eng. A*, vol. 260, no. 1, pp. 260–268, Feb. 1999.

[139]   B. P. Fairand, A. H. Clauer, R. G. Jung, and B. A. Wilcox, "Quantitative assessment of laser-induced stress waves generated at confined surfaces," *Appl. Phys. Lett.*, vol. 25, no. 8, pp. 431–433, Oct. 1974.

[140]   B. P. Fairand and A. H. Clauer, "Use Of Laser Generated Shocks To Improve The Properties Of Metals And Alloys," in *Industrial Applications of High Power Laser Technology*, 1976, vol. 0086, pp. 112–122.

[141]   A. H. Clauer, B. P. Fairand, and B. A. Wilcox, "Laser shock hardening of weld zones in aluminum alloys," *Metall. Trans. A*, vol. 8, no. 12, pp. 1871–1876, Dec. 1977.

[142]   D. Devaux, R. Fabbro, L. Tollier, and E. Bartnicki, "Generation of shock waves by laser-induced plasma in confined geometry," *J. Appl. Phys.*, vol. 74, no. 4, pp. 2268–2273, Aug. 1993.

[143]   "Laser Shock Peening - 1st Edition." [Online]. Available: https://www.elsevier.com/books/laser-shock-peening/ding/978-1-85573-929-1. [Accessed: 30-Jul-2018].

[144]   P. Mallozzi and B. Fairand, "Altering material properties," US3850698A, 26-Nov-1974.

[145]   A. H. Clauer, B. P. Fairand, S. C. Ford, and C. T. Walters, "Laser shock processing," US4401477A, 30-Aug-1983.

[146]   S. Mannava, A. E. McDaniel, and W. D. Cowie, "Laser shock peened rotor components for turbomachinery," US5492447A, 20-Feb-1996.

[147]   S. Mannava, A. E. McDaniel, W. D. Cowie, H. Halila, J. E. Rhoda, and J. E. Gutknecht, "Laser shock peened gas turbine engine fan blade edges," US5591009A, 07-Jan-1997.

[148]   S. J. Ferrigno, K. G. McAllister, and S. Mannava, "Laser shock peened gas turbine engine seal teeth," US6200689B1, 13-Mar-2001.

[149]   "Curtiss-Wright Surface Technologies," *Aerospace Technology*. .

[150]   D. A. Casarcia, W. D. Cowie, and S. Mannava, "Laser shock peened bearings," US5584586A, 17-Dec-1996.

[151]   R. SUNDAR *et al.*, "Laser shock peening of steam turbine blade for enhanced service life," *Pramana*, vol. 82, no. 2, pp. 347–351, Feb. 2014.

[152]   M. Yoda and B. Newton, "UNDERWATER LASER PEENING," p. 10, 2008.

[153]   M. P. Sealy and Y. B. Guo, "Surface integrity and process mechanics of laser shock peening of novel biodegradable magnesium-calcium (Mg-Ca) alloy," *J. Mech. Behav. Biomed. Mater.*, vol. 3, no. 7, pp. 488–496, Oct. 2010.

[154]   Y. Guo, M. P. Sealy, and C. Guo, "Significant improvement of corrosion resistance of biodegradable metallic implants processed by laser shock peening," *CIRP Ann. - Manuf. Technol.*, vol. 61, no. 1, pp. 583–586, 2012.

[155]   "Laser shock peening - Aviation Industry - 镭宝光电." [Online]. Available: http://www.beamtech-laser.com/lbgd_en/lbgd_en/html/2015/wrew_1105/42.html. [Accessed: 11-Aug-2018].

[156]   "Overview." [Online]. Available: https://cwst.com/laser-peening/overview/. [Accessed: 11-Aug-2018].

[157]   "Laser Peening - ROI." [Online]. Available: https://www.lsptechnologies.com/laser-peening-roi.php. [Accessed: 11-Aug-2018].

[158]   Evren Yasa, Jan Deckers, and Jean-Pierre Kruth, "The investigation of the influence of laser re-melting on density, surface quality and microstructure of selective laser melting partsnull," *Rapid Prototyp. J.*, vol. 17, no. 5, pp. 312–327, Aug. 2011.

[159]   E. Yasa and J. Kruth, "Application of laser re-melting on selective laser melting parts," *Adv. Prod. Eng. Manag.*, vol. 6, no. 4, pp. 259–270, 2011.

[160]   E. Yasa, J.-P. Kruth, and J. Deckers, "Manufacturing by combining Selective Laser Melting and Selective Laser Erosion/laser re-melting," *CIRP Ann.*, vol. 60, no. 1, pp. 263–266, Jan. 2011.

[161]   L. Zumofen, C. Beck, A. Kirchheim, and H.-J. Dennig, "Quality Related Effects of the Preheating Temperature on Laser Melted High Carbon Content Steels," in *Industrializing Additive Manufacturing - Proceedings of Additive Manufacturing in Products and Applications - AMPA2017*, 2017, pp. 210–219.

[162]   Q. Liu, Y. Danlos, B. Song, B. Zhang, S. Yin, and H. Liao, "Effect of high-temperature preheating on the selective laser melting of yttria-stabilized zirconia ceramic," *J. Mater. Process. Technol.*, vol. 222, pp. 61–74, Aug. 2015.

[163]   Y.-C. Hagedorn, J. Risse, W. Meiners, and et al, "Processing of nickel based superalloy MAR M-247 by means of high-temperature - selective laser melting (HT - SLM)," in *High Value Manufacturing. Advanced Research Virtual Rapid Prototyping*, 2014, pp. 291–295.

[164]   P. J. da S. Bartolo *et al.*, *High Value Manufacturing: Advanced Research in Virtual and Rapid Prototyping: Proceedings of the 6th International Conference on Advanced Research in Virtual and Rapid Prototyping, Leiria, Portugal, 1-5 October, 2013*. CRC Press, 2013.

[165]   H. K. Rafi, N. V. Karthik, H. Gong, T. L. Starr, and B. E. Stucker, "Microstructures and Mechanical Properties of Ti6Al4V Parts Fabricated by Selective Laser Melting and Electron Beam Melting," *J. Mater. Eng. Perform.*, vol. 22, no. 12, pp. 3872–3883, Dec. 2013.

[166]   B. Vrancken, S. Buls, J.-P. Kruth, and J. Van Humbeeck, "Influence of preheating and oxygen content on Selective Laser Melting of Ti6Al4V," in *Proceedings of the 16th RAPDASA Conference*, 20151101.

[167]   H. V. Atkinson and S. Davies, "Fundamental aspects of hot isostatic pressing: An overview," *Metall. Mater. Trans. A*, vol. 31, no. 12, pp. 2981–3000, Dec. 2000.

[168]   N. L. Loh and K. Y. Sia, "An overview of hot isostatic pressing," *J. Mater. Process. Technol.*, vol. 30, no. 1, pp. 45–65, Feb. 1992.

[169]   Z. G. Wang, Y. S. Shi, R. D. Li, Q. S. Wei, and J. H. Liu, "Manufacturing AISI316L Components via Selective Laser Melting Coupled with Hot Isostatic Pressing," *Materials Science Forum*, 2011. [Online]. Available: https://www.scientific.net/MSF.675-677.853. [Accessed: 01-Aug-2018].

[170]   N. P. Lavery *et al.*, "Effects of hot isostatic pressing on the elastic modulus and tensile properties of 316L parts made by powder bed laser fusion," *Mater. Sci. Eng. A*, vol. 693, pp. 186–213, May 2017.

[171]   "HIPing - What Is It and What are The Advantages for Engineering Ceramics?," *AZoM.com*, 27-Jul-2011. [Online]. Available: https://www.azom.com/article.aspx?ArticleID=5769. [Accessed: 01-Aug-2018].

[172]   S. Leuders, T. Lieneke, S. Lammers, T. Tröster, and T. Niendorf, "On the fatigue properties of metals manufactured by selective laser melting – The role of ductility," *J. Mater. Res.*, vol. 29, no. 17, pp. 1911–1919, Sep. 2014.

[173]   A. Riemer, S. Leuders, M. Thöne, H. A. Richard, T. Tröster, and T. Niendorf, "On the fatigue crack growth behavior in 316L stainless steel manufactured by selective laser melting," *Eng. Fract. Mech.*, vol. 120, pp. 15–25, Apr. 2014.

[174]   "Matsuura Machinery Corporation | LUMEX Avance-25." [Online]. Available: http://www.matsuura.co.jp/english/contents/products/lumex.html. [Accessed: 10-Aug-2018].

[175]   T. A. Book and M. D. Sangid, "Evaluation of Select Surface Processing Techniques for In Situ Application During the Additive Manufacturing Build Process," *JOM - J. Miner. Met. Mater. Soc.*, vol. 68, no. 7, pp. 1780–1792, 2016.

[176]   N. Kalentics *et al.*, "3D Laser Shock Peening – A new method for the 3D control of residual stresses in Selective Laser Melting," *Mater. Des.*, vol. 130, pp. 350–356, Sep. 2017.

[177]   Y. Estrin and A. Vinogradov, "Extreme grain refinement by severe plastic deformation: A wealth of challenging science," *Acta Mater.*, vol. 61, no. 3, pp. 782–817, Feb. 2013.

[178]   A. Mahato, Y. Guo, H. Yeung, and S. Chandrasekar, "Surface flow in severe plastic deformation of metals by sliding," *IOP Conf. Ser. Mater. Sci. Eng.*, vol. 63, no. 1, p. 012016, 2014.

[179]   S. Bagheri and M. Guagliano, "Review of shot peening processes to obtain nanocrystalline surfaces in metal alloys," *Surf. Eng.*, vol. 25, no. 1, pp. 3–14, Jan. 2009.

[180]   "Progressive Surface - process services: high pressure waterjet stripping, shot peening, grit blasting, waterjet & abrasive waterjet cutting, thermal spray coating." [Online]. Available: https://www.progressivesurface.com/services_process.htm. [Accessed: 10-Aug-2018].

[181]   B. AlMangour and J.-M. Yang, "Improving the surface quality and mechanical properties by shot-peening of 17-4 stainless steel fabricated by additive manufacturing," *Mater. Des.*, vol. 110, pp. 914–924, Nov. 2016.

[182]   C. Kanger *et al.*, "Effect of Process Parameters and Shot Peening on Mechanical Behavior of ABS Parts Manufactured by Fused Filament Fabrication (FFF)," p. 15.

[183]   G. Madireddy *et al.*, "Effect of Process Parameters and Shot Peening on the Tensile Strength and Deflection of Polymer Parts Made using Mask Image Projection Stereolithography (MIP-SLA)," p. 10.

[184]   S. Tekeli, "Enhancement of fatigue strength of SAE 9245 steel by shot peening," *Mater. Lett.*, vol. 57, no. 3, pp. 604–608, Dec. 2002.

[185]   N. Kalentics, R. Logé, and E. BOILLAT, "Method and Device for Implementing Laser Shock Peening or Warm Laser Shock Peening During Selective Laser Melting," US20170087670 A1, 30-Mar-2017.

[186]   N. Kalentics, E. Boillat, P. Peyre, S. Ćirić-Kostić, N. Bogojević, and R. E. Logé, "Tailoring residual stress profile of Selective Laser Melted parts by Laser Shock Peening," *Addit. Manuf.*, vol. 16, pp. 90–97, Aug. 2017.

[187]   R. A. Brockman *et al.*, "Prediction and characterization of residual stresses from laser shock peening," *Int. J. Fatigue*, vol. 36, no. 1, pp. 96–108, Mar. 2012.

156

[188]   Z. Zhou *et al.*, "A finite element study of thermal relaxation of residual stress in laser shock peened IN718 superalloy," *Int. J. Impact Eng.*, vol. 38, no. 7, pp. 590–596, Jul. 2011.

[189]   B. Sun, H. Qiao, and J. Zhao, "Accurate numerical modeling of residual stress fields induced by laser shock peening," *AIP Adv.*, vol. 8, no. 9, p. 095203, Sep. 2018.

[190]   M. Morales, C. Molpeceres, J. A. Porro, A. García-Beltrán, and J. L. Ocaña, "Numerical Thermo-Mechanical Modelling of Stress Fields and Residual Constraints in Metallic Targets Subject to Laser Shock Processing," *Materials Science Forum*, 2010. [Online]. Available: https://www.scientific.net/MSF.638-642.2682. [Accessed: 29-Nov-2018].

[191]   C. Correa, A. Gil-Santos, J. A. Porro, M. Díaz, and J. L. Ocaña, "Eigenstrain simulation of residual stresses induced by laser shock processing in a Ti6Al4V hip replacement," *Mater. Des.*, vol. 79, pp. 106–114, Aug. 2015.

[192]   D. Lin, C. Ye, Y. Liao, S. Suslov, R. Liu, and G. J. Cheng, "Mechanism of fatigue performance enhancement in a laser sintered superhard nanoparticles reinforced nanocomposite followed by laser shock peening," *J. Appl. Phys.*, Apr. 2013.

Curriculum Vitae

Nikola Kalentics   nikolakalentic@gmail.com

Education

2015-2018	PhD – "A new hybrid Additive Manufacturing process combining Selective Laser Melting and Laser Shock Peening"
	Laboratory of Thermomechanical Metallurgy (LMTM)
	École Polytechnique Fédérale de Lausanne (EPFL), Switzerland
2008-2010	MSc in Mechanical Engineering
	Faculty of Technical Sciences, University of Novi Sad, Serbia
2005-2008	BSc in Mechanical Engineering
	Faculty of Technical Sciences, University of Novi Sad, Serbia

Work Experience

2009-2014	Research, development and production of molds for injection and blow molding
	Tehnoplast, Serbia

Awards

1. Faculty of Technical Sciences, University of Novi Sad, Serbia, Award for Academic Results – Best Student of the Generation (2010)

2. 1000 Best Students, Ministry of Youth and Sport, Republic of Serbia (2009/2010)

Publications

1. N. Kalentics et al., "Tailoring residual stress profile of Selective Laser Melted parts by Laser Shock Peening," *Additive Manufacturing*, vol. 16, pp. 90–97, Aug. 2017. doi: 10.1016/j.addma.2017.05.008

2. N. Kalentics et al., "3D Laser Shock Peening – A new method for the 3D control of residual stresses in Selective Laser Melting," *Materials & Design*, vol. 130, pp. 350–356, Sep. 2017. doi: 10.1016/j.matdes.2017.05.083

3. N. Kalentics et al., "Laser shock peening: a promising tool for tailoring metallic microstructures in selective laser melting", *Journal of Materials Processing Technology, Nov. 2018. doi: 10.1016/j.jmatprotec.2018.11.024*

4. N. Kalentics, R. E. Logé, "3D LSP as a way to improve geometrical accuracy in Selective Laser Melting", *The International Journal of Advanced Manufacturing Technology, Nov. 2018. doi: 10.1007/s00170-018-3033-3*

5. N. Kalentics, R. E. Logé, "Hybrid Additive Manufacturing of ultra-durable metal parts", (To be submitted)

6. Nikola Kalentics et al., "Reducing crack density in Selective Laser Melting by 3D Laser Shock Peening", (To be submitted)

Patents

1. N. Kalentics, R. Logé, and E. Boillat, "Method and Device for Implementing Laser Shock Peening or Warm Laser Shock Peening During Selective Laser Melting," US20170087670 A1, 30-Mar-2017.

2. N. Kalentics, R. Logé, "Method and device for fabrication of 3D multi - material (composite) parts by selective laser melting combined with laser welding and cutting", WO2017108645A1, 29-Jun-2017.

Languages

Serbian, English, French, Hungarian